KWAME NKRUMAH UNIVERSITY OF SCIENCE AND TECHNOLOGY, KUMASI, GHANA

CLIMATE-INDUCED RICE ROOT-ZONE SALINITY IN THE TIDAL SWAMP RICE PRODUCTION ZONES OF THE GAMBIA

A thesis submitted to the Department of Civil Engineering, in partial fulfillment of the requirements for the degree of

DOCTOR OF PHI LOSOPHY
IN
CLIMATE CHANGE AND LAND USE

BY

JALAMANG CAMARA

(BSc Agriculture and Environmental Sciences, MPhil Soil Science)

SEPTEMBER, 2023

DECLARATION

I hereby declare that this submission is my work towards the Ph.D. in Climate Change and Land Use and that, to the best of my knowledge and belief, it contains no material previously published or written by another person nor material which, to a substantial extent has been accepted for the award of any degree or diploma at Kwame Nkrumah University of Science and Technology, Kumasi or other educational institution, except where due acknowledgment is made in this thesis.

Jalamang Camara	…….....	…….....
(ID PG 20447827)	Signature	Date
(Student)		

Certified by:

Prof. Antinuke O. Adebanji	…….....	…….....
(Main Supervisor)	Signature	Date

Prof. Emmanuel K. Appiah-Adjei	…….....	…….....
(Co-Supervisor)	Signature	Date

Prof. Sampson Oduro-Kwarten	…….....	…….....
(Head of Department)	Signature	Date

DEDICATION

To the Loving Memory of

Dr. Balla Musa Boiang,

Director General, National Agricultural Research Institute (NARI) from 2004 to 2007.

May Allah grant him Jannatul Firdaus. Ameen!

ACKNOWLEDGMENT

My sincere gratitude goes to the supervisory team, principal supervisor, Prof. ATINUKE O. ADEBANJI, Co-supervisor, Prof. EMMANUEL K. APPIAH-ADJEI, Dr. MICHEAL THIEL and my mentor, Dr. CHARLES GYAMFI, for their immense and remarkable contributions to the success of this research. Their guidance and constructive criticisms of the numerous drafts of this work have given me an in-depth understanding of scientific research. My special thanks and appreciation to Prof. Sampson K. AGODZO for the guidance and technical support during the research.

My appreciation goes to the Federal Ministry of Education and Research (BMBF) of Germany for the decade commitment to building regional capacity on climate change and the West African Science Centre on Climate Change and Adapted Land Use (WASCAL) in Ghana, Accra, for providing the scholarship and financial support for this program.

I am grateful to the Directorate of WASCAL CCLU coordination unit, Director Prof. Wilson Agyei Agyare; Deputy Director, Prof. Eric Forkuo; Scientific Coordinator, Dr. William Amponsah; Financial Officer, Mr. Ampong Kwabena; and the Senior Secretary, Miss. Theresa Sarpong, Akua Osaa Awuah, the WASCAL CCLU support and teaching staff, and the professors for their dedication and commitment to providing the next generation of climate experts in the West African Sub-region. The memorable advisory roles and support rendered by the WASCAL CCLU community in KNUST, the Batch 4 mates during the study, are worth noting.

Thanks to the Agroforestry and Cropping System Research Doctorate staff, NARI, Special appreciation to the institute's staff Soil laboratory, especially Fa Mamudu, Mr. Amadou Nyassi, and Mr. Dembo Manjang, who also deputies as field assistants, to Mr.Salifu Ceesay, Edrisa Manneh and Ebrima Bah during the entire field research. I am expressing my sincere appreciation to the National Agricultural Research Institute (NARI), Gambia. I sincerely thank NARI's current and previous management for creating an enabling capacity-building environment. I render appreciation and profound gestures in loving memories of the late Dr. Balla Musa Bojang and Dr. Babou Ousman Jobe, Mr. Ansumana Jarju, former Director General of NARI.

I notably thank all members of the Camara Kunda family, both at home and abroad, for their continuous moral support and prayers. I also owe special thanks to my wife,

Mrs. Fatoumatta Camara Yarbo, whose encouragement and steadfast support have brought me this far. I pray that God the Almighty Allah grants everyone their goodwill heart desires.

ABSTRACT

This research focused on the effects of soil salinity and climate variability on rice cultivation and agricultural productivity in the Lower River Region (LRR) and Central River Region South (CRRS) of The Gambia. The research employed a multidisciplinary approach, utilizing machine learning models, satellite reflectance, soil salinity (EC_e) data, and statistical analyses to assess soil salinity dynamics, its impact on rice yield, and potential adaptive strategies for sustainable agriculture. The Random Forest model demonstrates strong predictive capability using Landsat 8 reflectance values. Results indicate significant changes in salinity-affected areas in LRR from 66.34% of the total territory in 2014 to 72.15% in 2021, marking a substantial 9.56% increase. The results indicated a contraction in the combined salinity-affected area in CRRS, dropping from 93.46% of the region's land in 2014 to 80.29% in 2021, translating to a significant percentage decrease of -13.94 % during the same timeframe. The seasonal variability of root-zone salinity and its impact on rice yield shows that the soils predominantly exhibit acidity, with pH values ranging from 4.0 to 5.8. The GLM offers robust goodness of fit with an impressive R-squared value of 0.98. Tonitaba and Kudang express opposing coefficients on soil ESP, with t estimates (0.84994) and (-1.18268), respectively. The results indicated a statistically significant negative relationship between ESP and sampling time in August, indicating seasonality in salinity conditions. Sodium concentration (Na meq/100g) emerges as the most influential predictor of ESP, soil pH (pHsoil), calcium (Ca^{+2} meq/100g), potassium (K meq/100), and magnesium (Mg meq/100) manifest a negative association with ESP. The results show a substantial variation in rice yield across these study fields, with Mandina and Tonitaba yielding 30% less than Kudang. Maximum temperature exhibited a robust negative correlation with rainfall in both regions, while minimum temperature showed a medium to strong positive relationship with rain. Linear regression models explained 67% of rice yield variability in LRR and 64% in CRRS, highlighting the substantial influence of year-to-year changes. Random Forest prediction models revealed a 24% change between predicted and actual historical yield in LRR and a 54% change in CRRS. Maximum temperature significantly impacted rice yield, followed by rainfall.

Keywords: ESP; Climate variability; Soil salinity; root-zone

TABLE OF CONTENTS

LIST OF TABLES

LIST OF FIGURES

CHAPTER ONE
INTRODUCTION

1.1 Background

The agricultural industry and global food security are seriously threatened by climate change, especially in developing countries (Rondhi et al., 2019). IPCC (2014) identified climate change as a significant factor undermining food security, mainly impacting agricultural productivity. According to projections, agricultural output losses from the combined effects of temperature and precipitation might reach 32% by 2100 (IPCC, 2022). Fitton et al. (2019) estimated that by 2050, 11 % of cropland globally will be susceptible to climate-induced water scarcity.

Climate change directly affects precipitation and temperature, leading to water shortages, altering soil and soil moisture conditions, and amplifying the incidence of pests and diseases (Kawasaki and Herath, 2011; Krishnan et al., 2016). According to Vogel et al. (2019), there was an estimated 25% yield loss globally between 1961 and 2006, with climate and climatic extremes being responsible for 20–49% of the variation in yield anomalies and 18–45% of the variance being ascribed to drought and heatwaves. Iizumi et al. (2018) report that lower worldwide mean yields of maize (4.1%), wheat (1.8%), and soybeans (4.5%) were caused by variations in precipitation and temperature, with rice yield showing a global variability of almost 32%.

Ray et al. (2019) noted detrimental effects on essential crops owing to decreasing precipitation without irrigation in semi-arid locations, including the Mediterranean, Sub-Saharan Africa, South Asia, and Australia. According to Sultan et al. (2019), between 2000 and 2009, drought and other climatic factors in West Africa caused yield losses of 10–20% for millet and 5–15% for sorghum. Climate change impact studies in The Gambia revealed yield reductions for millet (-15%), groundnut (-18%), maize (-22%), and sorghum (-25 to -15%) (Njie and Corr, 2006; Sonko et al., 2019).

The 2007 IPCC report highlighted the projected rise in abnormally high sea levels as a vital component contributing to the salinization of water used for agriculture at estuaries, thereby reducing the availability of freshwater systems. Additionally, Bayabil et al. (2021) reiterated that saltwater intrusion resulting from rising sea levels leads to soil salinity, causing damage to soil health and agricultural productivity. Soil salinity and alkalinity are significant forms of land degradation directly threatening

food security in many parts of the world, including The Gambia. Most lowland rice ecosystems in The Gambia are adversely affected by salt intrusion caused by rising sea levels and unprecedented fluctuations in river flow. In the lower saline stretches of the River Gambia, rice cropping under tidal irrigation is currently encountering notable disruptions due to elevated salinity levels (Mungai et al., 2019).

Soil salinity is a dominant form of land degradation that significantly impacts vegetable and rice cultivation in different regions of The Gambia. A significant area of alluvial soils is found in the floodplain of the River Gambia, which can be permanently or intermittently influenced by saline water (Dunsmore et al., 1976; Peat et al., 1979; Sylla et al., 2016). The saltwater influx and sulfur deposition from marine sediments have significantly impacted the soil characteristics in the swampy conditions of river floodplains (Jørgensen et al., 2019).

Furthermore, sulfur deposition from marine sediments results in acid-sulfate soils with low pH levels and high concentrations of toxic substances like aluminum and iron (Virtasalo et al., 2023). This leads to the buildup of salts in the ground, increasing salinity levels and reducing soil fertility. These conditions have negatively affected plant growth and soil microbial activity, diminishing the potential for rice cultivation in swampy conditions despite the soil's inherent fertility (Sari et al., 2023).

The River Gambia is strategically important for the Gambia River Basin Organization (OMVG) countries, including The Gambia, Guinea, Bissau, Guinea, and Senegal. However, critical gaps in understanding the basin's biophysical conditions and human activities have been identified (Kramer et al., 2019). Specifically, there is a lack of comprehensive soil surveys to determine the total area of the floodplain suitable for vegetable and rice irrigation (Verkerk and Rens, 2005). There is also no systematic assessment of the interactions between soil, surface, groundwater, and soil salinity along the tidal swamps of the River Gambia.

Assessing and monitoring soil salinity degradation will be essential for effective natural resource management and regional agricultural sustainability (Shahbaz and Ashraf, 2013; Talat, 2020). Soil salinity maps play a critical role in decision-making processes for managing salinity and water resources at various scales (Shahbaz and Ashraf, 2013). By enabling early detection and mapping of soil salinity, stakeholders

can identify problem areas and understand temporal and spatial changes in salt occurrence, ensuring efficient soil and water management, particularly in water-scarce regions (Ravi et al., 2020).

Moreover, monitoring changes in soil salinity over time is of utmost importance to assess the impact of management practices and optimize fertilizer and cropping inputs, particularly for rice production (Ravi et al., 2020; Radanielson et al., 2018). Accurate and timely soil salinity assessment is crucial for developing effective strategies to mitigate the detrimental effects of soil salinization on rice production and overall agricultural sustainability in The Gambia.

Establishing a systematic soil salinity monitoring framework provides valuable evidence for decision-makers, farmers, and researchers, allowing for better management of soil and water resources (Ravi et al., 2020; Talat, 2020). This framework enables targeted soil amendments and appropriate soil management techniques to improve soil structure and fertility, enhancing the region's agricultural potential (Shahbaz and Ashraf, 2013).

The Gambia faces increasing challenges from climate change, including a rise in drought frequency, salinization, short growing seasons, variability in rainfall (GOTG, 2016), and the lack of short-duration rice varieties has adversely impacted rice productivity, limiting the potential for rainfed rice production in The Gambia. As climate change continues to intensify, implementing a comprehensive soil salinity monitoring framework in The Gambia becomes increasingly critical to mitigate the impacts of saltwater intrusion (Adger et al., 2011; Munns et al., 2010). The availability of accurate soil salinity data supports informed policy-making and decision-support systems at both national and regional levels, facilitating the development of agricultural policies, water management strategies, and land-use planning (Shahbaz and Ashraf, 2013; Talat, 2020). Integrating soil monitoring into policy frameworks enhances The Gambia's capacity to address agricultural challenges. It will promote sustainable land and water management practices, contributing to achieving long-term food security goals for the region.

1.2 Problem Statement

The two prominent threats to sustainable agriculture are population increase and the decline in cultivable land (Shahbaz and Ashraf, 2013; Talat, 2020). The area ofitable for farming in semi-arid regions is diminishing at an annual rate of 10%. It is expected to cover 50% of the overall arable land by the year 2050, according to Jamil et al. (2021). Soil salinity, a significant environmental challenge for crop production, affects plant sensitivity and overall agricultural productivity (Tahir et al., 2019). Climate change exacerbates salinization processes through alterations in precipitation, temperature, rising sea levels, and evaporation patterns (Munns et al., 2010; Tahir et al., 2019).

Climate-induced sea level rise, associated flooding risks, and saltwater intrusion have aggravated soil salinity, particularly in coastal regions (Torres et al., 2016; Talat, 2020). This situation is worsened by alterations in precipitation patterns and rising evaporation rates, which contribute to the elevation of soil salinity levels (Torres et al., 2016; Talat, 2020). The collective impacts of sea level rise, alterations in land use, and climate-related factors heighten the vulnerability to saltwater intrusion in coastal regions, exacerbating the problems associated with soil salinity (Torres et al., 2016; Talat, 2020).

Climate change is estimated to significantly impact river flows and freshwater availability in West Africa, as indicated by a study conducted by Roudier et al. (2014) that found considerable uncertainty in future streamflow developments. While the overall uncertainty was reported to be 0%, suggesting a lack of clear direction, the Gambia River showed a noteworthy negative change with a median of -4.5%.

Projections indicated that natural flows in the perennial freshwater section of the River Gambia would decrease by 9% compared to historical flows at Kuntaur in the 1970s and 1980s ($168m^3/s$) (GOTG, 2016). Furthermore, the downstream area of the Gambia River basin is influenced by seasonal and annual rainfall variations over the Gambia, Senegal, and Guinea (Adger et al., 2011), exacerbating the potential impacts of climate change on freshwater resources.

Human activities, including deforestation, land cover change, upstream freshwater diversions, inappropriate irrigation practices, and pollution, significantly contribute to

soil salinity globally (Mukhopadhyay et al., 2020). Within the Gambia River Basin framework, the suggested development of the Trans-Gambia Bridge and the Sambangalou Dam, endorsed by UNDP, is expected to yield various advantages. These include enhanced water storage capacity, increased hydropower generation, and expanded irrigation possibilities. These measures aim to strengthen agriculture, bolster hydropower production, and augment water supply for the states along the river (Bodian et al., 2018).

Nonetheless, it is crucial to consider the potential adverse consequences on the water supply, which could affect the affected nations' energy production and agriculture sectors (Bodian et al., 2018). Additionally, concerns regarding water resources in The Gambia, linked to climate change, are projected to influence the River Gambia's water flow due to heightened evaporation losses from the river. This could result in increased evaporation rates and potential reductions in water availability, as previously established at 11 m^3/s (Kramer et al., 2019).

The increased level of climate-induced soil salinization of the floodplain of River Gambia renders it unsuitable for irrigation practices, reducing water and land availability for crop production (Adger et al., 2011). Rice, in particular, is susceptible to salinity stress, affecting various aspects of plant growth and development, including seedling growth, establishment, yield, and yield components (Asch & Wopereis, 2001; Talat, 2020). Although tolerant rice varieties have been introduced, their potential yield still needs to be realized due to the need to adopt suitable cropping seasons and management technologies (Radanielson et al., 2018; Yadav et al., 2019).

1.3 Overall Aim of the Study

The main objective of the study was to assess the combined impacts of soil salinization and climate change on rice production in the tidal floodplain of the River Gambia within the Lower River Region (LRR) and Central River Region South (CRRS) of the Gambia.

1.3.1 Specific Objectives of the Study

The specific objectives were:

i. To assess the spatio-temporal dynamics of soil salinity in the study area, focusing on tidal swamps suitable for rice irrigation in the floodplain of the River Gambia.
ii. To investigate the seasonal variability of root-zone salinity under farmer-managed fields and its impact on rice yield and overall crop productivity.
iii. To assess the vulnerability of rice production to climate change in the Lower Central River Regions of the Gambia

1.3.2 Research Question

i. What is the spatial distribution of soil salinity in the tidal swamp rice production zones, and how does it vary across distinct land cover types within the floodplain of the River Gambia?
ii. How does root-zone salinity vary with other soil physicochemical properties throughout the rice-growing season, and what is its impact on rice yield under the management practices of local farmers in the tidal floodplain of the River Gambia?
iii. What are the historical trends in climate conditions within the Lower River Region (LRR) and Central River Region South (CRRS) of The Gambia, and how do these trends impact rice production over time?

1.4 Scope and Limitations

This research covers the enumeration of land degradation due to soil salinity, the determination of the distribution of seasonal variability of saline conditions, and the identification of suitable crop management practices for rice production along the flood plains of river Gambia in LRR and CRRS. The research further estimates the effect of soil salinity on rice production and productivity and assesses yield loss in the study area. Additionally, the study focused on farmers' technology adoption and coping strategies, including alternative land use and sustainable livelihood of farmers affected by soil salinity.

This research's limitations arose from insufficient historical soil data and the absence of daily meteorological records for the two regions under investigation. These constraints impeded the comprehensive assessment of the historical influence of climate factors, such as temperature and rainfall, on soil salinization. Furthermore, the

unavailability of daily meteorological data hampered the precise determination of the onset and conclusion of the rainy season, consequently restricting the ability to thoroughly analyze the vulnerability of rice production in the study areas.

1.5 Description of the Study Area

The study was conducted in some selected districts of the Lower River Region (LRR) and Central River Region South (CRRS) of the Gambia, shown in Figure 1.1.

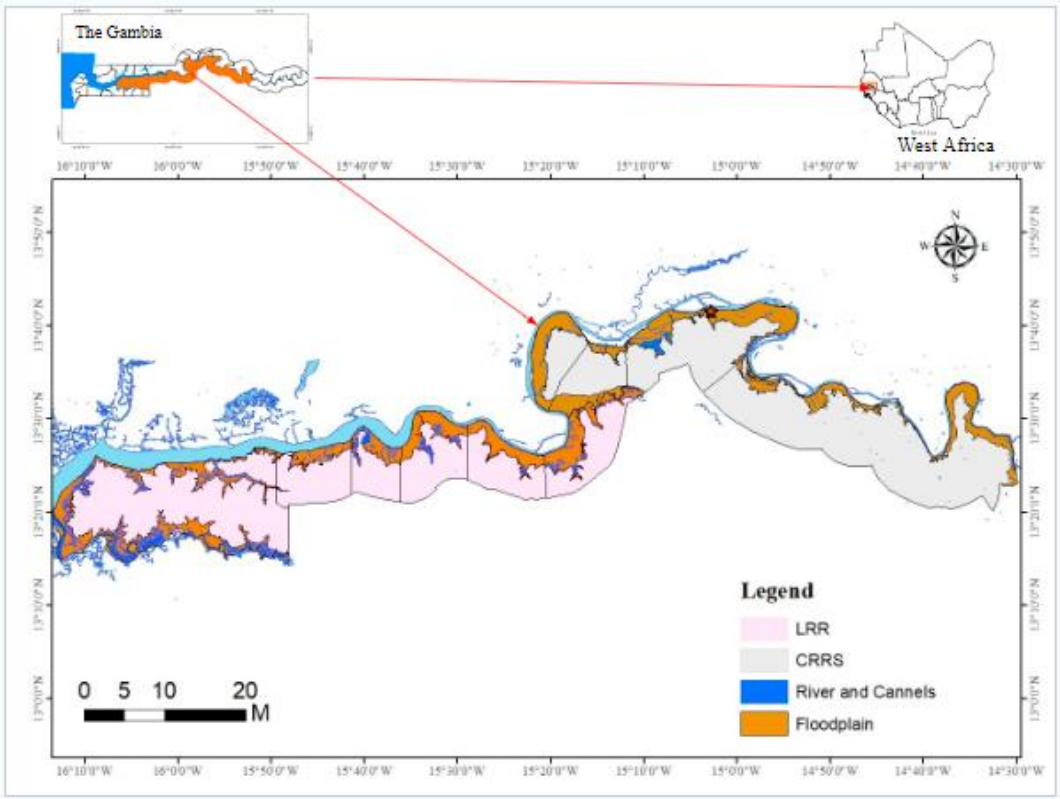

Figure 1.1 Map of the study area

Table 1.1 provides a comprehensive overview of land areas and the respective geographical coordinates for the specific regions. It also highlights the floodplain areas within these regions and the total floodplain area when combining both regions. The two regions have a Sudan-Sahelian climate characterized by savannah woodland vegetation interspersed with a tributary lowland valley systems network. These flood plains serve as excellent rice-growing catchments under tidal swamps and pump irrigation for rice production.

Table 1. 1 Geographical location and land areas (ha) of regions and floodplains

Region	Location		Area (ha)
	Longitude	Latitude	
LRR	-15.424459516829 ° W -15.1883353740675 ° W -15.5115289962543 ° W -15.6310647985023 ° W	13.453712190649° N 13.543396912821° N 13.481189881367° N 13.447324329627° N	149,064
CRRS	-15.3296256260678° W -15.3652108421198° W -15.3649035842031° W -15.3646737634526° W	13.629899889957°N 13.632079891759°N 13.633169967804°N 13.634305242712°N	145,190
Total Area			**294,254.4**
Floodplain			
LRR	-15.424459516829° W -15.1883353740675° W -15.5115289962543° W -15.6310647985023° W	13.4537121906487° N 13.5433969128207° N 13.4811898813669° N 13.4473243296266° N	41,021
CRRS	-15.3296256260678° W -15.2492807314256° W -15.0802336174757° W -14.8094297278412° W	13.602888488893° N 13.589362379631° N 13.633911618093° N 13.467075039242° N	32,563
Total Area			**73,584**

The zone has a short growing season from June/July to October, with mean annual rainfall varying from 900 mm in the southwest to about 600 mm in the northeast. The season is characterized by a few dry spells superimposed over fairly good rainfall distribution. The mean annual temperature ranges from 25 ^{o}C to 28 ^{o}C, with a higher mean in the eastern part of the country (Jarju, 2020).

Soil suitability assessments for this agroecological zone (AEZ) indicate that unsuitable land ranges between 28% and 58 %, while marginal land ranges between 7 % and 12% (FAO 1997). The soils on the upper edges of these flood plains are similar in texture and vary from friable clay to sandy loam, with distinctive crusting on the top that helps with significant runoff after heavy rains. These soils become stiff when dry and satisfiable but easy to cultivate when moist (FAO 1992; Gibba and Jallow, 2020). A considerable portion of the nation (492,999 hectares) is covered by the AEZ, of which 76% is farmed and provides for more than 60% of the country's agricultural output. The main grains produced in the region are primarily late varieties such as sorghum,

upland rice, and millet. Other important crops include vegetables, roots, tubers, and fruit trees (FAO, 1992; Sienta et al., 2019).

The river floodplain in LRR covers an area of 41,021 ha, and CRRS has a floodplain area of 32,563 ha. The combined floodplain area for both regions is approximately 73,584 ha. LRR covers an area of 149,064.1 ha, whereas CRRS encompasses an area of 145,190.3 ha. The total land area for the two regions is approximately 294,254.4 ha. The floodplain is characterized by thick mangrove forests and low-lying swamps, heavily influenced by tidal inundation. The mangrove forests provide vital ecosystem services such as carbon sequestration, shoreline protection, and nutrient cycling.

A substantial portion of the world's mangroves, approximately 19 %, is found in West-Central Africa, covering an area of around 20,410 km^2 (Feka and Ajonina, 2011; Feng et al., 2017). These mangroves hold great importance for the local population along the Atlantic Coast of Africa, particularly for the livelihoods of approximately five million people who depend on small-scale fisheries and rely on fish as a primary source of dietary protein(Boone & Bhomia, 2017). The site is rich in biodiversity and provides essential habitat for various species, including fish, crustaceans, and migratory birds.

The soil is primarily alluvial and colluvial, formed from the deposition of sediments carried by rivers and streams from the surrounding uplands. The soil texture is dominated by clay, with varying silt. As a result, the soil is generally rich in nutrients and organic matter. This can lead to soil compaction and poor drainage in some areas. However, the high clay content also means the soil has good water-holding capacity, which can benefit crop production.

Soil associations in the tidal zone with natural mangrove or reed vegetation are principally unripe and half-ripe gleys, basically grey or dark grey with very little mottling. The unripe saline soils are always sulphidic with fine texture and waterlogged. Their salinity decreases upstream and varies seasonally according to river flushing (Dunsmore., et al., 1976). Soil occurring in the upper part of the inter-tidal zone comprises nearly ripe saline gleys and almost mature acidic sulfate soils. The vegetation cover ranges from mangrove and reed to sparse grass or reed-sedge family beyond the saline limit (Peat et al., 1979). Under natural conditions, the ripe and nearly ripe saline gleys have a $pH < 5.1$ within the typical profile but severe acidity

reducing pH ≤ 4 following drainage or drying, and thus, they can be regarded as potential acid sulfate soils (Dong-Jin et al., 2007).

The nearly ripe soils can be cultivated provided the farm operation does not expose the sulphidic materials close to the surface and maintains a high water table. Soils found on the flood plain and terraces opposite the tidal zone are subject to wet season flooding. The saline association of this group of soil comprises ripe clays with slightly salty subsoils and variable salinity in the topsoil. The ground is acidic, with pH values < 4 in the subsoil. They contain adequate levels of both calcium and magnesium, with magnesium frequently serving as the primary cation in the exchange complex (Dunsmore et al., 1976; Peat et al., 1979). However, high exchangeable sodium concentrations could cause toxicity issues that precede other factors.

The soils are strongly acidic to neutral to within more than s50 cm of the surface, with high base saturation (BS) of less than 90 % throughout, a predominance of Mg in the exchange complex in the order of Mg> Ca > K but with ESP < 20 (Dunsmore et al., 1976). These saline soils can be used for rice production, provided leaching and liming requirements are met. The no-saline group comprises ripe soils of heavy texture and moderately acid to calcareous profile. They are suitable for irrigated agriculture, provided they are protected from wet season flooding. These soils are also characterized as having a water table within 2 m of the surface at the end of the dry season and are thus susceptible to salinization (Dunsmore et al., 1976).

Regions characterized by elevated water tables encounter issues related to soil salinization due to heightened capillary rise and recharge from salty groundwater sources (Bates et al., 2008; Fall, 2017; Talat, 2020). The area is also utilized for rain-fed rice cultivation during the short rain that lasts 3 to 4 months following the long dry season. However, the re-emergence of saline conditions as the rains cease poses a challenge to rice cultivation in the area.

1.5.1 Organization of Thesis

The thesis is organized into six chapters. Chapter 1 gives the background, problem statement, justification, objectives, and study area description. Chapter 2 presents the literature review of the subject matter, and chapters 3 – 5 focus on specific objectives 1 – 3, respectively. Chapter 6 presents a general discussion, conclusion, and recommendation based on the study findings for policy and future research.

CHAPTER TWO
LITERATURE REVIEW

2.1 Impact of climate change on soil salinity

2.1.1 Climate change

According to WMO (2013), the world recorded the highest number of decadal extreme climate events from 2001 – 2010 since the advent of modern measurement in 1850. IPCC (2013) confidently stated that 1983 to 2012 was probably the warmest 30-year period in 800 years. It was also probably the most generous 30-year period over 1400 years. The decade ending 2010 records an unprecedented era of extreme climate events with evidence of heat waves in Humid regions (EU and Russia), drought in The Amazon Basin, Australia, West Africa, and East Africa, and severe storms like Tropical cyclone Nagris (2008) and Hurricane Katrina (2005).

Recent climate-related events, including heat wildfires, droughts, cyclones, waves, and floods, have impacted many human systems and shown how vulnerable some ecosystems are to present climatic variability (Bell et al., 2018). Lomborg (2020) reported 15,000 weather-related loss events from 1980 to 2016, most of which were storms and floods. Climate forecasts with the A1B emission scenario show a substantial rise in temperature from 0.9 to 1.4 ^{o}C by 2035 to 2.0 to 2.9 ^{o}C by 2060, with significantly drier summers (Fischer et al., 2013). The worldwide temperature variations in 2016 demonstrate that temperatures in several regions in 2016 were 1 to 5 °C higher than in 1961 to 1990 (Adesina et al., 2016).

Dynamic crop growth models were used to simulate how climate change might affect agricultural yields, and the results showed that productivity varied with temperature variations (Webber et al., 2018). The expected changes in rainfall trends by the 2050s are still being determined for large parts of the region. Climate models disagree on whether rainfall will increase or decrease. Models frequently exhibit strong trends in both directions, from -40% to +20% (Sylla et al., 2016). Despite this difference, more than 80% of climate models predict less precipitation for various regions of southern and northern Africa in the future (Bathiany et al., 2018; Rosenstock et al., 2019). In West African countries, the IPCC 5th AR predicts that temperature increases will likely produce particularly negative consequences for making cereals such as sorghum, millet, and rice (Jones et al., 2014; Belle et al., 2016). In 2016, the UNDP reported that a 2 °C could substantially impact African agriculture.

2.2 Soil Salinization

Globally, more than 1,000 million ha of land is affected by the twin problems of salinity and sodicity and waterlogging in lowland areas of arid and semi-arid regions (Shrivastava and Kumar, 2015; Qureshi et al., 2019). According to Basak et al. (2020), 19 million acres of land in sub-Saharan Africa are affected by soil salinization. These are mainly found in the countries of Eastern Africa, along the coast of Western Africa, countries in the Lake Chad Basin, and sections of Southern Africa (Tully et al., 2019; Qureshi et al., 2019).

Soil salinity is influenced by climate, and the topographic conditions of soil type, water quality, and depth of the groundwater level affect salinity build-up (Akça et al., 2020). Qureshi et al. (2019) identify rising sea levels, seawater intrusion into coastal lands, and rising groundwater levels due to inefficient drainage combined with poor irrigation and land management practices as the main drivers of salinity development. Akca et al. (2020) studied the distribution and variability of soil salinity at the Akyatan and Seyhan basins in Adana, the eastern Mediterranean part of Turkey. Their results showed that distributions of salt-affected soils corresponded to the high electrical conductivity of the groundwater.

Soil salinity affects the environment, agro-ecosystems, agricultural output, and sustainability due to the compound degradation dynamics of soil and water resources, which directly impact food security and livelihood, societal biophysical and socioeconomic base (Gebremeskel et al., 2018). Salinization can change habitats, resulting in considerable ecosystem changes, including migration or death of flora (Rahman et al., 2019).

In The Gambia, salinization is anticipated to cause mangrove stands to move into adjacent swamp-rice farming regions and the flooding of marginal croplands in tidal floodplains on lower estuary areas by tides (GoGT, 2016). Salinization reduces agricultural potentials through salt accumulation in the root zone, interfering with several plant functions, including the decreased germination rate, shoot, and root development, eventually resulting in low crop yield (Rahman et al., 2019).

A multifaceted array of alluvial and fluvial marine deposits exist in the floodplain of the Gambia River and its significant streams. These wetland ecosystems cover almost

20% of the total land area, comprising mangrove forests (64%), uncultivated swamps (7.8%), and cultivated swamps (3.2%) (Sienta et al., 2019) principally. Mangrove tidal swamplands boarded the tributaries and were within reach of wet-season freshwater floods during the 4-6 months of the year. The freshwater zone adjacent to the river is inundated by the daily tidal floods in reaches that have not been subject to saline water for more than ten months.

These lands are essential to the country's food basket, where salinization has forced many small-scale farmers to terminate rice cultivation. The dominant soil types are heavy clays with acid-sulfate conditions and are predominant in the Gambia River Basin floodplain and other lowlands. The combination of tidal brackish water, geography, climate, and soil-vegetation elements creates the salinity gradient in the marsh (Rahman et al., 2019).

The continual silt deposits from floods make the soils in the mangrove zone significantly more productive than those in other rice ecologies, such as the upland and interior valley irrigated marshes. During the dry season, these soils are enhanced by the daily deposit of silt from the ocean and microbial activity inside the root zone (Yang et al., 2020). However, changes in soil salinity due to land elevation, capillary rise, and evaporation from the shallow saline groundwater table are the critical factors affecting their micro-scale and farm-level management.

In the Gambia, the increasing prevalence of salinization affects the functionality and sustainability of land and water quality (rivers and groundwater), the reduction of biodiversity, lowland irrigated agriculture and livestock productivity. During the reduced streamflows, the wet rice ecozone was also severely stressed. Downstream river Gambia, the elevated saline concentrations of root-zone influence by several interrelated macro-climactic and edaphic factors made rice production a marginal option. Lower streamflows meant the swamp rice yields would decrease due to saline water inundation (Chakroff and DuBois, 1982; Njie and Corr, 2006).

The productivity of rice is controlled by natural mechanisms, and cropping season in the mangrove swamps is highly dependent on rainfall to leach out the extra salt concentration to non-harmful levels (Baggie et al., 2018; Yang et al., 2020). In addition, the spatial extent of the saline area increases over time due to a decrease in

freshwater inflow into the rivers from the upstream increase in high tidal water level (Mondal and Bhat, 2021).

Population growth, food security, and rural livelihood improvement remain challenging in the Gambia. Food insecurity is especially true for LRR and CRRS, which are regarded as the most vulnerable communities with widespread malnutrition records of over 10% and specific deficiency of vitamins C and A (Sienta et al., 2019). The government deployed several attempts to mitigate and adapt to salinity through projects and development programs. These include land development in the form of anti-salt intrusion dams, spillways, and dikes.

The introduction, dissemination, and adoption of salt-tolerant varieties develop through the collaboration of NARS with AfricaRice and other regional and international partners. At the farm level, salinity management relied mainly on the farmer's decision and ability to adopt adaptation practices such as bounding and incorporating organic residues and water management practices.

2.2.1 Modeling Approaches in Soil Salinity Studies

The modeling of solute movement in soil has gained growing importance as it aids in comprehending the dynamics of salt within the soil. Similarly, evaluating the effects of salt build-up and forecasting the behavior of soluble salts under diverse natural and management circumstances in crop cultivation is crucial for ensuring sustainable crop production (Li et al., 2013; Radanielson et al., 2018; González-Gómez et al., 2021). These modeling endeavors have also integrated plant reactions to salinity on a crop-specific basis, encompassing crops such as wheat, beans, tomatoes, and rice (Corwin et al., 2007; Webber et al., 2010; Mondal et al., 2015). Most of these models rely on empirical descriptions of salinity effects, offering simplicity and reliability in estimating yield losses (Mondal et al., 2015).

Li et al. (2017) reported that among rice models, ORYZA v3 stands out as a comprehensive representation of rice knowledge and is extensively used to explore rice production challenges and opportunities in diverse environmental conditions and regions (Li et al., 2013; Feng et al., 2017). This model has been employed for physiological analysis, spatial and temporal simulations, and management optimization in the rice-growing sector.

Mondal and Bhat (2021) applied the AquaCrop model to simulate rice yield responses to salinity in Gazipur, Bangladesh. They parameterized and validated the model using data from field experiments and local climate information. The model exhibited good performance, with simulations closely matching observed parameters, indicating its potential for predicting the impact of salinity and climate changes on rice crops.

Radanielson et al. (2018) enhanced rice models, specifically ORYZA v3 and APSIM, to evaluate osmotic stress on rice due to salinity. Their results demonstrated the models' ability to characterize rice biomass and yield under salt-affected conditions despite slightly overestimating crop yield under severe salinity. Kumar et al. (2014) assessed the efficacy of the SAWAP model in modeling salt dynamics and yield for several wheat cultivars under differing saline water irrigation regimes. Their findings showed that the model predicted salt dynamics in the crop root zone and relative wheat yields under saline conditions, particularly for salt-tolerant varieties.

Other modeling approaches, such as support vector regression and fuzzy logic, have also been used to estimate soil moisture and surface parameters (Saleh et al., 2006; Singh, 2005). Gupta et al. (2014) explored the potential of the radial basis function artificial neural network (RBFANN) model for estimating soil moisture on irregular surfaces using biostatic scatter meter data. The RBFANN model showed promise in estimating soil moisture, particularly at VV-polarization. Kasim et al. (2018) utilized remote sensing and statistical methods to establish Partial Least Squares Regression (PLSR) models for evaluating soil salinity based on remotely sensed data and field-measured salinity (EC_a). Their results indicated strong correlations between EC_a and various indices derived from satellite images, with the PLSR model-D performing exceptionally well predicting EC_a.

2.2.2 Mapping of Soil Salinity Using Remote Sensing

Remote sensing techniques, particularly multispectral satellite sensors, have emerged as valuable tools for assessing and mapping soil salinity (Fernandez-Buces et al., 2006; Fan et al., 2012). These methods, often combined with Geographic Information Systems (GIS), offer fast and reliable approaches for regional and global scale applications (Dewitte et al., 2012; Gorji et al., 2015). Remote sensing, including geostatistics and modeling, has proven effective in evaluating soil salinity, creating maps, and enabling continuous monitoring (Gorji et al., 2015).

One significant advantage of remote sensing is its ability to capture soil properties through reflectance measurements, such as particle size distribution, moisture content, organic matter composition, and surface conditions (Nanni & Demattê, 2006; Gorji et al., 2015). This capability enhances our understanding of the spatiotemporal variation in soil physicochemical properties. Abuelgasim et al. (2018) developed a soil salinity index and model utilizing Landsat 8 OLI imagery data, particularly near-infrared and shortwave infrared spectral information in non-agricultural desert arid and semi-arid areas. The model displayed outstanding precision in mapping, outperforming other models based on salinity indexes, achieving an impressive accuracy rate of 60%. It efficiently pinpointed regions with elevated salinity and highly saline soils.

Wei et al. (2020) adopted a mixed data approach, incorporating multiple Landsat OLI datasets, vegetation type, land use, and terrain factors. They used the Random Forest (RF) and Cubist algorithms to predict soil salinity, accounting for 78.19% and 78.42% of the variation, respectively. The models exhibited predictive solid performance, with reasonable accuracy metrics, indicating the effectiveness of both algorithms. However, the Cubist model outperformed the RF model regarding prediction accuracy.

2.2.3 Limitations of Mapping Soil Salinity

The utilization of remote sensing for soil salinity assessment faces several significant challenges. These limitations stem from the soil profile's spatial, temporal, and vertical variability (Allbed and Kumar, 2013). Spectral reflectance sensors employed in remote sensing can only capture information from the soil's surface, lacking the capacity to observe the entire soil profile (Engman, 1998; Schmugge et al., 2002; Negi et al., 2010). This poses difficulties in accurately measuring salt concentration, especially when it falls below 10-15% (Allbed and Kumar, 2013). Furthermore, when halophytic plants dominate the vegetation cover, relying on proxies like remotely sensed vegetation reflectance becomes less reliable (Allbed & Kumar, 2013). Distinguishing between barren and severely saline land can also be problematic using multispectral imagery. Fraser (2009) noted that Landsat's spectral resolution is inadequate for determining the difference between saline and waterlogged ground.

Despite these challenges, multispectral satellite sensors have recently been widely employed to assess and map soil salinity (Akbarzadeh and Mehrijardi, 2010). These

sensors encompass a range of systems, including Landsat Thematic Mapper (TM), Landsat Multispectral Scanner System (MSS), Landsat 7, Landsat 8, Landsat Enhanced Thematic Mapper (ETM), Spot, Advanced Spaceborne Thematic Emission and Reflectance Radiometer (ASTER), IKONOS, MODIS, and IRS (Gorji et al., 2015). Due to their affordability and ability to detect prominent surface indicators of salt, multispectral satellite sensors are the favored option for monitoring and mapping soil salinity (Allbed and Kumar, 2013; Gorji et al., 2015). However, they must work on discerning salt concentrations within the soil profile and distinguishing between saline and waterlogged areas (Allbed and Kumar, 2013; Fraser, 2009).

Conversely, hyperspectral imagery, characterized by its greater spatial and spectral resolutions, provides enhanced detailed soil salinity mapping capabilities. Hyperspectral modeling has proven to be effective in this context. Nevertheless, the limited accessibility of hyperspectral satellite imagery constrains its extensive utilization for salinity mapping (Kumar et al., 2020).

2.3 Agricultural Production

Recent climate trends indicated adverse effects on global yield levels of the six most widely grown crops (sorghum, maize, soybeans, barley, wheat, and rice) (Lobell and Field, 2007). Guo., et al. (2021) identified north of 30 °N and included southwestern Europe, Eastern Europe, Central Asia, and West Asia as major high-risk rice drought areas. Maize and beans growing areas are estimated to experience 12–40% yield reductions by the 2050s.

Rippke et al. (2016) reported that Africa's two staple crops, beans and maize, are anticipated to decline. The climate suitability of most significant crops is also projected to shift as climate warms (Zabel et al., 2014; Rippke et al., 2016). Wheat, rice, maize, and soybean are the four essential crops capable of attaining global food security. These crops account for 85% of the world's cereal exports. This has resulted in adverse effects on significant crops across Africa, with regional yield variability estimates of a 19% reduction in maize yield and 68% in bean yields.

Maize yields in southern Africa are expected to fall by 18% on average, with the total crop output falling by as much as 30% (Schlenker and Lobell, 2010; Zinyengere et al., 2014). According to Lal (2017), crop reaction to rising temperatures can affect grain

output by up to 10% in rice for every 1oC increase in night-time temperature. Furthermore, vegetables are relatively sensitive to high temperatures.

Several conflicting precipitation projections concern the severity, timing, and geographical dissemination of future wetting and drying in Africa (Hoerling et al., 2010; Biasutti et al., 2019). Projections for precipitation are complex partly due to gaps in observed historical climate data and high variability at the local level across the continent (Rosenstock et al., 2019). For example, under a higher emission scenario (RCP 8.5), a median of the CMIP5 models indicates that by 2050, annual precipitation will rise in much of eastern and central Africa while falling in southern, western, and northern Africa (Sillmann et al., 2013; Rippke et al., 2016; Rosenstock et al., 2019). Overall agricultural production changes in West Africa are similarly predicted to be regional, with median yield losses of -11 % by the end of the 21st century (Roudier et al., 2011).

Global model results within the context of IPCC AR5 over West Africa show a significant increase and decrease in rainfall. As a result, the yield of several critical crops and animals is expected to fall, threatening food security (Solomon et al., 2007). Reduced crop-growing seasons will likely result in a shift from mixed-crop-livestock production systems to systems that are dominated by livestock (Thornton, 2010). This change will probably occur in transition zones in the West African Sahel and midaltitude regions of eastern and southern Africa by 2050 (Gebreyes et al., 2017). The increased occurrence of extreme temperatures is probably to surpass the comfort threshold of livestock, reducing feed intake (Gebreyes et al., 2017) and with the possibility of an increase in diseases and pests in the future to adding extra limitations on livestock production (IPCC, 2014).

Reduced growing season duration and a rise in the chance of failed seasons will almost certainly be an essential aspect of future climate. As a result, agricultural production systems face increased strain and have a significant negative impact (Thornton 2010). In Mali, Lacy et al. (2006) found a propensity for farmers to switch some of their sorghum production to a variety with a shorter cycle than the conventional one due to the shortening of the rainy season. Nielsen and Reenberg (2010) reported that the amount of rain-fed grain produced in Burkina Faso is decreasing due to climate change and the country's reliance on migration, livestock, small-scale trade, and gardening.

Seasonal rainfall patterns significantly impacted the productivity of rain-fed agricultural production in the Gambia. Notably, due to a shortened rainy season, it continues to have a very harmful duction of rice, maize, and groundnuts (Sienta et al., 2019). For example, based on estimates of historical annual precipitation minimum and maximum temperatures, Sonko et al. (2019) noted decreasing patterns in the cultivation of two primary cereal crops, which they attributed to fluctuations in rainfall. They reported an estimated decrease in maize yield of 19% and a substantial reduction in rice yield, possibly reaching as high as 50%, covering the period from 1987 to 2016 within the Lower River. These changes in production are reflected in the cereal supply/demand equilibrium for the 2021 marketing year for sub-Saharan African countries.

Domestic production in these countries shows a negative trend against increasing food utilization, mainly dependent on high import requirements (FAO, 2020). Food security challenges remain high on the agenda for governments, international and national development agencies, and professionals to confront the negative impact of climate change on livelihood and help farmers adapt (Shackleton et al., 2015).

2.3.1 Vulnerability of Agriculture to climate change

In Sub-Saharan Africa (SSA), agriculture faces significant vulnerability to climate change due to its heavy dependence on rainfed crop production and the region's susceptibility to climate hazards (Kamali et al., 2018). This vulnerability results from exposure, sensitivity, and limited adaptive capacity. Exposure represents the degree to which the agricultural system is exposed to climate hazards, sensitivity reflects how sensitive the system is to changes in climate, and adaptive capacity signifies the ability to respond and adapt to these changes (IPCC, 2014).

The dependence on rainfed agriculture in SSA makes the region highly vulnerable to the inherent rainfall variability. Approximately 90% of SSA relies on rainfall for food production, with over 79% of the population depending on agriculture for their livelihoods. Climate change introduces additional stressors, including increased temperatures, extreme weather events, and changes in precipitation patterns, all of which impact crop yields and food security (Morgan, 2011).

Climate variability, characterized by unpredictable rainfall patterns, poses a significant challenge to agriculture in SSA. Droughts and floods are frequent, leading to crop loss and yield instability and making certain regions less appropriate for traditional crops (Bhavnani et al., 2008). The scheduling of agricultural activities, such as planting and harvesting, becomes uncertain, affecting crop management practices and food production. Poverty exacerbates vulnerability, limiting the capacity of communities to cope with these climate-related challenges (Shiferaw et al., 2014).

Unsustainable land use and resource management practices further contribute to vulnerability. Smallholder farmers in degraded areas are particularly at risk, with limited resources and exposure to multiple risks (Shiferaw et al., 2014). Changes in land use and policies, along with unstable commodity prices, reduce adaptive capacity and hinder efforts to mitigate climate-induced challenges (Morton, 2007). Alterations in temperature and precipitation directly impact food production and security in Sub-Saharan Africa (SSA). Rainfed crop cultivation, widespread in this area, becomes highly susceptible to even minor fluctuations in climate conditions (Bathiany et al., 2018). Increasing temperatures, rainfall shifts, and weather variability exacerbate smallholder farmers' challenges (Sivakumar et al., 2014).

Rainfall variability, in particular, significantly impacts food production and livelihoods. Droughts and floods account for a substantial portion of loss of life and economic losses in SSA (Bhavnani et al., 2008). Changes in rainfall patterns lead to alterations in the timing of the growing season, affecting agricultural decisions, input use, and crop management practices (Rosenstock et al., 2019).

Various studies have explored agricultural vulnerability to climate change using different approaches, including socioeconomic, biophysical, and integrated assessments (Kamali et al., 2018). These studies emphasize that new agricultural investment alternatives, legislative reforms, and institutional innovations are required to manage climate risks effectively. However, the inability to compare data from various researchers is hindered by the need for standardized assessment criteria or indicator systems (Wilhelmi and Wilhite, 2002).

2.3.2 Model Application in Agriculture and Climate Change

Understanding the impact of climate change on agriculture is a complex task, partly due to the variability in climate modeling projections (Jones et al., 2014). While controlled field experiments provide valuable data for calibrating crop models, their availability is limited due to resource constraints and inconsistent results stemming from various factors (Hunt and Boote, 1998; Kephe et al., 2021).

Researchers gain insights into how crops respond physiologically to environmental variables in controlled environments, but translating these findings into real-world simulations remains challenging. This is because crop growth is influenced by numerous complex factors, including weather events, soil conditions, water stress, and localized climate variations (Lamichhane et al., 2018; Liliane and Charles, 2020; Nkurunziza et al., 2020).

Crop models are crucial in assessing climate change's impact on agriculture, especially when conducting extensive scale assessments. These models, taking into account factors such as weather conditions, soil composition, genetic makeup, and management practices, can replicate the growth of crops, the dynamics of soil moisture, and nutrient-related processes on a daily or even more frequent basis, offering different levels of precision (Webber et al., 2010; Adesina et al., 2016).

One of the primary applications of crop models is exploring adaptation approaches to mitigate climate-related challenges in agriculture. They enable the evaluation of various management approaches for their effectiveness in addressing climate impacts (Beveridge et al., 2018; Corbeels et al., 2018; Peng et al., 2020). These models are broadly categorized into statistical and process models, offering insights into how crops respond to environmental conditions (Lambin et al., 2000; Jones et al., 2017; Peng et al., 2020).

2.4 The climate of The Gambia

2.4.1 Rainfall

The climate in West Africa is significantly influenced by the interface between the Inter-Tropical Convergence Zone (ITCZ) and the West African Monsoon (WAM). This climate is characterized by alternating wet and dry periods, and in some areas, two wet seasons are driven by the movements of the ITCZ and WAM. Oceanic

moisture transfer is governed by trade winds in the southern hemisphere and the ITCZ's low-pressure corridor, which moves northward as temperatures increase at the beginning of summer. This movement creates conditions favorable for rainfall.

The Gambia, located in the Sudan-bioclimatic zone driven by the WAM, experiences its rainy season from June to November, with most precipitation between July and September. The rain is often associated with squall lines and systems from the Ethiopian Highlands and influenced by the Indian monsoon's sub-tropical jet stream. These systems form hurricanes in the Atlantic Ocean (Giannini et al., 2001).

Variability in tropical sea surface temperatures in different ocean basins, including the El Niño/Southern Oscillation (ENSO), is a crucial factor influencing inter-annual rainfall variations in The Gambia. Changes in the high-pressure regions that control the weather system can lead to deviations from standard rainfall patterns, resulting in either insufficient or excess rainfall in the country (Gianini et al., 2001).

Climate-related studies conducted in The Gambia's Second National Communication (SNC) and Third National Communication (TNC) under the UNFCCC have analyzed temperature, precipitation, and evapotranspiration trends. This research produced an ensemble time series up to 2100 at decade intervals using three global circulation models (GCMs), CCC199, BMRC98, and GDFL90, with different radiative forcing. Using these models, projections for annual rainfall in The Gambia indicated a decreasing trend ranging from less than 1 % in 2020 to approximately 54 % by 2100 under the warm climate change scenario of MBRC98. Meanwhile, the estimate from CCM199 did not significantly differ from the current inter-annual rainfall variability, suggesting only a 2% reduction in rainfall by 2100 (McConnell & Jallow, 2022).

The annual rainfall pattern gradually declines from around 1,000 mm in the South and Southeast to 700 mm in the northernmost part of the country. However, considering the substantial variability in rainfall projections from different models, the possibility of a reverse climatological trend cannot be ruled out (GoTG, 2016). Regional climate models (RCMs) with complex orographic characteristics, according to predictions made by Sylla et al. (2016), may affect the direction of rainfall change. Additionally, research by Sanogo (2015) using climate simulations from HadGEM2 has shown an indication of optimistic trends in annual precipitation totals in most Sahel stations,

where yearly precipitation variability is significantly influenced by sea and land-surface interactions with the atmospheric boundary layer (Wei et al. 2014; Sanogo et al., 2015).

2.4.2 Temperature

Projections for temperature using GCMs indicate a warming trend in all parts of the country, with an estimated increase from 2000 by an annual mean increment of 1.7 to 2.1 ºC in 2050 and by 3.1 to 3.9 ºC in 2100 (McConnell & Jallow, 2022). Results of CCCM199 and GFDL90 estimated more substantial warming in the winter compared to the summer months (June, August, and September) over the following decades. During the dry season, average temperatures range between 18°C and 30°C and between 23°C and 33°C during the rainy season. The fastest and most significant increase in temperature was produced by BMRC98, indicating more substantial warming in the summer months.

The ocean and vast stretches of swamp/wetland have a role in regulating summertime temperatures, which can range from 13 ºC to 43 ºC. These have a similar moderating effect on winter temperatures ranging from 13 °C to 37 °C. Jenoi (Lower River Region) had the lowest daily temperature of 4 °C in 2003 and the maximum day temperature of 49.0 °C in 2001 (Barry et al., 2018). The combined effects of interplanetary, landscape, and pluviometric factors govern the spatial distribution of temperature. The distribution pattern generally exhibits an increasing temperature gradient landwards from the coastline. Routine observation also indicates an increase in minimum temperatures at a constant rate of 0.4 to 0.67 °C per decade across the country since 1950 (GOTG, 2012). During the dry season, the relative humidity is around 68% near the coast, 41% inland, and often exceeds 70% throughout the country during the rainy seasons.

Seasonal Northeast trade winds, commonly referred to as "Harmattan," are famous for their cold effect and have an associated impact on atmospheric circulations. Substantial quantities of dust are picked up from the boundaries of the Sahara Desert. The sunshine hours during the dry season drift around 8 hours a day, falling abruptly to around 6 hours during the summer (Barry et al., 2018). Average ultraviolet (UV) indices are much higher (UV index = 12) between February and September and significantly lower (UV index = 9) around December.

2.4.3 Potential evapotranspiration (PET)

GFDL90 and BMRC98 simulations predict that PET will rise to 2% and 45% over historical levels annually (GOTG, 2012). Verkerk and van Rens (2005) projected PET based on Thornthwaite's methods, involving calibrated 24 years of observational data with an error estimate of 4% indicating PET at 2,400 mm. All scenarios projected estimated PET to be between 1,460 mm and 2,260 mm/year by 2050. Van Vuuren et al. (2011) projected sea level rise between 19 cm and 43 cm in The Gambia by 2050. Church et al. (2013) reported similar findings that estimate mean sea level changes generated from a process-based model under different greenhouse gas concentration scenarios.

In the coastal region of the Gambia, estimates of mean sea levels are expected to be within 20% of the worldwide mean sea level increase of 26 cm to 98 cm by 2100. However, the usage restrictions and uncertainties associated with these estimations are primarily due to our lack of a thorough knowledge of the underlying biophysical processes. In addition, because of their unpredictability, rainfall estimates may need a sensitivity analysis in contrast to temperature changes.

2.5 Soil and Water Resources of The Gambia

Good agricultural land has been a limited factor of production in The Gambia since post-World War II. Long-term agricultural processes have resulted in land use patterns characterized by upland fields in a rainfed or dry ecology for producing coarse grains, legumes, and oils seeds and the lowland fields in a riverain plain or wet swamp ecology typically for rice production. The twin problems of desertification and salinity confront the land resources. Frequent drought magnified by unsustainable farming practices and degradation of native vegetation in the upland rainfed crop production areas, soil salinity, and acidification of the lowland riverain agricultural are threats to land resources. The nation is primarily lowland with four important topographic landscapes that correlate to diverse soil types: the floodplain, colluvial slope, lower plateau, and upper plateau (Mcconnell & Jallow, 2022).

2.5.1 Upland Sandy Soils

The Continental terminal soils found in the uplands are made from the weathering products of the continental terminal acid complex parent material. The soils are well drained with low chemical fertility and cation exchange capacity (CEC) and have a

hard-to-tough consistency when dry. Most soils are ferralitic and ferruginous weathered tropical soils with medium to high base saturation, low cation exchange capacity, low intrinsic fertility, strong textures, and poorly formed structures (Silliman and James, 1980).

Short-duration rains, low inherent fertility, and poor water-holding capacity have significantly reduced the productivity of upland soils (FAO, 1997). Insufficient soil management practices additionally contributed to their impoverishment and loss of fertility. Consequently, obtaining accurate data on local soil classification through an updated soil map is required. This will enable the implementation of appropriate soil cultivation practices tailored to each soil type. Furthermore, promoting structural development by encouraging the widespread use of organic matter in soil management is essential.

2.5.2 Alluvial soil

Alluvial soil, deposited by the River Gambia and its tributaries, is often affected by temporary or permanent wet conditions. It covers around 30% of The Gambia, with the extent decreasing gradually from west to east, roughly corresponding to the limit of salty water incursion in the Gambia River during the dry season (Peat et al., 1979). These alluvial soils are typically hydromorphic, containing over 80% silt and clay throughout the profile, and they can also be saline due to inundation by salty water during high tide.

Mangrove species often colonize them, although some higher-lying areas remain unflooded by the tide and are devoid of vegetation, known as barren flats. These soils are primarily young, forming on recent fluvio-marine sediments. Within the mangrove area, a variety of soil conditions can be found. The river terrace consists of flat, low-lying extensions of the valley floor, featuring a complex network of temporary and permanent drainage depressions. These areas are periodically inundated and support sparse grassland vegetation, including halophytic species.

Clayey soils in upland depressions are suitable for rain-fed rice, while colluvial slopes and similar soils are ideal for rainfed crops like groundnut, upland cereals, and other fields. These inferior grey and ochre-brown upland soils are extensively used, and more intensive cultivation methods will, therefore, be increasingly required to increase

their productivity. Between the river swamps and upland are transitional lands comprising colluvial and alluvial soils suitable for irrigated crop production and as pasture land for livestock.

The transitional zone between the wetland and upland is inundated only during the season of high river flows, which are bunded to capture direct rainfall and runoffs from the uplands. These soils are prone to several climate-induced limiting factors, notably salinization and acidification. Progressive reduction in arable lowland for rice production due to climate-induced changes in precipitation and temperature and increased evapotranspiration, creating drier soil conditions and increasing soil salinity, is a significant threat to food security. These have an enormous socioeconomic impact on rural communities depending on subsistence rice-based production systems in tidal irrigated mangrove swamps.

2.5.3 Hydrology of the Gambia River Basin

Three significant West African rivers originating in Guinea's Futa Djalon constitute the Gambia River basin, including the Gambia River (Webb, 1992; Carney, 2017). The Gambia basin, which includes the nations of Guinea, Senegal, and The Gambia, stretches from 11° 22 North to 14° 40 North in latitude and from 11° 13 West to 16° 42 West (Banjul, mouth) in longitude (Carney, 2017). Three countries—Guinea, Senegal, and Gambia—share the roughly 77,100 km^2 region of the Gambia Basin. The Gambia Basin is located in the isohyet band 1700-700 mm. The marine section is below the isohyet 1000 mm. North of this isohyet, the river's contributions regarding water balance are meager and almost insignificant. The river system comprises the River Gambia, related freshwater and estuarine ecosystems, and marine and coastal zones along the western coast.

Within The Gambia, there are no notable tributaries; the majority of the wet season flow comes from Guinea, with substantial contributions from Senegal and minimal input from The Gambia itself. Similar to numerous river basins in West Africa, the Gambia River basin is anticipated to undergo transformations driven primarily by climate-related factors, alongside other elements like alterations in land use, human activities, and hydraulic infrastructure developments (Mbaye et al., 2020). Bodian et al. (2018) underlined a decrease in river discharge over The Gambia and the upper Senegal basins. According to Stanzel et al. (2018), there is a projected significant

decrease of over -10% in runoff for Senegal, Gambia, and Guinea-Bissau, while substantial increases of more than +10% are expected in the region bordering Liberia and Côte d'Ivoire. Similarly, Mbaye et al. (2020) found possible streamflow and soil moisture decreases over the Senegal River Basin.

On the other hand, findings from Stanzel et al. (2018) suggested that in a significant portion of West Africa, the anticipated effects of climate change do not lead to a considerable reduction in river discharge. However, there is a notable forecasted decrease in release for northern, eastern, and western regions of Africa, alongside a prominent increase in the southwest. The authors stated that the prediction model ensemble had a margin of error of approximately ± 50%. Nonetheless, their study's outcomes revealed that employing a substantial ensemble of climate models introduces significant uncertainty in the projections. However, it also highlights regions with considerable agreement among the results of various models. Prior research has shown a comparable pattern. However, most of these studies primarily examine individual river basins using climate change projections from Global Climate Models (GCMs) characterized by coarse spatial resolution or early iterations of dynamical downscaling with Regional Climate Models. (RCMs) (Roudier et al., 2014; Oyerinde et al.; 2016; Yira et al., 2017).

Most streams that feed The Gambia Basin have a tropical climate with lengthy, dry, and short rainy seasons. It is mainly in the Sudano-Guinean zone (Njie and Corr, 2006). From June to late October, the salt front is forced towards Banjul by heavy flows during and after the rainy season and then rises back up the river eastward by 32 - 60 km, depending on the surface area of the farmed tidal marsh from November to June (Verkerk and van Rens, 2005; Njie and Corr, 2006). Similarly, Mbaye et al. (2020) observed a decline in flow rate at both gauging stations throughout the peak flow season.

During the dry season in the Gambia River, spanning from kilometers 110 to 180, the freshwater flow remains relatively stable. Still, its presence is seasonal and influenced by rainfall in the broader watershed, extending from Guinea downstream. The river lowers barely one meter in gradient throughout the remaining 500 km to the sea from The Gambia's easternmost extremity to the river's mouth at Banjul. Due to the

extraordinarily flat nature of the river, tidal movements from the Atlantic Ocean are conveyed up the river as far as between Kaur and Kuntaur.

The upstream hydrological degradation has resulted in a reduced amount of freshwater flow toward the coastal estuaries of the Gambia River basin. Erosion and siltation in the Gambia River have diminished water flow and heightened saltwater intrusion into peripheral areas. Siltation and sedimentation persistently erode the feature agricultural feasibility and long-term prospects (National Rice Development Strategy (NRDS), 2014). This seriously affects the agricultural production systems of the country to meet the prerequisite demand for water and food under varying climate scenarios.

The significant uncertainty of the functionality of The Gambia River basin is the development of Sambangalo, a hydroelectrical dam. Such major engineering works planned for the River Gambia basin are projected to impact water resource regimes differently in the basins across the region, according to the Gambia River Basin Hydraulic Master Plan published in 1999 by The Gambia River Basin Development Organisation (OMVG). The project will impact the physical environment, the various water uses and demands, and socio-environmental (Verkerk and van Rens, 2005). These impacts are linked to the modification of water balance in the Senegalese and Gambian basins, loss of soil and vegetation, modification of topography and physicochemical characteristics of water, and erosion of segments of river banks.

Degradation of water quality in the reservoir and loss of biodiversity for aquatic fauna upstream of the dam will result in more significant saline intrusion, especially during the dry season in The Gambian reach, with irreversible consequences (OMVG, 2014). For example, Verkerk and van Rens (2005) projected salinity intrusion in river Gambia using the 1-D numerical model SALNST for three projected dam release scenarios. The study aims to keep saline intrusion downstream of Kilometre point (KP) 170 derived from the Gambia River Basin Hydraulic Master Plan.

The result of the study indicated that under scenario A, the maximum salt front would be between KP190 and KP243 and between KP176 and KP230 under scenario B, subjective to rainfall and the total area of tidal swamp cultivated. The results further indicated that combining all scenarios and accounting for future precipitation and evaporation shows that the salt front cannot be kept downstream of KP170. Similarly,

Mbaye et al. (2020) reported that these activities would likely significantly impact the availability of water resources and the river over the Faleme River basin in Senegal.

2.5.4 Agricultural Production in The Gambia

The Gambia's economy relies heavily on agriculture, contributing approximately 24-32% of the country's GDP and generating 30-40% of foreign exchange earnings (Mungai et al., 2019; Sienta et al., 2019). This sector provides employment and income for at least 75-80% of the rural population, significantly contributing to food security and nutrition (GBOS, 2017; Sienta et al., 2019; Mungai et al., 2019; Gibba and Jallow., 2020). With an estimated 69,100 farm households engaging in subsistence crop production and traditional livestock rearing, The Gambia's agriculture sector faces challenges related to underutilized irrigation potential (GoTG, 2012; Mungai et al., 2019).

Agricultural output in The Gambia can satisfy only half of the nation's domestic consumption requirements, resulting in importing about 50% of its essential agrarian products, including rice (Sienta et al., 2019). For instance, imported milled rice amounted to US$35.7 million in 2016, accounting for 3.7% of the GDP (FAO 2019). The agriculture sector primarily relies on small-scale subsistence rain-fed crop production, which is heavily dependent on a single rainy season from June to October (Sienta et al., 2019).

The country's arable land is approximately 188,000 hectares, with less than 2,000 hectares under irrigation (FAO/AQUASTAT, 2014; GoTG, 2016). Cereal crops, including rice, early and late millet, sorghum, and maize, occupy about 51.6% of the cultivated area. In contrast, cash crops such as groundnut, sesame, and other grains and oilseeds occupy the remaining 48.4%. Horticultural production, engaging over 65% of the agricultural labor force, significantly contributes to rural income. Groundnut is the most extensively produced cash crop, covering about 44 % of the cultivated area and generating 60-80% of income for many farm households. In 2017, the total groundnut harvest was estimated at 405,200 hectares, with a gross production value of $100.8 million US (FAOSTAT, 2019).

However, low soil fertility and increasingly drier climatic conditions in the form of decreased rainfall and increased evapotranspiration significantly influence the production of upland crops, especially groundnuts. Other problems, including

inadequate water supply and low plant-available nitrogen and phosphorus, contribute to yield levels 20-50% below their potential (Ceesay, 2004).

The agriculture sector in The Gambia is highly vulnerable to rainfall variability, with yields varying by as much as 100% from year to year based on rainfall patterns (GoTG, 2016). Over the years, crop yields have experienced declines, including a 36% decrease in rice yields, a 26% decrease in maize yields, a 17.7% decrease in millet yields, and an 8.7% decrease in groundnut yields between 2010 and 2016 (Mungai et al., 2019). These declines are attributed to reductions in rainfall, limited adoption of improved technologies, and widespread soil degradation (GOTG, 2003).

The Gambia's rice yields, for example, are only 35.6% of the average rice yield for West Africa, underscoring the sector's challenges (FAOSTAT, 2019). Soil fertility decline, inadequate crop responses to fertilizers, and increased soil salinity contribute to declining yields (Mungai et al., 2019). Agriculture is vulnerable to weather-related extremes and grown salinization in lowland rice-producing areas, reducing food production (GOTG, 2013).

Climate change projections, including increased drought frequency, pose additional uncertainties for crop production in The Gambia, except for developing suitable irrigation technologies and climate-focused agricultural interventions (GoTG, 2016). Despite these challenges, the agriculture sector has the potential to achieve food self-sufficiency and reduce poverty among a significant portion of the population (GoTG, 2016).

Realizing this potential requires addressing constraints through policy frameworks transforming agriculture from subsistence to commercially oriented production systems. Improvements in agricultural value chains, the development of social capital, more efficient extension services, stronger research-farmer-extension linkages, and the adoption of improved farming practices such as integrated soil fertility management and sustainable natural resources management are crucial to enhancing the sector's productivity and resilience (Mungai et al., 2019).

2.5.5 Rice Production in The Gambia

Rice is the staple food and the most important agricultural commodity in The Gambia, particularly in national development strategies (Mungai et al., 2019). The National Poverty Reduction Strategy Paper (2007-2011) identified rice as the primary food crop in the drive to attain food security (NRDS 2014). The projected national rice demand for 2024 in The Gambia was estimated to be 273,800 tonnes based on population census, per capita rice consumption, national need, and population growth rate (NRDS 2014). However, the country's crop sector meets only half of the need for basic staples, leading to increased reliance on imported rice and persistent food insecurity (Mungai et al., 2019). The drop in national rice production substantially impacted the rural population, reduced income and savings, and further exacerbated food security (NRDS 2014).

Different approaches have been used to characterize rice production zones in West Africa, primarily based on climatic or agroecological zones and edaphic features. For example, Balasubramanian et al. (2007) differentiated rice-growing agroecological zones across SSA into four (3) groups based on the growing period's length. These agroecological zones include the Sahel, which has an increasing duration of 65-90 days and is classified as arid and semi-arid. The dry savanna has a growing time of 90-180 days, the wet savanna has an increasing period of 180-270 days, corresponding to the sub-humid zone, and the forest has a growing period of more than 270 days, referred to as the humid zone.

Rice production systems comprise diverse ecologies of uplands, rainfed lowlands, irrigated lowlands, deep water, and mangroves (Balasubramanian et al., 2007). Niang et al. (2017) distinguish rice production based on climatic zones into arid, semi-arid, and humid areas across 14 West African countries. Rice is cultivated as a sole crop across all agroecologies (AEZs), including upland, rainfed hydromorphic soils, and seasonal saline mangrove swamps ecology in The Gambia (Ceesay, 2004). Rice production in the upland ecosystem is done in free-draining soil, entirely dependent on rainfall, with a water table permanently below the plant's root zone. In this rice-growing ecology, drought, caused by erratic and insufficient rainfall, leads to a shorter growing season. Additionally, limited utilization of mineral and organic fertilizers within a context characterized by declining soil fertility, pests, diseases, and weeds are

identified as significant production challenges (Manneh, 2004; Ceesay, 2004; Mungai et al., 2019).

Because of the variable nature of rainfall, upland rainfed systems have more significant production risk factors (Ceesay 2004). The rice self-sufficiency ratio was unaffected despite considerable increases in planted acreage and production throughout the 2001/02 to 2010/11 decade. The growth in developed areas can be attributed to the expansion of upland rice farming, which was made possible by introducing NERICA rice varieties (NRDS, 2014). The introduction of suitable rice varieties by the National Agricultural Research Institute (NARI) under the sub-regional NERICA Project supported by the Africa Rice Initiative (ARI) of Africa Rice Centre launched in 2004 has revived the production potential of the upland rice ecosystem in West Africa. Similar efforts to save rice production include the Taiwanese Mission's recently terminated four-year Upland Rice Expansion Project.

An upland rice expansion program to cultivate 8000 hectares each year for four years, with a projected output of up to 32,000 metric tonnes of paddy rice, was implemented as part of coordinated efforts to close the gap between domestic supply and demand. These endeavors reflected a progress yield increase to 1,400 in 2007 and a peak upland cultivation of 50,000 ha by 2013 (NRDS, 2014). Lowland rice cultivation for local consumption in The Gambia dates back to the pre-colonial era. The flat topography of the Gambia River Basin offers the country the advantage of developing more tidal swamps with much less expanse for irrigation through dependence on the gravitational flow of river floodplains (Webb, 1992). The Gambia River Basin also allows for more tidal irrigation schemes in the lowlands. Irrigated rice is generally produced in bunded paddy fields with tidal/pump irrigation, allowing for more than one crop per year in the river's freshwater zones, offering a reasonable security measure against erratic local rainfalls.

The swamp rice agriculture system inside the mangrove ecosystem's tidal wetlands provides approximately 10% of the total domestic rice output in West Africa (Adefurin and Zwart, 2017; Yang et al., 2020). Over the past 30 years, rice production in the lowland ecology, including mangrove swamps, comprises a significant fraction of rice production, accounting for about 52% of rice-growing ecologies in the Gambia (Manneh, 2004; Ceesay, 2011). Rice production occurs in three ecologies in the tidal

swamps: tidal mangrove swamps, tidal freshwater swamps, and pump-irrigated freshwater swamps. Water-controlled irrigation includes two sub-systems: pump irrigation and tidal irrigation.

The former is located in the alluvial levees and sloughs, which generally remain beyond the reach of tidal flooding. This technology is mainly found in the middle and Upper River regions. Tidal irrigation, in contrast, consists of controlling the tidal waves of the river water utilizing earthen dykes, with gates and conveyance distribution networks in low, riverine areas which are generally flooded by the tide. According to the National Agricultural Sample Survey (NASS) report (2013), the country has an estimated 216,121 ha of lowland ecologies suitable for rice production, of which 17,434 ha lowland with only 2332 ha irrigated area under rice production in 2013. These figures indicated an untapped lowland potential of 196,355 ha for rice production.

Lowland paddy rice production increased steadily from 5,000 tonnes in 2006 to a peak of around 17,500 tones in 2010, dipped to 12,500 tonnes in 2010, and soared to around 18,000 tones in 2013, whereas the corresponding yield per hectare fluctuated somewhat (NRDS, 2014; GoGT, 2020). Lowland ecologies have more potential for rice production, with irrigated rice yields between 2–4 metric tons per hectare (Segnon et al., 2020). Similarly, rice yields are expected to remain constant in lowland ecologies, provided crop cycle water demands are not well appraised or adoption of climate coping strategies and sustainable management of degraded land by soil salinity or acidification (NRDS, 2014). Increasing vegetable production and swamp rice yields depend on increased river flows to push back the salt tongue for a substantial increase in swamp rice cultivation, particularly in the Middle Eastern half-country. Salinity is a significant abiotic stress, devastating rice production in saline soils, including the mangrove ecology (Yang et al., 2020).

The mangrove soils in the Gambia are anaerobic and heavily impregnated with iron sulfates. Manneh et al. (2004) reported that low-temperature stress usually occurs in the irrigated lowland when rice is grown during the relatively cooler months from November to March in the dry season, adversely affecting yield. However, the author indicated that low soil fertility is rice's most widespread and endemic problem. In addition to these meteorological and edaphic characteristics and the production

systems, agricultural practices also impact farmers' rice yields. These practices are controlled by the farmers' resource endowment, which influences the production orientation, cropping intensity, and input utilization (Angulo et al., 2012).

Regional research efforts in rice varietal screening and selection for adaptability and yield in the mangrove ecologies and agronomic practices and subsequent dissemination of results are headed by NARI in collaboration with AfricaRice and International Rice Research Institute (IRRI) (NRDS, 2014). The newly developed Rice Sector Development Hubs provide a promising source of innovative technology, such as high-yielding and adaptable rice varieties.

2.6 Sustainability of Natural Resources, Climate Change, and Food Security Nexus

Natural resources, soil, water, vegetation, and the weather form the essence of all kinds of life and support its varied activities. Rapid growth in the global population over the last century has increased pressure on limited and fragile land resources. It leads to unsustainable resource exploitation and environmental degradation (Coser et al., 2020). Global food security and sustainability of the food system might be threatened due to the increasing pressure on natural resources and climate change (Sivakumar, 2017; FAO, 2015). Shrinking natural resources based on land and water, declining quality of water resources, and environmental degradation issues imply increased threats to our ability to meet the basic needs of the growing population. Conijn et al. (2018) state that current approximations predict global food demand will double within three decades. Therefore, meeting societal food needs is a worldwide challenge (Berners-Lee et al., 2018).

Food security is a persistent global challenge influenced by various factors, including land degradation, diminishing freshwater resources, population growth, insufficient agricultural infrastructure, and adverse climate conditions (Shepherd et al., 2016). The combination of environmental degradation and the effects of climate change poses dual challenges to the sustainability of natural resources essential for agricultural production and food security. Soil losses from global cropland are currently occurring at a rate of over 6-ton ha/year, 15 times the average loss rate of 0.4-ton ha/ year over the earth's geological history (Shepherd et al., 2016). Agricultural land formerly productive has been lost to urbanization and other human uses, as well as to

desertification, salinity, soil erosion, and other consequences of unsustainable land management (Anwar, 2013). Land use and land cover change (LULC) are critical due to their significant influence on global warming, loss of biodiversity, and impact on human life (Anwar, 2013).

LULC has reduced the ability of the land to provide ecosystem services globally (Pontius and Petrova, 2010; Coser et al., 2020). LULCs are critical drivers of anthropogenic environmental changes through the expansion of agriculture, urbanization, and industrial development (Liu et al., 2017). Furthermore, land management methods and land use intensity alter the mix of ecosystem functions and services (Petz, 2014).

The IPCC (2013) reported with high confidence that many semi-arid regions of the world would suffer a reduction in water resources due to climate change. Global climate change is expected to reduce crop yield and freshwater resources by the end of the 21st century (Talat, 2020). Globally, freshwater resources are depleting quickly due to the confounding effects of climate change and unparalleled growth in water demand for local, irrigation, and industrial sectors (John et al., 2020).

The effects of climate change heighten competition for progressively limited resources like fresh water and cultivable land (Niang et al., 2017). Climate change-induced sea level rise is recognized as one of the most severe dangers to coastal populations and ecosystems (Mengel et al., 2016). Coastal areas are regularly confronted by seawater intrusion in the groundwater aquifers, increasing the salinity of soil and thus reducing arable land (Panagea et al., 2016).

2.6.1 Sustainable Land Management

“Sustainable development” is defined as development that satisfies current needs without compromising the capacity of future generations to meet meetings" (Cavallaro and Dansero, 1998). Environmental sustainability focuses on preserving environmental capital to pass it on to future generations (Verbruggen and Kuik., 1991). Sustainability entails managing environmental, socioeconomic, and economic interactions among different groups. Achieving sustainability involves evaluating the quality of resource stocks and developing relevant processes, institutions, policies, and public support (Petz, 2014). Changes in land management practices can alter the

balance of ecosystem services, creating trade-offs between them (Rodríguez et al., 2006; Petz, 2014).

Adapting to climate change, including declining water resources, can involve changes in land management (Vigerstol and Aukema, 2011). Sustainable land management protects ecosystems and their services (Coser et al., 2020). Developing modeling and mapping tools and conducting impact assessments considering multiple functions are essential to sustainable land management (Vigerstol and Aukema, 2011).

Agriculture's multifunctionality extends beyond food and fiber production, including carbon sequestration, natural resource management, biodiversity conservation, and rural socioeconomic viability (Klein, 2012). Policy-making should consider agriculture's multifunctional role and balance economic, environmental, and social functions (Olesen and Bindi, 2002; Traerup, 2010). Therefore, to evaluate adaptation options, development frameworks should link sustainable development with climate change, accounting for costs and benefits.

2.6.2 Drivers of Land and Water Quality Degradation

Global climate change transforms land and water resources and the functions of ecosystems, leading to soil systems being affected by physical, biological, biochemical, and chemical deterioration (Adesina et al., 2016; Rosenstock et al., 2019). Climate change leads to land degradation, characterized by long-term loss of productivity, ecological integrity, or value to humans (IPCC, 2020). It exacerbates ongoing land degradation processes and introduces new patterns (Mishra, 2023). Rising global temperatures intensify the hydrological cycle, affecting land precipitation patterns (IPCC, 2007; Kadykalo et al., 2019). Climate change plays a role in extreme events such as droughts, floods, erosion, saltwater intrusion, soil structure degradation, biodiversity reduction, and disruptions to biochemical cycles (Adesina, 2016; Rosenstock et al., 2019).

Agriculture, the dominant land use globally, significantly influences climate and atmospheric gas composition (Shiferawa et al., 2014). Agricultural activities and forest degradation increase atmospheric carbon dioxide (IPCC, 2014). Unsustainable farming practices and land-use changes contribute to land degradation (Shiferaw et

al., 2011). Soil erosion and siltation result from these practices, leading to habitat loss, diminished soil productivity, and sedimentation in river basins (Markhi et al., 2019).

Due to changing rainfall and evapotranspiration patterns, climate change reduces water resources, especially in semi-arid regions (IPCC, 2007). This affects agricultural production and competition for land and water resources (Lotze-Campen et al., 2008). Water scarcity, extreme temperatures, droughts, soil salinity, and acidity impact arid and semi-arid regions (Calanca, 2007; Lotze-Campen et al., 2008).

Rising sea levels increase coastal erosion and flooding (McInnes et al., 2011; Thomson and Rogers, 2014; Day and Hodges, 2018). Coastal inundation, erosion, and increased salinity affect low-lying lands (Sarak, 2010; Dasgupta et al., 2016). Land degradation has complex social, political, cultural, and economic implications, with knowledge gaps in understanding its cumulative impacts on ecosystems and human societies (Kadykalo et al., 2019). Climate information is valuable for developing sustainable practices in the context of climate-induced soil and water quality degradation.

CHAPTER THREE

SPATIO-TEMPORAL DYNAMICS OF SOIL SALINITY IN THE FLOODPLAIN OF RIVER GAMBIA[1]

ABSTRACT

Land degradation due to soil salinity has become a critical challenge for African small-scale agriculture. With rising sea levels and climate-induced variability, ecological functions such as storm surges, flooding, and soil salinization are being altered. This research endeavors to compare machine learning models, analyze satellite reflectance data and quantify salt-degraded land in the Gambia River floodplain. The Super grid sampling approach at a minimum 50 -100 m² scale was used to obtain soil samples. Through a stepwise AIC procedure, Landsat 8 OLI image bands 2-5 were processed into TOA planetary reflectance using rescaling coefficients alongside eight Salinity Indices (SI) and the Normalized Vegetation Index to map soil salinity. Integrating OLI 8-band and SI reflectance values into a multilevel model facilitated evaluating and comparing soil ECe (d/Sm) based on the study regions' 2014 and 2021 soil data. RF and SVM machine learning models predicted soil salinity, with an 80% training set and a test set used for model training and evaluation. Model selection was guided by cross-validation, ranking models based on performance metrics. There were strong correlations between ECe, individual bands, and SI reflectance values, particularly with Landsat 8 bands 2-5 and SI II-VI. Model validation demonstrated good concordance between estimated and predicted ECe values for RF and SVM models in 2014, with R2 values of 0.94 and 0.74 and RMSE values of 0.26 and 0.52, respectively. In 2021, the RF model exhibited higher R^2 values (0.79 and 0.78) for LRR and CRR than the SVM model. The study revealed a slight reduction in the floodplain's total area from 41,021 ha in 2014 to 40,541 ha in 2021. Notably, a significant decrease of -51.09% was observed in the non-saline and very slightly saline classes, respectively, while CRRS saw marginal changes of -1.26% and -2.24% in these classes. However, the slightly saline class expanded by 9.82% in CRRS. The RF model demonstrated superior predictive capability using Landsat 8 reflectance values. The study's recommendations include incorporating ecosystem risk assessments, innovative soil reclamation techniques, and efficient utilization of saline water for agricultural purposes.

[1] A manuscript has been developed from this chapter to be publish in a journal

Keywords: Salinity; Cross-validation Machine Learning; Satellite Data, Random Forest

3.1 INTRODUCTION

Soil salinization is a global phenomenon that occurs on all continents and under almost all climatic conditions due to natural or human-induced processes causing a significant environmental hazard (Dehni et al., 2012; Zaman et al., 2018). In 2010, FAO reported that nearly 3% of the world's soil resources are salt-affected. Similarly, Wicke et al. (2011) mapped the global dispersal of soil salinity using a Geographic Information System and the Harmonised World Soil Database. According to their estimates, about 1100 m ha of land worldwide—of which salty, sodic, and saline-sodic soils make up around 60%, 26%, and 14%, respectively—have reduced productivity due to salt stress.

Ivushkin et al. (2019) estimated around 1 billion hectares of salt-affected grounds in 2016, with a clear increasing trend. Roughly 2000 ha of productive soil gets degraded daily due to extreme salts across 75 states of arid and semi-arid regions (Srivastava et al., 2019). Salinity in the soil renders over 6-7% of the Earth's surface unfit for agricultural purposes (Metternicht and Zinck, 2003; Yensen, 2008; Bado et al., 2016; Talat, 2020). Zaman et al. (2018) indicated that globally, salt-affected soils are divided into saline (412 million hectares) and sodic (618 million hectares), totaling 1030 million hectares. Recent reports indicated that saline and sodic soils cover about 10% of the world's total arable land (Li and Kang, 2020), affecting nearly 1 billion hectares worldwide and causing a substantial threat to ecosystems (Gorji et al., 2015; Tan et al., 2023).

Land degradation attributed to soil salinity problems has posed a significant threat to African small-scale agriculture. Reports indicate that approximately 1,899 million hectares of African land are affected by salinity, highlighting the extensive reach of the issue (Aredehey et al., 2018; Bannari et al., 2021). In Africa, 80 million hectares, particularly in the Sahel region of West Africa, are reported to be saline, sodic, or saline-sodic, making it the most affected area (Zaman et al., 2018). The salinization of water and soils affects freshwater availability and diminishes arable land's suitability for crop production (IPCC, 2007; Bayabil et al., 2021). Climate change and variability

drive rising sea levels, modifying several ecological functions in storm surges, flooding, and salinization of water and soils (Awal et al., 2016).

Soil salinization presents challenges in accurate mapping and monitoring its extent compared to other soil properties due to its dynamic nature and variations in affected areas. Traditional field surveys and laboratory methods for monitoring salinity are precise but labor-intensive, time-consuming, and expensive, leading to rough estimates and scattered information on the extent of salt-affected areas (Nanni & Dematte, 2006; Fan, 2016; Allbed & Kumar, 2013; Gorji et al., 2015). The limited accessibility of inhabitable areas and the massive coverage of salinity make it challenging to obtain accurate sampling distributions (Gorji et al., 2015).

In recent years, satellite remote sensing has emerged as an inexpensive and effective tool for mapping soil salinity at various spatiotemporal scales (Metternicht and Zinck, 2003; Günal et al., 2021). By analyzing surface reflectance characteristics and vegetation patterns influenced by salinity, remote sensing techniques, such as satellite imagery, can help identify and map salt-affected areas (Günal et al., 2021). Integrating remote sensing with statistical models, such as linear regression, offers a practical and cost-effective approach to modeling soil salinity (Allbed et al., 2014). Predictive algorithms can be developed, incorporating spectral bands, indices, image transformations, and various soil-related variables, to map soil salinity using electrical conductivity (ECe) as a salinity indicator (Ekercin & Ormeci, 2008; Bannari et al., 2021; Nawar et al., 2014; Masoud et al., 2019; Kumar et al., 2020).

Acquiring up-to-date information on soil salinity's spatial distributions and severity is crucial for agricultural development and precision soil resource management (Ivushkin et al., 2019; Duan & Zhang, 2021). Therefore, this study proposes to develop a predictive model for soil salinity in the floodplain of CRRS and LRR in The Gambia by integrating satellite remote sensing and soil electrical conductivity (EC) measurements. The study aims to compare machine learning models, analyze satellite reflectance values, and quantify the magnitude of salt-degraded land in the Gambia River floodplain. The findings of this study will contribute to improved natural resource management by identifying and monitoring salinity-prone sites and recommending appropriate soil salinity management practices for sustainable agriculture and environmental protection.

3.2 Materials and Methods

3.2.1 Soil Sampling

The Super grid sampling approach was adopted for good spatial and feature space coverage.

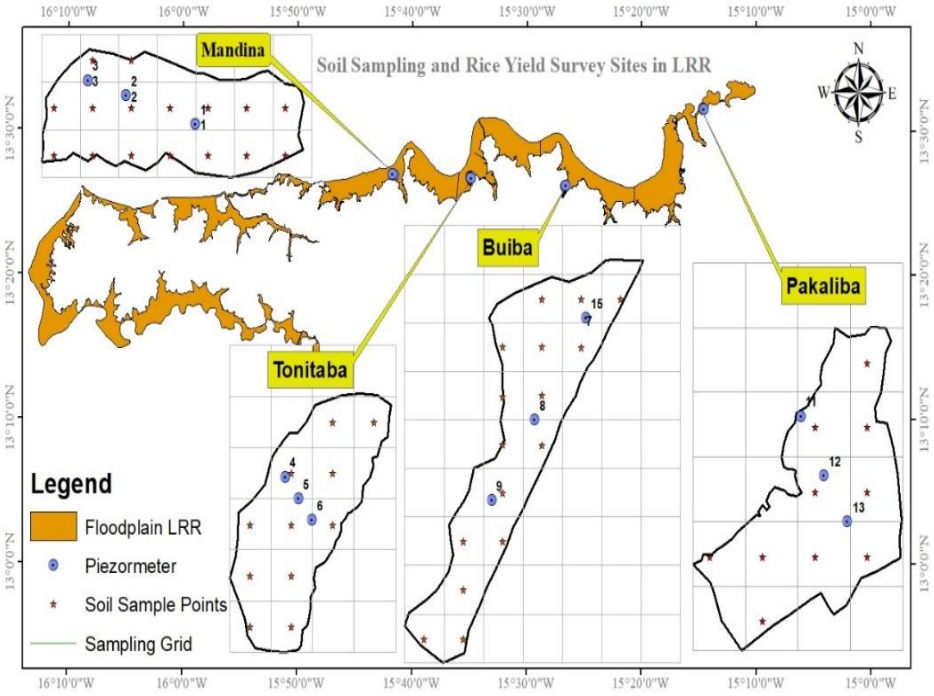

(a)

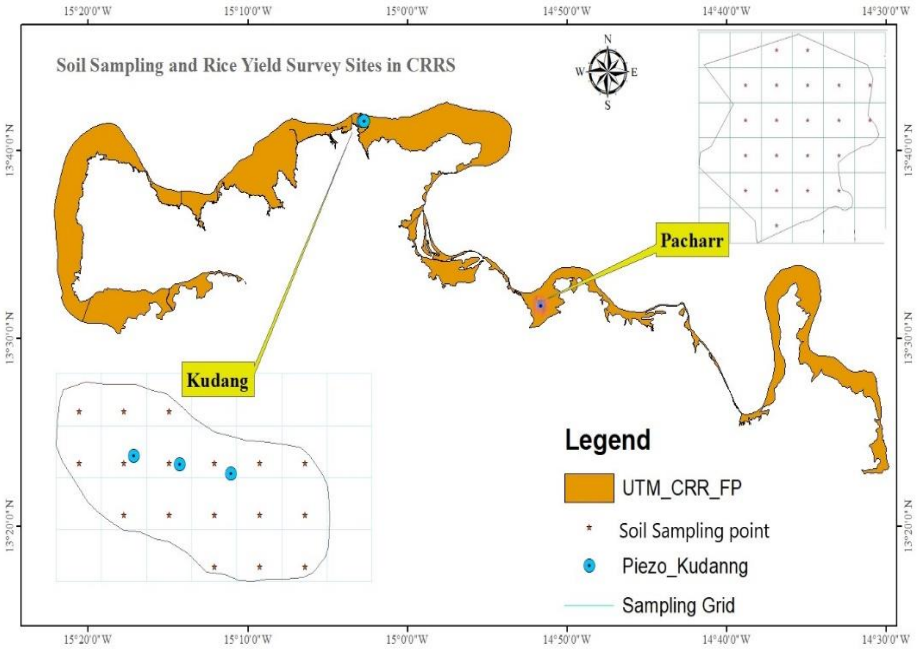

(b)

Figure 3. 1 Soil sampling and rice yield survey fields a) LRR b) CRRS

The super grid sampling method effectively achieves more precise spatial variability of farm field-level target variables with limited sample sizes (Wang et al., 2019). Using Data Management Tools in a GIS environment, a fishnet was created with a minimum sampling scale (50-100 m2). The centroid of each fishnet was determined as the sampling point for collecting soil samples across six community rice fields within the study regions. A portable global positioning "Garmin etrex 10" device was used to navigate the identified sampling points, and coordinates were entered at the field level. Composite soil samples for each sampling unit were obtained from 3 additional discrete subsamples collected at 3-5 feet adjacent to sampling points on a homogeneous physiographic land unit. Soil samples were obtained at a depth of 30 cm using a 15 cm graduated soil auger. In total, 196 composites (0.5 kg of soil per sampling point) of geo-referenced soil samples were packed in double plastic bags with internal and external labels for transportation to the laboratory. Soil samples were dried at room temperature, ground, and passed through a 2 mm sieve before laboratory analysis. Soil samples were analyzed for electrical conductivity (ECe) measured in deciSiemens per meter (dS/m).

3.2.2 Soil Salinity Classification

Richards (1954) defines saline soils as exhibiting electrical conductivity of more than 4 dS/m saturation extracts at 25 °C and uses measurable soil properties to quantify further characteristics of salt-affected soils, which have been widely applied for general classification of salt-affected soils.

Table 3. 1 Characteristics of salt-affected soils

Type of soil	pH	EC_e (dS/m)	ESP (%)	SAR
Saline	< 8.5	>4.0	< 15	< 13
Sodic	> 8.5	<4.0	> 15	≥ 13
Saline-sodic	> 8.5	>4.0	> 15	≥ 13

Salt-affected soils with a high content of soluble ions and an appreciable amount of sodium ions are known as saline-sodic soils. The high content of sodium ions in these soils causes the dispersion of clay and organic matter, which settles on the surfaces of soil particles to give them a brownish-black appearance. When sodium salts in these soils hydrolyze, the pH of the soil increases, and the soil changes to sodic soil (Zaman et al., 2018).

Sodic soils, salt-affected soils with high amounts of sodium ions, are sometimes called saline soils capable of alkaline hydrolysis(Rangesamy and Marchuk 2011). When the soluble salts remain high in the saline-sodic soils, the characteristics of the soils are like those of the saline soils. The dominant cations in salt-affected soils are Sodium (Na^{+}), Calcium (Ca^{2+}), Magnesium (Mg^{2+}), Potassium (K^{+}), and dominant anions are Chloride (Cl^{-}), Sulphate (SO^{-2}), Carbonate (CO^{-2}), Bicarbonate (HC_{O}^{-}), and Nitrates (NO^{-}) (Richards, 1954; Omuto et al, 2020).

Soil salinity classes in the scientific literature concerned with plant growth and agricultural importance are soils containing sufficiently high soluble salts in the root zone that negatively impact most crops' growth and development have been adequately reported (Lamond and Whitney 1992; Abd-elwahed, 2014). However, due to the difference in the degree of salt injury among plant species, the physiological growth stage, type and nature of salts, edaphic, and other environmental factors, saline soils are difficult to define precisely. For example, Kissell and Sonon (2008) identify six essential salinity ranges for plant growth and development.

Table 3. 2 Agronomic classification of soil salinity based on EC

Classification	EC (dS/m)	Crop yield
Non-saline soils	0–2	Not affected
Very slightly saline	2–4	Sensitive crop affected
Slightly saline soils	4–8	Yields of many crops are restricted
Moderately saline soil	8 -16	Only tolerant crops exhibit satisfactory yields
Strongly saline soils	>16	Few very tolerant crops can grow

Source: FAO and ICBA (2023)

Barrett-Lennard et al. (2008) propose classifying soil salinity into non-saline, low salinity, moderate salinity, high salinity, severe salinity, and extreme salinity to create a standardized classification system for soil salinity, consistency in research on the

salinity tolerance of potential salt-affected land fodder plants, and easily extrapolated results across Australia.

Similarly, Asfaw et al. (2018) identified classes of salinity with varying degrees based on the spatial overly salinity model result. Tian et al. (2020) suggest classifying salinity levels using remote sensing into non-saline (ECe = 0-2 dS m1), slightly saline (ECe= 2-4 dS m-1), moderately salty (ECe= 4-8 dS m-1), intensely saline (ECe= 8-16 dS m-1), and highly saline (ECe > 16 dS m-1) groups.

Bannari et al. (2021) group salt-affected soils into three classes based on their EC values: non-saline, low, moderate, high, very high, and extreme salinity. In this study, soils are classified as salt-affected soils according to the agronomic category of soil salinity (Hammam & Mohamed, 2020; FAO and ICBA, 2023)

3.2.3 Spatial Characteristics of Soil Salinity

A geo-database of study fields (shape files, coordinate of grid sampling points, and soil properties of physicochemical analysis and soil-water relationship) was created in a GIS environment for geo-statistical analysis. The inverse distance weighted (IDW) interpolation method with a stable semi-variogram was used to generate interpolation of soil salinity distribution across the study fields. The IDW method assumes that the interpolated surface should be influenced mainly by the nearby points and less by the more distanced points (Juglea et al., 2010).

The equation for the IDW method is given in Equations 1 and 2.

$$u(x)=\frac{\sum_{k=0}^{N} wk\,(x)uk}{\sum_{k=0}^{N} wk\,(x)} \quad \text{... equation(3.1)}$$

where the weight function is:

$$wk(x)=\frac{1}{d(x,xk)} \quad \text{... equation(3.2)}$$

According to Juglea et al. (2010), x denotes an interpolated, xk is the interpolated point, d is a given distance from the known point xk to the unknown point x, and N is the total number of known geographic reference points.

3.2.4 Remote sensing data and processing

The study uses multispectral Landsat 8 OLI satellite imageries of April (2014-2021) to map soil salinity. The images cover (Path/Row: 204/51, UTM WGS1984 Zone: 28 and were collected on (April 4th, 2014, April 15th and April 26th, 2021).

April imageries are beneficial for recognizing soil types due to their low cloud coverage and high surface exposure in the dry season. For example, Kumar et al. (2020) reported that satellite images of March or April offer the maximum contrast between SAS and cropland when the salt appearance on the surface is highest, unlike the images of May and June.

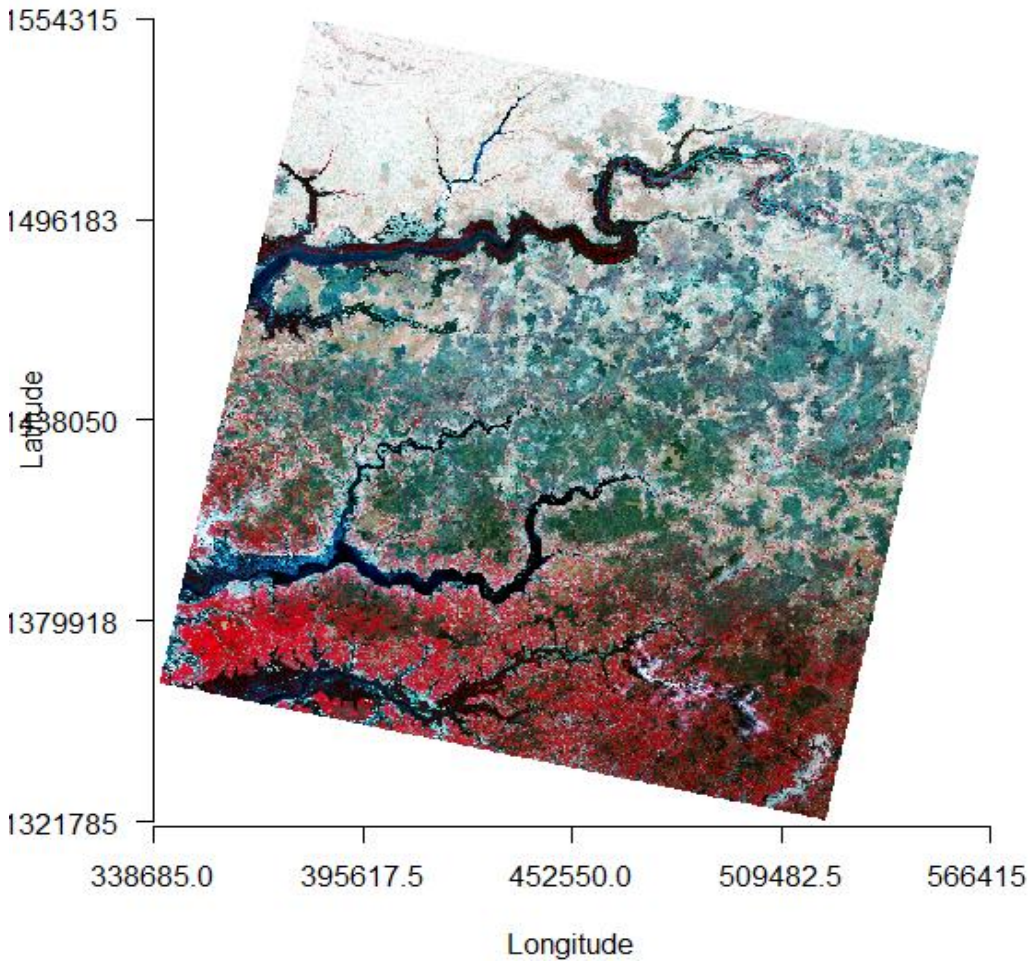

Figure 3. 2 FCC image of Landsat 8 OLI composite band over the study area

The Landsat 8 OLI (Operational Land Imager) consists of 11 spectral bands with a 30 m resolution. This study used Landsat 8 OLI bands 2-5 to generate various salinity and vegetation indices. These images provide information about the electromagnetic radiation reflected by the Earth's surface at different wavelengths. In this study, the visible bands selected for extraction of Reflectance values and salinity mapping are obtained from multispectral bands (2-5).

The acquired Landsat 8 OLI image data were converted to TOA planetary reflectance using reflectance rescaling coefficients provided in the remote sensing imageries'

product metadata file (MTL). Equations 3.1 and 3.2 equation were used to convert DN values to TOA reflectance for OLI data sets as follows:

$$\rho\lambda' = M\rho Qcal + A\rho \quad \text{... equation(3.1)}$$

where:

$\rho\lambda'$ = TOA planetary reflectance, without correction for solar angle

$M\rho$ = Band-specific multiplicative rescaling factor (Reflectance Mult Band x, where x is the band number)

$A\rho$ = Band-specific additive rescaling (Reflectance Add Band x, where x is the band number)

Qcal = Quantized and calibrated standard product pixel values (DN)

TOA reflectance with a correction for the sun angle is then:

$$\rho\lambda = \frac{\rho\lambda'}{\cos(\theta sz)} = \frac{\rho\lambda'}{\sin(\theta se)} \quad \text{... equation(3.2)}$$

where:

$\rho\lambda$ = TOA planetary reflectance

θse = Local sun elevation angle

θsz = Local solar zenith angle; $\theta sz = 90° - \theta se$

The reflectance values of the salinity and vegetation indices were calculated using the point database of EC values obtained during fieldwork using satellite image bands and band combinations. The Extract Values to Points tool from the 'raster' package in R statistical software (version 4.2.3) was utilized for this analysis.

Composite band imagery consisting of the band (2-5) was developed and visualized using False Color Composite (FCC) in RGB color code. Based on some salinity and vegetation indicators in the literature, eight salinity indicators were selected and utilized to map soil salinity regularly (Table 3.1). Salinity and vegetation indices were calculated from various band combinations using the raster calculator in the map algebra of Arc Toolbox of ArcGIS 10.6.

Table 3. 3 Salinity indices used for the delineation of soil

Salinity Indices (SI)	Band Ratios	References
Normalized Difference Salinity Index	$NDSI=\frac{(R-NIR)}{(R+NIR)}$	Dehni et al., 2012
SI I	$SI=\sqrt{G \text{ X } R}$	Khan et al., 2001
SI II	$SI=\sqrt{G^2+R^2+NIR^2}$	Douaoui et al., 2005
SI III	$SI=\frac{G \text{ X } R}{B}$	Khan et al., 2001
SI V	$SI=\frac{B \text{ X } R}{G}$	Khan et al., 2001
SI VI	$SI=(R \text{ X } NIR) \div G$	Khan et al, 2007
Brightness Index (VII)	$BI=\sqrt{R^2+NIR^2}$	Dehni et al., 2012
Soil Adjusted Vegetation Index (L = 0.5) SAVI	$SI=\frac{(NIR-R)X\ (1+L)}{(NIR+R+L)}$	Dehni et al., 2012
Normalized Vegetation Index	$NDVI=\frac{NIR-R}{NIR+R}$	Rouse et al., 1974

R = Red Band, B= Blue Band, G=Green Band, NIR=Near Infrared, Band, L=0.5

Finally, images of floodplains with a spatial resolution of 30 m were clipped in ArcGIS 10.6.

3.3 Statistical Analysis

3.3.1 Data Preprocessing

The dataset analysis underwent several rigorous steps to ensure the integrity of the regression model in climate science. Outlier detection and removal of non-significant variables were performed. Collinearity detection involved examining variables with high correlation coefficients, and any aliased coefficients were subsequently eliminated from the model (Daoud et al., 2017). Multicollinearity was assessed to guarantee the stability and reliability of the regression model by calculating the variance inflation factor (VIF) for each independent variable. Variables with high VIF values were considered potential indicators of multicollinearity (Daoud et al., 2017). Non-significant variables were identified through high p-values in the model's sum. This refinement process aimed to retain only the independent variables that

significantly influenced soil ECe based on a pre-defined threshold ($p > 0.05$). Furthermore, a Pearson correlation coefficient analysis was conducted between soil EC values and remote sensing data to compare the relationships and identify significant variables associated with increasing soil salinity.

3.3.2 Stepwise Variable Selection

In predictive modeling, selecting relevant predictors is crucial for accurate predictions in climate science (Kano & Harada, 2000). The choice of predictors directly impacts the model's performance and ability to capture the underlying relationships within the data. Stepwise variable selection is a systematic technique employed to select a subset of predictors from a larger pool of candidate predictors, resulting in improved goodness-of-fit statistics for the model (Yoshida, 2023).

Stepwise variable selection typically involves two main steps: forward selection and backward elimination. In the forward selection, variables are sequentially added to the model one at a time, starting from an empty model. At each step, the variable that provides the most significant improvement in the model's performance, as determined by the Akaike Information Criterion (AIC), is selected and included. In backward elimination, the model begins with all potential predictors included.

At each step, the variable with the least significant contribution or significant impact, as determined by a specified criterion, is removed from the model. This process continues until no further improvement is observed, or removing any remaining variables would significantly decrease the model's performance. Stepwise variable selection has been widely used in soil characteristics studies to refine models by selecting the best set of variables (Khaledian et al., 2017). Based on the stepwise AIC procedure, the OLI 8-band and SI reflectance values were incorporated into the multilevel model evaluation and comparison to predict soil ECe (d/Sm) in the two study regions.

3.4 Prediction of Soil Salinity

Accurate prediction of soil salinity plays a vital role in understanding and managing soil health in agricultural areas. This study aimed to develop a predictive model for soil salinity in the floodplain of CRRS and LRR in The Gambia by leveraging satellite reflectance values and soil electrical conductivity (EC) measurements (Tan et al.,

2023). The satellite reflectance data encompassed multiple spectral bands obtained from remote sensing imagery, enabling the capture of electromagnetic radiation reflected from the Earth's surface. The satellite reflectance data and soil EC measurements spanned from 2014 to 2021 in the floodplain of CRRS and LRR in The Gambia. The soil EC measurements provided quantitative information on soil salinity levels. Two machine learning models, Random Forest (RF) and Support Vector Machine (SVM), were used to predict soil salinity reliably.

3.4.1 Cross-Validation Settings:

The cross-validation approach was employed to assess the performance of various machine learning models. Cross-validation serves a dual purpose of parameter tuning and performance evaluation. The dataset is divided into k (in this case, 10) folds. Each fold functions as a validation set, while the remaining folds are used for model training. This systematic testing over several data sections reduces the danger of overfitting and assesses the model's capacity for generalization. Results from every iteration are averaged to give a reliable performance assessment across various data subsets. Cross-validation ensures a trustworthy evaluation of the model's forecasting ability while preventing overfitting and obtaining reliable model performance metrics.

3.4.2 Model Training and Development

The dataset was divided into a training set and a test set using a stratified random sampling approach. The training set comprised 80 % of the model training and development data. The selected predictor variables (OLI bands and SI reflectance values) and the target variable, soil salinity represented by ECe dS/m, were used to fit each model. The aim was to capture the relationship between satellite reflectance values and soil EC to predict soil salinity in the floodplain.

3.4.3 Model Evaluation and Comparison

After training the models, they were evaluated using the test set to assess their performance in predicting soil salinity. Evaluation metrics, including root mean squared error (RMSE), mean absolute error (MAE), Mean Absolute Percentage Error (MAPE), and R-squared (R^2), were calculated. These metrics provided insights into the accuracy and precision of the model's predictions. The models were compared based on their performance, and the best-performing model was selected based on R^2

and RMSE values for predicting soil salinity in the floodplain of CRRS and LRR in The Gambia.

3.4.5 Model Selection

A comprehensive comparison was conducted using the cross-validation method to identify the best-performing model. Cross-validation is a statistical procedure used to evaluate the performance of machine learning models by partitioning the available data into multiple subsets for training and testing. The method assesses a predictive model's performance and generalization ability and detects potential overfitting or underfitting.

Cross-validation enables tuning model hyperparameters effectively and evaluates the model's performance on different subsets of the data. The data was divided into k folds of 10, each serving as the validation set, while the remaining folds were used for training. This process was repeated multiple times, with each fold taking turns as the validation set. The performance metrics from each iteration were averaged to obtain a reliable estimate of the model's performance.

The models were ranked based on their average performance metrics across all iterations. The trained model was evaluated on the validation set using metrics such as R-squared, RMSE, MAE, or MAPE. The evaluation metrics, particularly the R-squared value, were carefully analyzed to determine the model's ability to explain the variance in soil salinity. The model with the lowest RMSE and the highest R^2 was identified as the best for predicting soil salinity.

The models were then used to analyze an independent dataset from 2014 to 2021 for validation and performance monitoring. These datasets served as test or validation sets. They were deliberately excluded from the model development process to evaluate the model's capacity to generalize and provide precise predictions throughout the study period.

3.4.5 Mapping of soil salinity

The selected models were used to map and quantify historical salinity levels in 2014 and compare them with the current conditions in 2021 for both study areas. The reflectance images of the independent variables were combined with the normalized

variable importance derived from the chosen model. Variable importance values quantify the contribution or relevance of each reflectance band in predicting or explaining soil EC_e (dS/m).

A weighted combination of reflectance images and variable importance values were used to obtain the predicted soil salinity values. The weighted combination involves assigning weights or importance values to each reflectance band based on their respective variable importance values, multiplying each reflectance value by its corresponding weight, and summing the results across all bands. The higher the importance value of a reflectance band, the more weight it receives in the combination process. This process was conducted pixel-wise across the study area, resulting in a raster dataset to generate soil salinity maps that produce a single continuous value for each pixel, representing the estimated EC_e (dS/m) level.

The final maps of soil salinity predictions provided a continuous spatial distribution of soil salinity across the study area, with higher values demonstrating higher salinity levels and lower values indicating lower salinity levels. A comparative map analysis was done to estimate the changes in salinity and visualize the extent of salinity in the study areas for the periods under review (2014 – 2021).

3.5 RESULTS AND DISCUSSION

3.5.1 Spatial Distribution of Soil Salinity

The spatial distribution of soil salinity of five surveyed fields within the floodplains of LRR and CRRS shows the characteristics and extent of soil salinization processes (Figure 3.3).

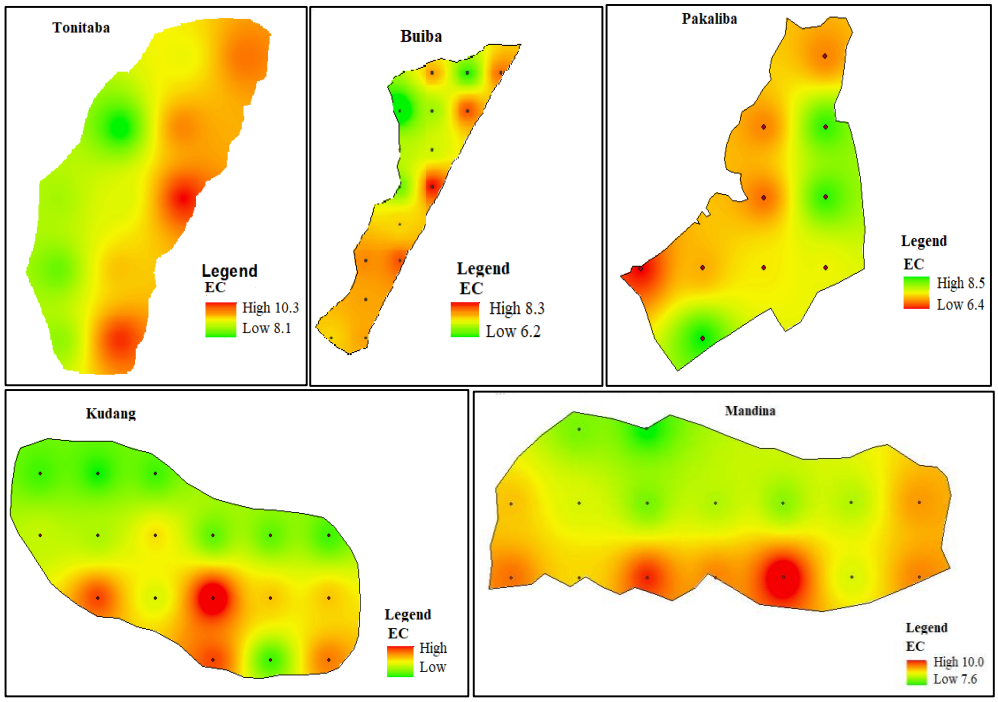

Figure 3. 3 Spatial distribution of soil salinity across the study fields based on ECe

The maps indicate the degrees or intensity of soil salinity across the surface of study fields. The visual interpretation shows that (Mandina, Tonitaba, Buiba, and Pakaliba) have more than 70 % of the total area classified as slightly saline (ECe 4 - 8 dS/m) and strongly saline (ECe 4 - 16 dS/m).

Table 3. 4 Summary statistics of electrical conductivity (EC dS/m)

Region	LRR	CRRS
Min.	6.2	0.3
Max.	10.3	4.1
Mean	8.34	2.1
Std. Error	0.11	0.23

The spatial distribution further suggests that surface salinity levels decrease toward the eastern parts of the country, where ECe values range between 0.3 and 4.0 dS/m, except for some patches where more than > 4 dS/m are reached. The highest salinity values were observed in fields in the western part of the study area, which is influenced by seawater intrusion from the Atlantic Ocean. Other factors, such as soil high SO_2^4 and Cl^- content, were observed, specifically in Mandina, Tonitaba, and Buiba.

3.5.2 Variable Selection for Regression Model

Figure 4 shows the Pearson correlations of ECe (dS/m) of the soil data with individual band data, band combinations, and designated salinity spectral indices of Landsat 8 OLI image. Comparatively, more significant and positive correlation coefficients were observed between ECe, individual bands, and SI reflectance values.

Table 3. 5 Correlation matrix of soil ECe, OLI 8 reflectance, and salinity indices spectral reflectance values

Visible Bands	**LRR**	**CRRS**
Band 2 Blue	-0.15	0.53
Band 3 Green	-0.22	0.53
Band 4 Red	-0.33	0.55
Band 5 Near Infrared (NIR)	-0.46	0.57
Indices Indices		
NDSI	0.44	-0.42
SI_II	-0.28	0.54
SI_III	-0.4	0.62
SI_IV	-0.35	0.56
SI_V	-0.29	0.55
SI_VI	-0.33	0.57
SAVI	-0.53	0.34
NDVI	-0.51	0.26

The ECe has a strong positive correlation with Landsat 8 band 2 – 5 ($r > 0.54$) and SI II ($r = 0.54$), SI III ($r=0.62$), SI IV ($r=0.56$), SI V ($r=0.55$), and SI VI (0.57). The highest positive correlation coefficient was obtained between ECe, the Near Infrared Band (NIR) ($r=57$), the Red Band, the Green Band, and SI II. A lower correlation coefficient was observed between OLI reflectance Bands (2-5), NDVI, NDSI, and SAVI, whereas a robust negative relationship was between NDSI and SAVI ($r= -0.80$), and NDSI and NDVI ($r= - 0.78$).

Based on the strength of the association between ECe and the indices for the two regions (LRR and CRRS), Band 5, SI III, SI IV, and SI VI all indicate coefficient correlation values ($r > 0.55$) and could be considered suitable for determining the soil salinity, respectively. However, R-square (R^2) and Adjusted R-square (Adj. R^2) values of the linear regression between soil ECe and spectral reflectance of individual salinity indices were low despite having significant p-values. The highest $R^2 = 0.39$, and Adj. $R^2 = 0.28$ was obtained for SAVI. This result is similar to the finding of Günal et al. (2021), who reported an equal correlation coefficient (R^2) for the SAVI index using

soil ECe values as the dependent variable for salinity modeling. Therefore, incorporating multiple variables into the modeling and using the stepwise selection process will enhance the explanatory capacity of the models in assessing soil salinity in the floodplain of LRR and CRRS, The Gambia.

Equation 3.2 shows the results of the stepwise variable selection process using the AIC criterion for choosing the best model for modeling soil salinity. The models with the lowest AIC= (-58.06) and AIC value (-12.83) are selected as the best predictor outcome variable for LRR and CRRS, respectively. The equations of the best-fitted model for LRR and CRRS are shown in equations 3.3 and 3.4. These regression models demonstrated superior predictive performance and effectively captured the complex relationships between the predictor variables derived from satellite reflectance data and soil ECe (dS/m).

$$\begin{aligned} ECe \; = \; & -2462.58 \times Band_2 - 9246.70 \times Band_3 - 4206.68 \times Band_4 - \\ & 28.49 \times Band_5 + 29056.61 \times NDSI + 13533.26 \times SI_{II} - \\ & 149.08 \times SI_{IV} - 2310.45 \times SI_V - 29137.09 \times SI_{IX} + \\ & \varepsilon \end{aligned} \quad \ldots \text{equation (3.3)}$$

$$\begin{aligned} ECe = \; & -32675.77 + 2341.49 \times Band\_2 - 9084.79 \times Band\_3 - \\ & 4387.11 \times Band\_4 - 29.84 \times Band\_5 - 126513.59 \times RF\_NDSI + \\ & 13420.79 \times RF\_SI\_II - 85.18 \times RF\_SI\_IV - 2121.47 \times RF\_SI\_V - \\ & 173529.94 \times RF\_SI\_IX + \varepsilon \end{aligned} \quad \ldots \text{equation(3.4)}$$

where:

EC_e (dS/m) is the predicted soil electrical conductivity

The R-square metric measures the proportion of the variance in the target variable that is predictable from the predictor variables. RMSE measures the average deviation between predicted and actual values, with lower values indicating better model performance. The precision of the model fitting increases as R^2 gets closer to 1. The model's accuracy is inversely correlated with the RMSE value.

The more closely this value approaches 0, the less difference between the measured value and the value projected by the model, and the more accurate the prediction (Wang et al., 2021). The Stepwise variable selection for multiple linear models shows R^2 values of 0.67 and 0.62 and RMSE of 0.5769 dS/m. This suggests that the model explains a significant portion of the variance, indicating that the indicates that the model explains 67 and 62 % of the variance in the dependent variable of LRR and CRRS, respectively.

3.5.3 Model Evaluation and Comparison Based on Predicted Values

Figure 3.5 presents model performance results on the training dataset for predicting soil salinity (ECe) in LRR and CRRS of The Gambia. Two models use reflectance values from Landsat 8 as predictor variables. The SVM model has the highest coefficient of determination (R^2) value of 0.77 and RMSE value of 0.51, meaning that approximately 0.77 of the dependent variable ECe variance is explained by the independent variables in the SVM model for LRR.

The RF and SVM models have RMSE values of 0.63 and 0.51, which suggests that, on average, the predictions of the RF and SVM models deviate from the actual values by approximately 0.63 and 0.51 EC_e (dS/m) for LRR (Figure 3.4b). This result is higher than those reported by Hihi et al. (2019), who use a linear regression model to predict EC from Sentinel 2 bands and spectral indices of soil salinity. Their results indicated that a combination of predictor variables from Sentinel_2 bands and soil salinity indices produced a significant coefficient of determination R^2 0.48 and an estimated RMSE of about 4.8 dS/m.

The models predict salinity content per the observed truth in the field. For example, the measured ECe (dS/m) values in CRRS indicate non-saline to saline soils within the ranges of 0.3 to 4.1 (Table 3.3). The model-predicted estimated values of salt content in the soil of CRRS are categorized into non-saline and saline classes, which concurs with the region's logical sense of the minimal problem of soil salinity.

Nawar et al. (2014) reported similar minimum and maximum estimated ECe values with measured laboratory spectral data for predicting soil salinity from Landsat images using PLSR and Multivariate Adaptive Regression Splines (MARS) models. Linear and PR have the same R^2 values (0.24), lower than RF. Despite recording the lowest RSME, RF has the lowest R^2 value, suggesting that it explains the least variance in ECe. Overall, the two models have similar R^2 and RMSE, MAE (0.44), MAPE (5.0), and RSS (0.62).

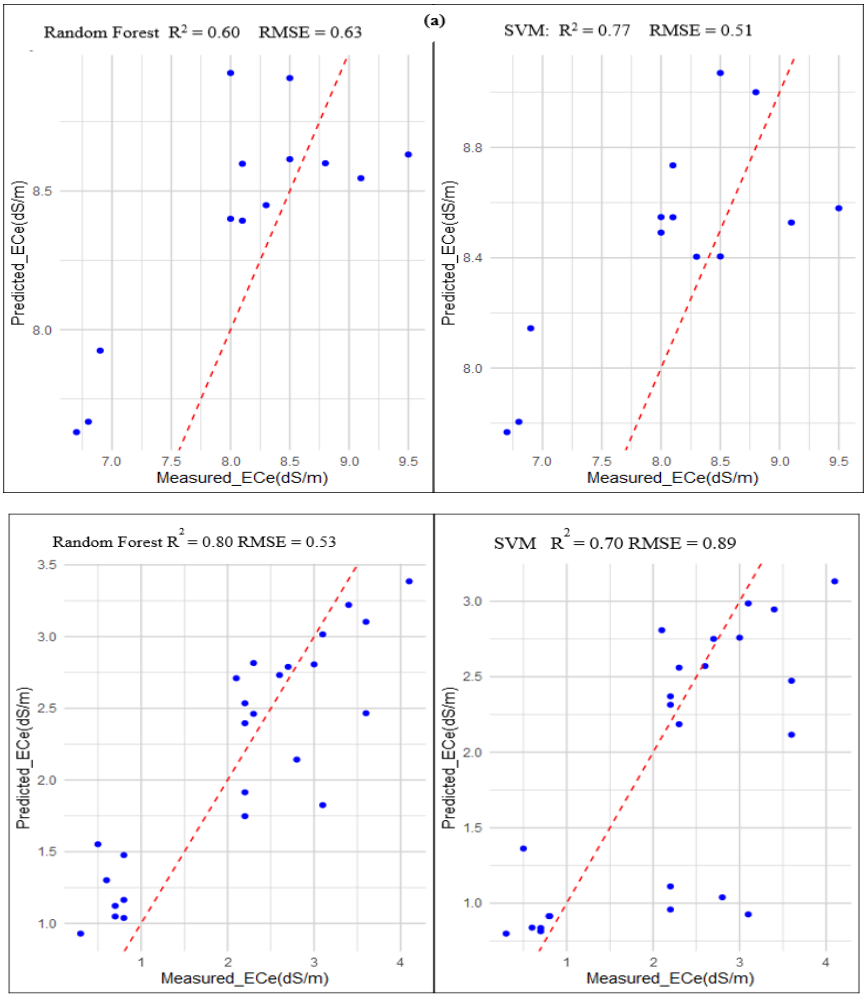

Figure 3. 4 Evaluation of the two predictive models on the trainset for Soil salinity a) CRRS b) LRRS

Therefore, using the minimum RMSE with the highest coefficient of determination (R^2) as the decision criterion, the Random Forest and SVM models offered promising results on the training dataset and are thus considered suitable for model validation on the test dataset.

3.5.4 Model validation

Model validation was conducted to assess the performance of the RF and SVM models on the test dataset for LRR and CRRS, respectively.

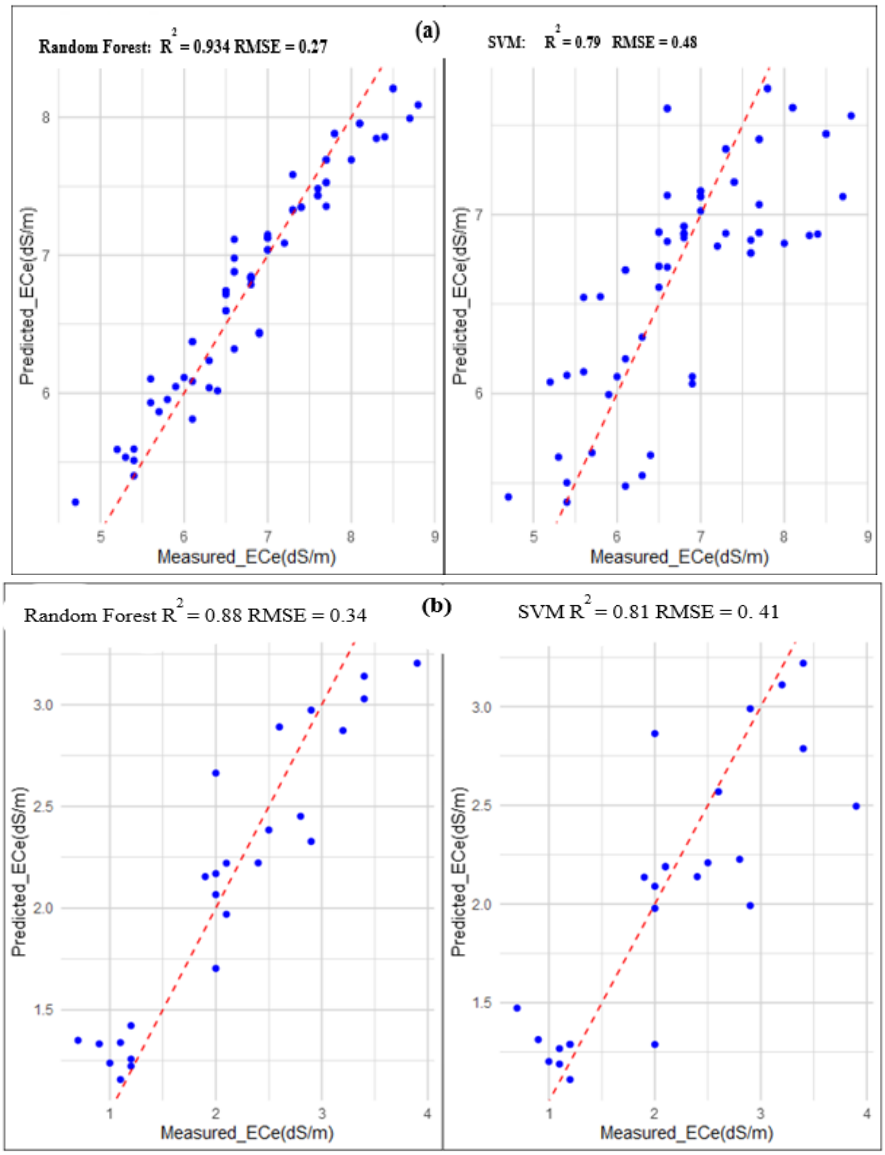

Figure 3. 5 Validation of the Random Forest and SVM model on the test dataset a) LRR and b) CRRS.

Figures 3.5a and 3.5b depict the expected and measured values, demonstrating a good relationship between the estimated data. In LRR, the RF model predicted soil salinity with an R^2 of 0.93, and the SVM model achieved an R^2 of 0.78 and an RMSE of 0.48 (Figure 3.8a). Similarly, in CRRS, the RF model achieved an R^2 of 0.89 and RMSE of 0.34, while the SVM model achieved an R^2 of 0.81 and RMSE of 0.42 (Figure 3.5b).

The validation results confirmed the strong association between the estimated data and estimated ECe values, as indicated by high R^2 values and relatively low RMSE values for both LRR and CRRS. Like the model evaluation, the RF model outperformed the SVM model in terms of accuracy, with R^2 values of 0.93 and 0.88 for LRR and CRRS,

respectively. The RF model captured 93 % and 88 % of the variance in ECe, with a lower prediction error of 0.27 and 0.34 dS/m from the actual values.

Contrary to the model evaluation results, the validation results demonstrated that the RF model exhibited higher accuracy and lower prediction errors for both regions. These findings align with previous studies that have utilized reflectance values from Landsat imageries to estimate and map soil salinity in arid and semiarid environments (Nawar et al., 2014; Bannari et al., 2021). The results suggest that the RF model, employing Landsat reflectance data, is stable and slightly superior to the SVM model for estimating soil salinity in the study area.

3.5.5 Application RF and SVM Model for Mapping Soil Salinity in LRR and CRRS

The RF and SVM models' were applied to 60 and 40 independent soil samples obtained in 2014 and 2021 for mapping soil salinity in LRR and CRRS, respectively. The predicted and measured values are plotted in Figures 3.6 a, b, and 3.7a, b. The results indicated a good association between the estimated data and predicted ECe values (R^2 = 0.94 and 0.74 and RMSE = 02.6 and 0.52) for RF and SVM models in 2014, respectively (Figure 3.7 a, b). Applying the RF and SVM model on the independent dataset was slightly better in predicting ECe (d/Sm) than the 2014 validation results for RF (R^2 = 0.93 and RMSE = 0.27). In contrast, SVM explains a high variance (79 %) of soil ECe for the validation dataset, although with a relatively high RMSE value (0.48) compared to the independent validation set of 2014 for LRR respectively. Comparatively, the application of RF and SVM models performs better for estimating soil salinity in CRRS than LRR from the 2014 independent dataset.

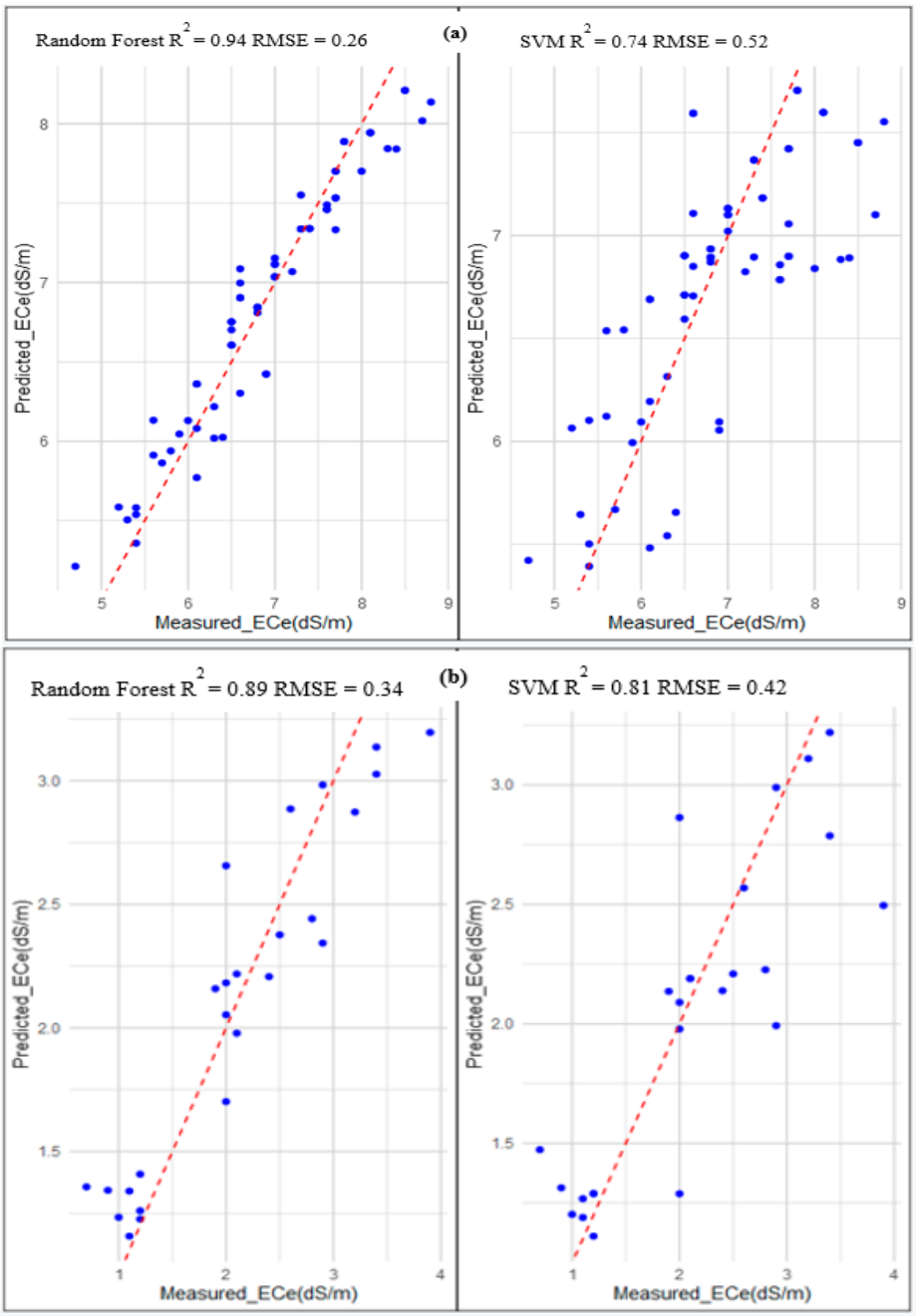

Figure 3. 6 Application of RF and SVM model of the Random Forest and SVM model on the 2014 independent dataset a) LRR and b) CRRS

The values obtained in this study are high than those reported by Wang et al. (2020), who identified the RF model as the best regression model (R^2 = 0.75) for revealing the spatial characteristics of salt dispersal in Southern Xinjiang, China. Both models explain more than 80 % of the variance in soil salinity, with the RF having high R^2 values (0.89) and lower RMSE (0.34) compared to the SVM model (R^2 = 8.1) and RMSE value of 0.42 (Figure 6b).

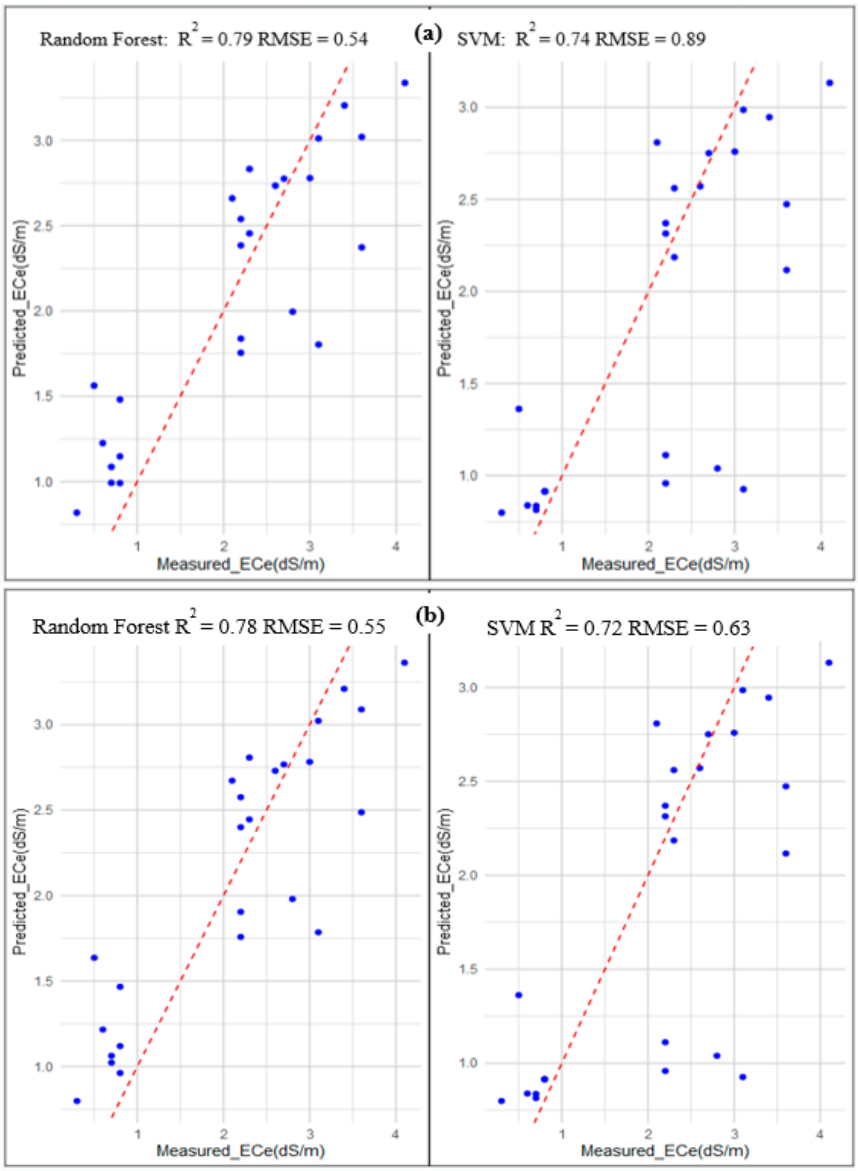

Figure 3. 7 Application of RF and SVM model of the Random Forest and SVM model on the 2021 independent dataset a) LRR and b) CRRS

The 2021 independent set shows a similar quality of model performance in estimating soil salinity for both regions (Figure 3.6 a, b). The RF model shows high R^2 values (0.79 and 0.78) for LRR and CRRS compared to the SVM model for 2021. However, both models show high accuracy ($R^2 > 0.70$) for predicting soil salinity in the two study regions.

This result is contrary to the findings of Wang et al. (2021), who compare three machine learning algorithm estimation models (ANN, RF, and SVM) to map soil salinity using sentinel-2 MSI and soil electrical conductivity (EC) in arid areas in

China. Their results indicated that the SVM model estimation soil EC attained a higher performance and accuracy (R^2 = 0.88) than those achieved with the soil EC estimation models established with the RF and ANN models. The empirical relationship between measured and predicted EC_e values is a reasonable estimation of the predicted electrical conductivity values. The result obtained from this study indicates that both the Random Forest and SVM models are suitable for mapping, monitoring, and predicting soil salinity in the floodplain of CRRS and LRR in The Gambia regions (LRR and CRRS). The two perform relatively similarly in predicting soil salinity (EC_e) using reflectance values from Landsat 8 OLI bands as predictors of The Gambia's Lower and Central River Region.

3.5.6 Map of Soil Salinity in LRR and CRRS

Originating in a mountainous region in Guinea, the River Gambia winds its way through Senegal, ultimately emptying into the Atlantic Ocean at Banjul, traversing the Gambia's entire length. The floodplains, extending from the sources of the river in the FUTA Jallon Highland to its mouth at the Atlantic Ocean, exhibit a noticeable increase in surface salinity towards the western regions.

This pattern suggests a westward trend of increasing salinity levels along the river basin. The salinization process in the floodplains follows a continuous uniform distribution, characterized by a gradual increase in soil salinity levels from the eastern to the western part of The Gambia, particularly in the coastal areas. This pattern is primarily driven by saltwater intrusion resulting from seepage from the Atlantic Ocean. Similar observations have been made in other river basin floodplain systems, supporting the influence of saltwater intrusion on soil salinity levels (Arslan & Demir, 2013; Bayabil et al., 2021).

The unique characteristics of the floodplain, including its relatively flat topography, shallow groundwater table, and high ratio of evaporation to precipitation, contribute to the accumulation of salt on the surface and subsequent soil salinization. The analysis reveals an increase in soil salinity levels in all categories in LRR, particularly in the upper slope of the floodplain.

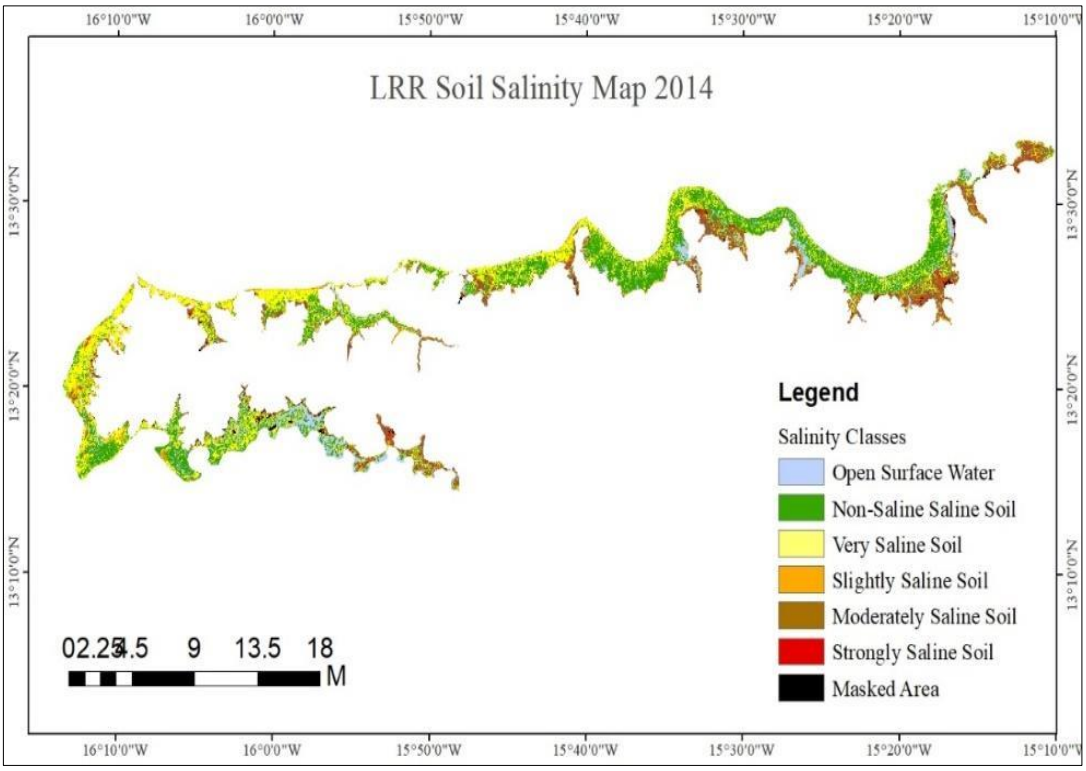

(a)

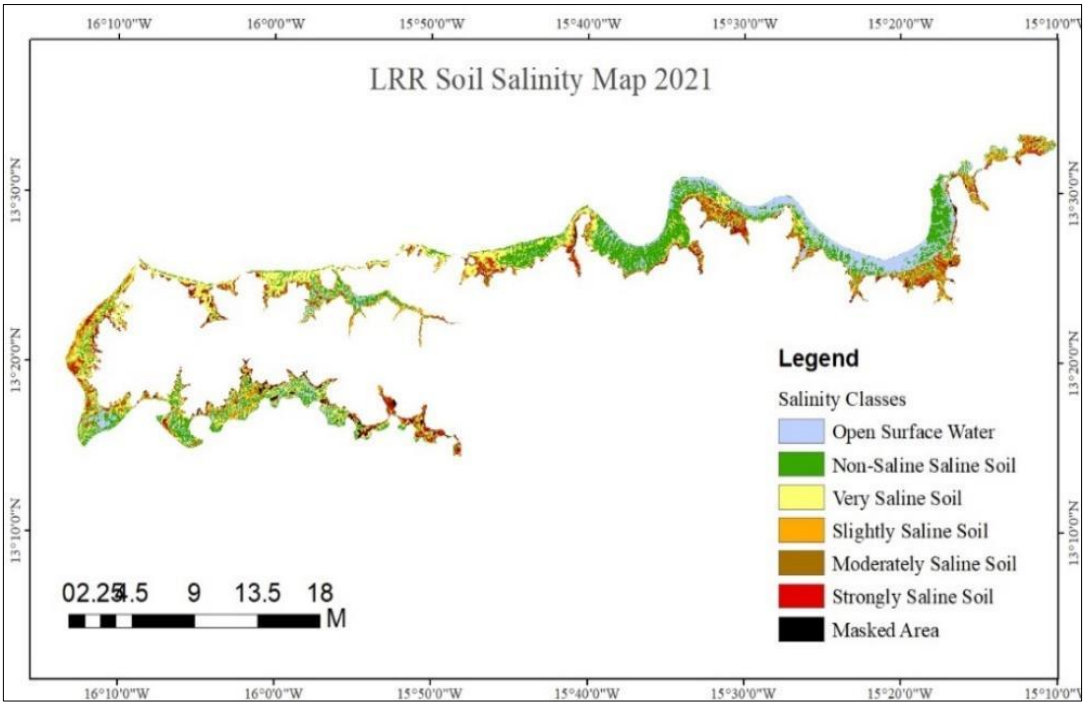

(b)

Figure 3. 8 Continuous spatial distribution of Soil Salinity in LRR using Random Forest a) 2014, b) 2021

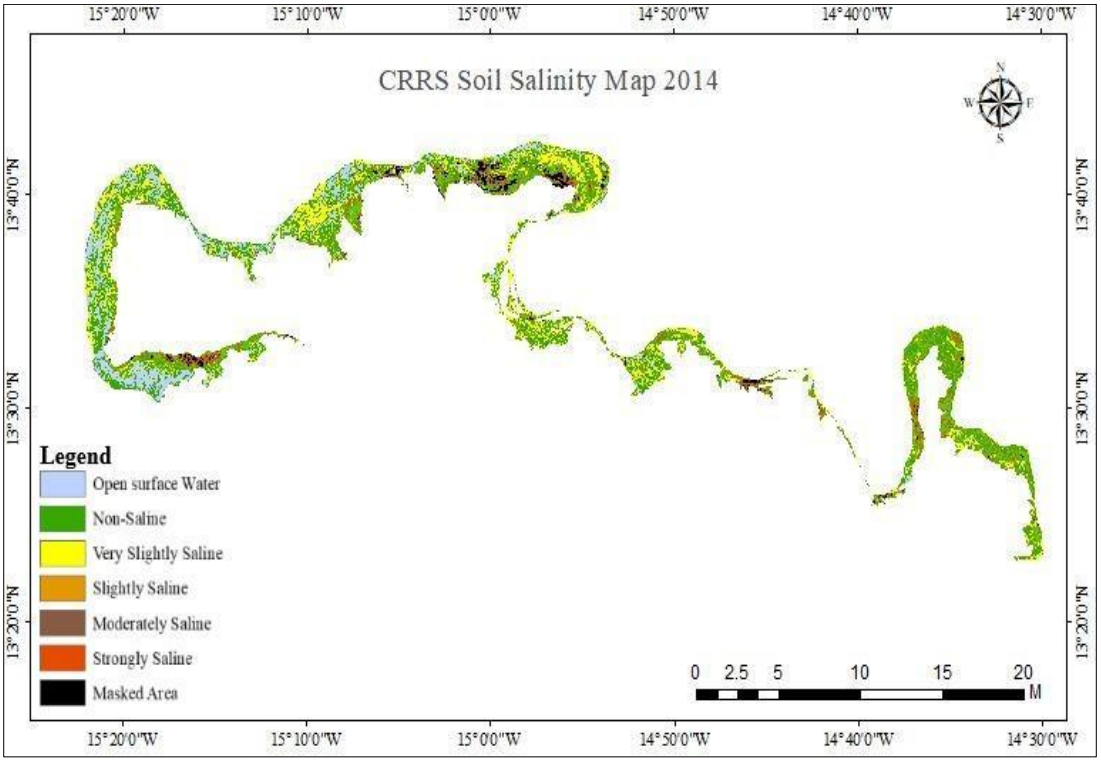

(a)

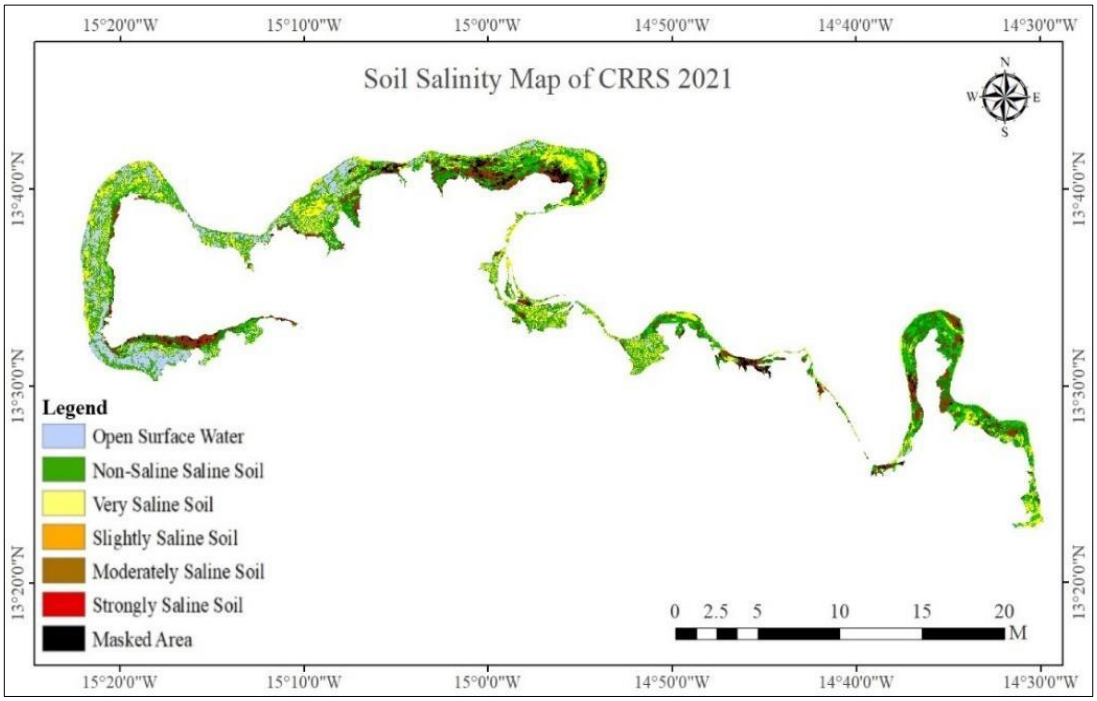

(b)

Figure 3. 9 Continuous spatial distribution of Soil Salinity in LRR using Random Forest a) 2014, b) 2021

Hotspot areas characterized by strongly saline soils (ECe dS/m >16) are found in the lower southern parts of LRR, farther away from the river channels, tributaries, and areas that experience regular flooding. The increasing trend of salinity upslope can be

attributed to the high evaporative effect in these areas. During the period of analysis within the CRRS, a predominant and continuous spatial distribution of the Very Slightly Saline salinity class was observed. Additionally, isolated hotspots featuring salinity classes ranging from slightly to moderately saline were detected in various parts of the region. Further investigations are required to ascertain whether these hotspots result from specific land management practices. Overall, there has been a noticeable reduction in salinization across all salinity classes in the CRRS region from 2014 to 2021. This trend might be attributed to an increase in rainfall patterns, as indicated by the findings of the Man-Kendall trend analysis.

The lower reaches of The Gambia River Basin experience high temperatures and a long dry season, leading to enhanced evaporation rates. Consequently, surface water in river channels, estuaries, and flooded areas evaporates rapidly, leaving behind concentrated salts and higher salinity levels. The absence of significant vegetation cover exacerbates the evaporative effect, contributing to the concentration of salts in the remaining water and the subsequent increase in salinity levels on the broader upslope of the floodplain.

The intensive and prolonged dry season in the Sudano-Sahelian climatic zone of the study area further limits vegetation cover. Although transpiration is reduced in areas with minimal vegetation, vegetation's absence allows direct and intense solar radiation to reach the surface, leading to heightened evaporation rates. This absence of significant vegetation cover further exacerbates the evaporative effect and contributes to the concentration of salts in the remaining water.

The combination of high temperatures, limited vegetation cover, and high evaporation rates results in unique surface features, such as salt entrustments, salt marshes, and wet desert islands. Increasing land surface temperature enhances evapotranspiration and rapidly accumulating salt in flat areas (Zhang et al., 2019). Masoud et al. (2014) pointed out that elevated land surface temperatures increase evaporation and evapotranspiration, accelerating salt accumulation in flat regions. This is per the conclusions drawn by Masoud et al. (2019), who investigated the factors influencing salinization in arid areas. They noted a consistent rise in high land surface temperatures near heavily salinized areas within flat depressions from 2001 to 2014.

As water evaporates, it leaves behind salt deposits, causing salt encrustment on the surface. Wet-desert islands refer to areas where the water table remains high due to limited drainage, resulting in localized wet areas surrounded by drier surroundings. These unique surface features are often characterized by high radiometric reflectance values, indicating the presence of salts at higher salinity levels. Tables 3.5 and 3.6 provide the distribution of salinity classes and their corresponding areas in hectares (ha) for the Lower River Region (LRR) and Central River Region (CRRS).

In the Lower River Region (LRR) floodplain, salinity classes with their corresponding areas for 2014 and 2021 show a total land area slightly decreased from 41,021 ha in 2014 to 40,541 ha in 2021, indicating a subtle shift in land cover or other regional factors such as climate. Similarly, for the periods under review, changes in soil salinity levels have led to significant shifts in land use and potential implications for agricultural practices. The water bodies within the region experienced a minor increase in area, growing from 220 ha (0.54 % of the total area) in 2014 to 375 ha (0.92 % of the total area) in 2021.

This change represents a 70.45 % expansion of open water bodies, likely influenced by hydrological variations, as indicated by the significant trend in rainfall observed in both regions (Figure 5.4). A substantial reduction was observed in the non-saline class, with the area decreasing from 5,159 ha (12.64 % of the total area) in 2014 to 3,786 ha (9.34 % of the total area) in 2021. This substantial decline of -26.67 % suggests a significant transition within this class, possibly due to changes in land use or shifts in hydrological regimes. In contrast, a remarkable increase occurred in the slightly saline category, growing from 10,618 ha (26.01 % of the total area) in 2014 to 13,446 ha (33.17 % of the total area) in 2021.

This change reflects a substantial percentage increase of 26.62 %, suggesting potential land usage shifts or adaptive agricultural practices in response to changing conditions. Moreover, the strongly saline areas exhibited growth, from 3,703 ha (9.07 % of the total area) in 2014 to 5,630 ha (13.89 %) in 2021. This change indicates a percentage increase of 51.94 %, suggesting ongoing dynamics within this highly saline range.

Table 3. 6 Dynamics of soil salinity in LRR for two periods (2014 and 2021)

Year Soil Salinity Class	EC_e (dS/m)	2014		2021		% Change
		Area (ha)	% Land Area	Area (ha)	% Land Area	
Open Water	NA	220	0.54	375	0.92	70.45
Non-Saline	0–2	5,159	12.64	3,786	9.34	-26.67
Very Slightly Saline	2-4	16,349	40.05	8,443	20.83	-48.32
Slightly Saline	4-8	10,618	26.01	13,446	33.17	26.62
Moderately Saline	8-16	4,312	10.56	8,093	19.96	87.56
Strongly Saline	> 16	3,703	9.07	5,630	13.89	51.94
Masked Area	NA	660	1.62	768	1.89	16.36

The regions categorized as Masked areas, which include non-cultivable lands such as rock outcrops or hardpans, access roads, and farmhouses, saw an expansion from 660 ha (1.62 % of the total area) in 2014 to 768 ha (1.89 % of the total area) in 2021. This represents a 16.36 % increase in the area of these masked areas, where no salinity measurements were taken.

Table 3.5 presents the changing soil salinity characteristics within the Central River Region (CRRS) between 2014 and 2021. The results highlight shifts in salinity levels and their potential implications for land use and agricultural productivity. As in LRR, open surface water bodies within the CRRS displayed notable changes, expanding from 484 ha (1.49 % of total area) in 2014 to 571 ha (1.80 % of total area) in 2021. This considerable increase of 17.98 % suggests hydrological dynamics that have influenced the distribution of open water areas.

The Non-saline areas in the CRRS saw a minor increase, growing from 6,648 ha (20.41 % of total area) in 2014 to 6,910 ha (21.73 % of total area) in 2021. This change corresponds to a moderate percentage increase of 3.94 %, indicating stability within this class. Similarly, the very slightly saline areas experienced a small expansion, increasing from 8,221 ha (27.62 % of the total area) in 2014 to 8,408 ha (26.53 % of the total area) in 2021. This shift reflects a modest percentage increase of 2.27 %, suggesting relative stability within this salinity range. Similarly, the very slightly saline areas experienced a slight expansion, increasing from 8,221 ha (27.62 % of total area) in 2014 to 8,408 ha (26.53 % of total area) in 2021.

Table 3. 7 Soil salinity dynamic in CRRS for two periods (2014 and 2021)

Year	**2014**			**2021**		
Salinity Class	Ece (dS/m)	Area (ha)	% Land Area	Area (ha)	% Land Area	**% Change**
Open Water	NA	484	1.49	571	1.80	17.98
Non-Saline	0 - 2	6648	20.41	6910	21.73	3.94
Very Slightly Saline	2 - 4	8221	25.25	8408	26.53	2.27
Slightly Saline	4 -8	8995	27.62	8193	25.76	-8.92
Moderately Saline	8 - 16	5349	16.43	4212	13.24	-21.26
Strongly Saline	>16	927	2.85	1050	3.30	13.27
Masked Area	NA	1939	5.95	2460	7.73	26.87

This shift reflects a modest percentage increase of 2.27 %, suggesting relative stability within this salinity range. The moderately saline regions experienced a significant reduction, decreasing from 5,349 ha (2.85 % of total area) in 2014 to 4,212 ha (13.24 % of total area) in 2021. This substantial change reflects a percentage decrease of -21.26 %, indicative of pronounced differences within this class. The strongly saline areas exhibited a modest increase, growing from 927 ha (5.95 % of total area) in 2014 to 1,050 ha (3.30 % of total area) in 2021. This change signifies a percentage increase of 13.27 %, suggesting ongoing dynamics within this highly saline range. The masked areas of CRRS expanded from 1,939 ha (19.25 % of total area) in 2014 to 2,460 ha (7.73 % of total area) in 2021. This change represents a 26.87 % increase in these areas, underscoring the importance of understanding and managing these regions for sustainable land utilization.

In both the Lower River Region (LRR) and the Central River Region South (CRRS), the analysis of combined salinity classes reveals varying patterns of salinity distribution and their implications for land use. However, these two regions exhibit different trends in how salinity has changed. In the Lower River Region (LRR), the

combined area covered by all saline categories was 27,078 hectares in 2014, constituting approximately 66.34 % of the entire region. By 2021, this combined area had expanded to 29,669 hectares, representing around 72.15 % of the territory. This indicates a percentage change of 9.56 % over the analyzed period.

In contrast, the Central River Region South (CRRS) exhibited a different pattern. In 2014, the combined area covered by these salinity classes accounted for 29,572 hectares, constituting about 93.46 % of the total region. However, by 2021, this combined area had contracted to 25,455 hectares, representing approximately 80.29 % of the region. This indicates a percentage change of -13.94 % over the analyzed period.

3.6 SUMMARY

The study successfully utilized regression models and Landsat OLI 8 reflectance data, along with Salinity Indices (SI) reflectance, to predict and delineate spatiotemporal variation of soil salinity in Lower River Region (LRR) and Central River Region South (CRRS), The Gambia. The Random Forest (RF) model emerged as the most effective predictor, demonstrating high accuracy and reliability in estimating soil salinity based on Landsat 8 reflectance values.

LRR faces potential ecosystem degradation and agricultural impacts from declining non-saline areas (-26.67 %), while the expansion of slightly saline soils (26.62 %) challenges agricultural diversification. The contraction in Slightly Saline (-8.92%) and Moderately Saline (-21.26%) areas in CRRS presents distinct challenges and opportunities for agricultural productivity and ecosystem preservation.

For the period under review (2014 -2021), LRR indicates a percentage % increase in salt-affected areas of 9.56 %. The noticeable expansion of these salinity classes underscores the evolving nature of cover and ecosystem dynamics in the LRR, potentially influencing agricultural practices and the ecological balance. In contrast, the results show a percentage contraction of 15.54 % in the salt-affected area in CRRS. The shift in these salinity class distributions highlights potential changes in land management practices and ecosystem health in the CRRS, which may affect agricultural productivity and sustainable land utilization.

CHAPTER FOUR
VARIABILITY OF ROOT-ZONE SALINITY ON RICE YIELD[2]

ABSTRACT

Rice cultivation in the floodplain of the River Gambia in The Gambia faces significant challenges due to soil salinity, resulting in grain yield reduction. Soil salinity poses substantial obstacles to agricultural production in this region. This study aimed to analyze the impact of seasonal variability in root-zone salinity on rice yield under farmer-managed fields in CRRS and LRR, The Gambia. The research focused on soil properties, groundwater level and quality, and their influence on soil salinity. The initial physicochemical characterization of the soil revealed clay texture with low pH values (ranging from 4.1 to 4.3) and high electrical conductivity (ECe), indicating highly acidic and saline conditions, respectively. The exchangeable sodium percentage (ESP) values were also relatively high, indicating the presence of sodic soils. Correlation analysis highlighted significant relationships between soil variables, groundwater quality, and levels, and their correlations with rice growth and yield, showing their influence on soil salinity. GLM demonstrated strong goodness of fit (R2 = 0.98), indicating that high ESP variability could be attributed to specific field locations, soil properties, and seasonal factors. Tonitaba and Kudang exhibited significant and opposing influences on soil ESP, with Tonitaba associated with an increase (0.84994) and Kudang with a decrease (-1.18268). At the same time, the analysis also revealed a statistically significant ($p < 0.05$) reduction in ESP during August, indicating a seasonal effect. Nonparametric MANOVA analysis demonstrated substantial differences in rice yield across treatment groups ($p < 0.05$). Multiple comparison tests showed significantly higher rice yields of 254(kg/ha) in Kudang than in Mandina. The study, emphasizing the importance of understanding specific soil variables critical in influencing root zone salinity, provides valuable insights for sustainable rice production in mangrove swamp areas and informs evidence-based decision-making in rice farming in The Gambia. The study recommends adopting and applying suitable soil amendments, implementing effective drainage systems, selecting salt-tolerant and short-duration rice varieties, and regularly monitoring soil physicochemical properties. Further research should investigate the long-term trends

[2]A manuscript has been developed from this chapter to be publish in a journal

and effects of various soil salinity management strategies, including the impact of specific practices on soil salinity.

Keywords: Root-zone; Salinity; Nonparametric MANOVA; ESP

4.1 INTRODUCTION

This chapter focuses on the impact of soil salinity on agricultural production, particularly in the context of rice cultivation in the floodplain of the River Gambia in Gambia. Soil salinity significantly threatens agricultural production and ecosystems worldwide, especially in arid and semiarid regions where irrigation is used to grow crops (Corwin and Scudiero, 2019; Tian et al., 2020).

In Africa, soil salinity poses a significant challenge to small-scale agriculture, with approximately 1,899 million hectares of land affected by salinity (Aredehey et al., 2018; Bannari et al., 2021).

The Sahel region in West Africa, including The Gambia, is particularly impacted. The increasing salinization of farmland significantly threatens the long-term sustainability of food production and productivity systems (Li and Kang, 2020). Its direct impact on cultivated lands is evident in crop failures while triggering other forms of land degradation, such as soil dispersion, waterlogging, amplified soil erosion, and hindering engineering programs (Metternicht and Zinck, 2003; Fan et al., 2016). These consequences further compound the challenges of the growing global population and the demand for increased arable lands to meet future food requirements (Fan et al., 2016).

Global climate change further exacerbates the challenges associated with soil salinity. It is projected to reduce crop yield and freshwater resources through alterations in hydrologic cycles by the end of the 21st century (Bodian et al., 2018; Talat, 2020). Using the River Gambia as an irrigation water source plays a vital role in agricultural development in The Gambia, addressing water scarcity and food security concerns (Jarju, 2009). However, the interrelationship between seasonal flow and salinity limits its potential. The reduction in streamflow contributes to the salinity increment in rivers and estuarine waters (Njie and Corr, 2006). During the long dry season, low flow and saline water intrusion upstream restrict the availability of suitable flood plains for rice production.

Rice is susceptible to salt, with most cultivated species showing a tolerance limit of 3 dS/m, beyond which their yield declines (Hoang et al., 2016; Rahman et al., 2019; Mariama, 2019). Consequently, this susceptibility to salinity stress poses significant challenges for rice during critical growth stages, resulting in reduced grain yield (Asch & Wopereis, 2001; Talat, 2020). In The Gambia, lowland rice is primarily cultivated by raising seedlings in salt-free conditions and then transplanting them into the fields. Salinity becomes a recurring problem as the dry season approaches, coinciding with critical growth stages like panicle formation and flowering, resulting in reduced grain yield (Fahad et al., 2019).

According to Baggie et al. (2018), soil salinity tends to be elevated at the start of the rainy season, a critical period for seedling establishment. Such salt-affected soils often contain high levels of sodium ions Na^+, which can harm rice plants' proper growth and development. Excess Na^+ in the soil can negatively impact photosynthesis, reducing plant growth, lowering chlorophyll content, and disrupting various metabolic processes (Munns and Gilliham, 2015; Rahman et al., 2019).

This study aims to analyze rice yield under seasonal variability of root-zone salinity in the lowland rice production areas of LRR and CRRS in The Gambia. It seeks to address the research gap regarding rice production in saline conditions and contribute to knowledge about sustainable rice cultivation in salinity-affected regions. Additionally, the research investigates the influence of groundwater fluctuation and quality on soil root zone salinity during the rice growing season to understand the impact of environmental factors and potential management strategies. The study's findings are expected to provide valuable insights into enhancing rice productivity and promoting regional food security.

4.2 Material and Method

4.2.1 Site Selection

Five study sites/fields were selected to assess the seasonal variability of root zone soil salinity, rice production, and yield under farmer management systems across LRR and CRRS. Figures 3.1a and b show the floodplain in LRR and CRRS with studies of farmer fields, soil sample collection points, and groundwater monitoring networks. The site was selected based on the track history of the National Agricultural Research Institute's (NARI) research activities in the rice production zones of the two regions. Similarly, an initial reconnaissance tour was conducted to verify which communities are actively involved in rice production.

4.2.2 Soil Data

The initial soil characterization of the study area was conducted during the dry season in May/April, providing a baseline assessment of the soil conditions before the rainy season. During the growth season of rice, spanning from June to October, repeated measurements of soil variables were collected to capture the significant changes in soil characteristics expected during this period. Soil samples were collected from three landforms in the study area: river swamps, tidal flats, and colluvial flatlands.

A survey plot of 300 m^2 was established at the beginning of the growing season to ensure representative sampling. Within this plot, three permanent sub-sampling quadrats of 1 m^2 each were designated along a 100 m transect. Soil samples were taken at 0-30 cm depths, corresponding to the root zone, at different physiological growth stages of rice.

4.2.3 Agronomic Data

In addition to soil sampling, data was collected on various agronomic variables throughout the rice crop's growth stages. This included measurements of plant density, height, and the number of tillers. Yield and yield components, such as filled grain, unfilled grain, 1000 grain weight, and grain weight in kg/ha, were assessed from the sub-sampling plots within the 1 m^2 quadrats. All panicles within the quadrat were removed, threshed, and weighed to obtain the dry grain weight and adjusted to a moisture content of 14 %.

4.2.4 Groundwater

During the 2021 rice growing season, an assessment was conducted to investigate the effects of groundwater fluctuation and quality on soil root zone salinity in alluvial soils of a lowland tidal floodplain of LRR and CRRS, The Gambia. A groundwater salinity observation network was constructed at each sub-sampling plot in the five community fields. Wells were dug using auger drilling, fitted with PVC pipes (50 mm in diameter), and screened at the bottom with an outer lining of cloth material. PVC pipes were extended 0.5 - 1 m above the ground level to avoid the inflow of surface water, depending on the depth of the surface water during tidal inundation.

In total, 15 piezometers were installed (1 m depth) from the surface to the groundwater levels. Groundwater level measurements and water samples were collected in the middle of every month for the study period to determine their influence on root-zone soil salinity. Groundwater levels were measured at regular intervals using a groundwater level sensor. Water samples were collected using cleaned sample bottles rinsed with distilled water. Samples were sent to the Central Water Quality Monitoring Laboratory Division, Department of Water Resource, Ministry of Fisheries and Water Resources, The Gambia. The water samples were analyzed for physicochemical parameters such as pH, total dissolved solids (TDS), and electrical conductivity (EC).

4.3 Laboratory Analysis

The soil samples collected in polyethylene bags labeled for laboratory analyses were air-dried, crushed, and passed through a 2 mm sieve. According to Soil Survey Staff (2014), the soil analyses were performed.

4.3.1 pH

The pH can be defined as the negative logarithm (base 10) of the activity of hydrogen ions (H^+) at 25°C. The pH value depends on the features of the soil, concentration of dissolved CO_2, and moisture content. The pH of the soil samples was determined using the saturation paste method (pHs) using 1:2.5 soil-water suspension and measuring the pH of the resulting mixture. The pH meter was calibrated using Standard buffer solutions of pH 7.0 and 9.2 before the analysis. The saturated soil paste was allowed to stand for at least one hour, and then the electrodes were inserted into the paste to measure and record the pH reading.

4.3.2 Electrical Conductivity

The electrical conductivity (EC) of the saturation extract (ECe) was determined to assess the soil's salinity. EC is defined as the reciprocal of electrical resistivity and is expressed in reciprocal ohms per cm (mhos per cm). A standard potassium chloride solution was prepared by dissolving 1.4912 g of KCl in water to make a 1-liter solution with an electrical conductivity of 2.768 dS/m at 25°C. The analysis procedure consisted of two steps:

(a) Determination of cell constant: The conductivity cell was rinsed and filled with the standard 0.02 N KCl solution. The cell constant (K) was determined by measuring the electrical conductance (C) of the standard KCl solution. The equation for determining K was:

$$K = L / C \qquad \text{... equation (4.1)}$$

where L is the standard solution's known specific electrical conductance (dS/m)

(b) Determination of conductivity of saturation extract: The cell was rinsed and filled with the saturation extract of the soil sample, and its conductance was recorded. The specific conductance (dS/m) was calculated using the equation:

$$Lt = K \times C \qquad \text{... equation}(4.2)$$

where Lt is the electrical conductivity of the test solution

The temperature factor (ft) was considered to correct the conductivity value to 25°C:

$$L25 = Lt \times ft \qquad \text{... equation}(4.3)$$

4.3.3 Cations and Anions Analysis

Specific methods were employed to determine the concentrations of cations and anions in the soil-saturated paste. A flame photometer measured the exchangeable sodium (Na^+) and potassium (K^+) in the soil paste extracts. The concentrations of calcium (Ca^{2+}) and magnesium (Mg^{2+}) were determined using standard titration techniques with the use of ethylenediaminetetraacetic acid (EDTA) as the titrant and Eriochrome Black T as the indicator. In these extracts, the concentrations of Na^+ and K^+ were measured using the flame photometer, while the attention of Ca^{2+}, Mg^{2+}, Cl–, $HCO^3{}^-$, and $CO_3{}^{2-}$ were determined using standard titration methods. The exchangeable sodium (Ex. Na) was determined using the ammonium acetate at pH 7.0 method. Include $SO_2{}^4$ (meq/100g) and Cl^- (meq/100g).

4.4 Statistical analyses

Before data analysis, all data sets were assessed for multivariate normality using the multivariate Shapiro-Wilk test for each group in the independent variable field and sampling time. The Shapiro-Wilk test evaluates the hypothesis that the data distribution deviates from a multivariate normal distribution. If the resulting p-value is less than 0.05, indicating a significant difference from normality, we reject the multivariate normality hypothesis. Conversely, if the test is non-significant ($p > 0.05$), we accept the normality hypothesis and conclude that the sample follows a normal distribution. Box's M test was performed for each combination of groups in the independent variables to evaluate the homogeneity of variance-covariance matrices. This test examines the null hypothesis that the variance-covariance matrices are equal for each combination of groups. If the resulting p-value is less than 0.05, it suggests that variations in sample variances are not likely to have occurred based on random sampling. Consequently, the null hypothesis of equal variances is rejected, providing evidence to conclude that variances differ in the population.

4.4.1 Correlation and Regression Analysis

Correlation analysis is an essential statistical procedure used to investigate the relationships among variables (Senthilnathan, 2019). In this study, Pearson's product-moment correlation analysis was conducted among individual soil physicochemical properties, groundwater quality, agronomic variables, yield, and yield components of rice. The purpose was to characterize the relationships between these variables and determine their influence on root zone salinization and yield of rice in the mangrove swamp rice production areas in the Lower River Region (LRR) and Central River Region South (CRRS).

The correlation analysis allows us to identify significant associations between soil properties, groundwater quality, agronomic variables, yield, and yield components, providing insights into the interplay of these factors in root zone salinization and rice yield. Furthermore, multiple linear regression was employed to examine the relationship between the EC_e (dS/m) within the root zone and soil physicochemical properties, groundwater quality, agronomic variables, sampling time, and site. This analysis enables us to quantify the contributions of each independent variable and assess their significance in explaining variations in root zone salinization. Sampling

month and site as independent variables to determine the effects of different seasons and locations along the middle-reach River Gambia. The correlation and multiple linear regression analyses comprehensively understand the relationships between salinity, soil properties, month of the season, different locations, and rice yield. These analyses are crucial in elucidating the factors influencing root zone salinization and guiding effective management strategies for sustainable rice production in the mangrove swamp areas.

4.4.2 Nonparametric Multiple Analysis of Variance (MANOVA)

Nonparametric Multiple Analysis of variance (MANOVA) was used to analyze differences among study fields in soil physicochemical properties, groundwater quality, and agronomic variables (Plant density, plant height, number of tillers, grain yield per meter, and yield in kg/ha) at various physiological growth stages of rice. The MANOVA is an analysis of variance (ANOVA) that has two or more dependent variables (Warne, 2014), which is a mathematical extension of ANOVA applied to situations where there is more than one dependent variable (Zientek and Thompson, 2009; Warne, 2014).

The null hypothesis for this study is that the two or more independent variables are equal on the soil physicochemical and rice agronomic dependent variables. In other words, all groups' mean vectors are the same. The alternative hypothesis, on the other hand, states a significant difference between the means of the groups compared, indicating that the group mean vectors are not the same for all groups.

Hypotheses:

Null hypothesis (H_0): All groups' mean vectors are identical

Alternative hypothesis (H_1): All groups' mean vectors differ

Based on classical procedures, the null hypothesis in MANOVA is tested against the alternative hypothesis using a statistical test, such as the Wilks' Lambda test, Pillai's Trace test, Lawley-Hotelling, Roy's largest root, or generalized linear mixed models (Davis, 2002; Anderson, 2001; Johnson and Wichern, 2007). Classical MANOVA approaches, on the other hand, are based on the assumptions of equal covariance matrices for each group and multivariate normality. Which may not be attainable in

actual data (Ellis et al., 2017). These assumptions are difficult to verify, leading to inflated type-I errors, especially with small sample sizes and increased dimensions. Furthermore, traditional MANOVA approaches do not give consistent information on which subsets of response variables or factor levels are responsible for the overall significance (Woodrow et al., 2017).

To overcome these limitations, several alternative methods have been developed, including simulation studies (Friedrich et al., 2017; Livacic-Rojas et al., 2017; Friedrich and Pauly, 2017) and nonparametric rank-based approaches (Ellis et al., 2017). Nonparametric rank-based methods are preferred when the assumptions of multivariate normality or homogeneous covariance matrices are not satisfied (Kherad-Pajouh and Renaud, 2015; Konietschke et al., 2015). These methods provide robust and applicable statistical inferences for all data types, including factorial repeated measures, split-plot design, and longitudinal data (Akritas, 2011).

In this study, nonparametric multivariate analysis was conducted using the R package "npmv" to overcome the limitations of classical MANOVA (Ellis et al., 2017). The "npmv" package provides a nonparametric approach that complements the global test with a comprehensive means of identifying significant response variables and factor levels while controlling the familywise error rate (Ellis et al., 2017). The package computes global nonparametric test statistics, p-values for each statistic, and nonparametric relative treatment effects using the F approximation and permutation (randomization) method (Woodrow et al., 2017).

The relative effects quantify the tendencies observed in the data regarding probabilities. Specifically, the Relative Treatment Effect (RTE) for treatment "k" is characterized as the likelihood that an individual chosen at random from treatment group "k" exhibits a superior response compared to an individual randomly selected from any of the treatment groups, including treatment "k" itself (Cohen, 1992; Acion et al., 2005; Sullivan & Feinn, 2012; He et al., 2017).

A permutation test (also known as a randomization test) is employed to determine if there is a significant difference between the groups by re-assigning the observations to the groups at random and calculating the test statistic for each re-assigned data set (Basso and Salmaso, 2011; Pesarin and Salmaso, 2012). Multiple comparisons of the different multivariate samples were conducted using a subset algorithm comprising

factor levels and variables to determine which variables or factors contribute to the significant differences (Liu et al., 2011; Ellis et al., 2017).

4.5 RESULTS AND DISCUSSION

4.5.1 Initial Soil Physicochemical

Table 4.1 shows the initial physicochemical properties of soil in the rice production zones of the River Gambia floodplain in LRR and CRRS South of the study area. The soil's particle size distribution and textural composition in the study area was mainly clay. An essential characteristic of the local classification system of alluvial soils is the high proportion of silt and clay, usually greater than 80 % (Dunsmore et al., 1976).

The results show the varying composition of silt between the different fields, which also varies along with clay and sand content in the 30 cm surface horizon. The variable textural distribution of clay and silt suggests much of the variations are probably depositional, with little influence on pedogenesis from the textural profile (Peat et al., 1979). The land resource survey (1976) indicated that while the alluvial soil has a narrow structure with less surface layer, the underlying soils commonly show strong or very strong blocky structures, which may become coarser with depth (Dunsmore et al., 1976).

Likewise, according to Sylla (1994), the development of soil profiles in a mangrove environment is primarily influenced by physical processes such as soil structure formation, shrinkage, ripening, subsidence, and desalinization. Additionally, chemical processes like oxidation and decalcification play a significant role. As much as between 8 - 12 % sand compositions are recorded in Pakaliba and Kudang. This might be due to coarse-textured colluvial material overlaying finer-textured layers. For example, Thornton and Giglioli (1965) reported the presence of sandy layers in some parts of the mangrove swamps of Keneba.

Table 4. 1 Initial physicochemical composition of soil in swamp rice production zones

Properties	Mandina	Tonitaba	Buiba	Pakaliba	Kudang
pH	4.2	4.2	4.3	4.2	4.1
EC_e (dSm/m)	8.5	9	7.5	7	3
SAR	9.50	11.26	18.64	19.23	0.32
ESP (%)	39.4	39.3	34.1	31.1	6.9
Ca^{+2} meq/100g	3.9	4.35	6.15	5.1	4.1
Mg^{+2} meq/100g	5.5	6	11	14	0.4
Na^{+} meq/100g	6.2	7	9	8.8	0.3
K^{+} meq/100g	0.2	0.48	0.25	0.22	0.1
Cl^{-} meq/100g	787	543	328	328	180
SO_2^4 meq/100g	6.8	7.39	8.1	5.48	4
Particle size distribution					
% Sand	5.96	7.96	6.0	8.0	12.0
% Silt	8.44	6.44	12.0	12.0	12.4
% Clay	85.6	85.6	82.0	80.0	75.6
Clay + Silt	94.04	92.04	94.0	92.0	88.0
Textural Class	Clay	Clay	Clay	Clay	Clay

Note: ECe = Electrical conductivity of saturated soil extract; ESP=Exchangeable Sodium Percentage; all cations and ions are measured in meq/100g

The mean values of the initial physicochemical composition of soil taken in April in the swamp rice production zones of LRR and CRRS show low pH values ranging from 4 to 4.3. Additionally, high concentrations of SO_2^4 indicate highly acidic sulfuric conditions. These observations are consistent with acid sulfate soils, characterized by highly acidic conditions resulting from sulfuric acid, iron, and aluminum sulfates derived mainly from marine sediment and pyrites. The oxidation of pyrite (FeS_2) in marine sediments leads to sulfates and sulfuric acid (H_2SO_4) formation, contributing to the extreme acidification of acid-sulfate soils.

The soil electrical conductivity (ECe) values from saturated extract indicate values exceeding 4 dS/m for all sites except Kudang, where a value of 3 was recorded. The high ECe values in most fields correspond to a high exchangeable sodium percentage (ESP) above the threshold for classifying soil as sodic (> 15 %). Na^{+} is the dominant cation for exchangeable cations, followed by Mg^{2+}, Ca^{+2}, and K^{+} in Mandina and Tonitaba. In Buiba and Pakaliba, magnesium is the predominant cation, followed by Na^{+}, Ca^{+2}, and K^{+}. Similarly, the two fields express sodicity conditions, showing SAR

values of 18.64 and 19.23, respectively. Kudang, on the other hand, exhibits a non-saline, strong acid condition where calcium forms the dominant cation. These observations suggest an eastward decrease in conductivity values, indicating the influence of seawater intrusion.

The combination of low pH values, high SO_2^4 concentrations, and elevated ECe and ESP values in specific fields signifies the presence of soil conditions that may pose challenges for vegetable and rice production. The variability in soil properties across the sites reflects the complex interactions between soil characteristics and environmental factors in the rice production zones of the floodplain in LRR and CRRS.

4.5.2 Determinants of soil salinity in the lowland Floodplain of LRR and CRRS

The correlation between soil physicochemical properties indicates soil pH has a strong significant (p-values <0.001) negative relationship with EC_e, Na^+, and ESP. Soils with lower pH (acidic soils) indicate a considerable amount of hydrogen ions and show a higher rate of electrical conductivity (Bruckner, 2012). Although pH significantly affects EC, soil conductivity is influenced by several other factors, including soil texture, mineral composition, organic matter content, porosity, soil moisture, and soil temperature (USDA, 2011; Mohd-Aizat et al., 2014).

Similarly, soil ECe has a strong, significant positive relationship with Na^+ (r= 0.7) and ESP (r= 0.89), whereas ESP and Na^+ recorded a similar relationship (r= 0.58), as expected (Table 4.2). A significant negative correlation exists between the Ca^{+2} and Na^+ content of the soils in the study area, meaning an increase in Ca^{+2} will lead to a decrease in the Na^+ composition of the soil. This is important for their management since reclaiming these soils aims to bring the soil ESP below the threshold value of 15 %. This can be attained by adding amendments that increase the concentration of calcium ions (Ca^{+2}) in the soil.

Table 4. 2 Pearson's correlation matrix of physicochemical properties of soil in the floodplain of CRRS and LRR, The Gambia.

Variable 1	Variable2	r	95 %	CI	t	p-value
pH	EC_e(dS/m)	-0.64	-0.75	-0.48	-7.05	< .001***
pH	Na^+	-0.45	-0.61	-0.24	-4.26	< .001***
pH	ESP (%)	-0.57	-0.71	-0.4	-5.96	< .001***
EC_e(dS/m)	Na^+	0.7	0.56	0.8	8.3	< .001***
EC_e(dS/m)	ESP (%)	0.89	0.82	0.93	16.28	< .001***
Na^+	ESP (%)	0.85	0.77	0.9	13.84	< .001***
Ca^{+2}	Na^+	-0.24	-0.01	-0.44	-2.09	0.040*
EC_e(dS/m)	K	-0.25	-0.45	0.2	-2.19	0.031*
EC_e(dS/m)	Mg^{2+}	-0.5	-0.65	-0.31	-4.95	< .001***
K^+	Mg^{2+}	0.31	0.09	0.5	2.75	0.008**
K^+	ESP (%)	-0.3	-0.50	0.8	-2.73	0.008**
Mg^{+2}	ESP (%)	-0.47	-0.63	-0.2	-4.58	< .001***

All other cations (K^+ and Mg^{2+}) composition of the soil show weak to medium negative significant ($p < 0.05$) correlation between soil EC_e and ESP. A similar correlation analysis was conducted on soil and groundwater parameters, and the results show that soil physicochemical properties and groundwater quality are highly correlated (Table 4.2). Soil ECe and groundwater ECw show a significant positive correlation value of 0.84 and a p-value of <0.001, and ESP increases with an increase in the groundwater level depth (r=0.41). This is in line with the findings of Feng et al. (2017), who reported a rise in ECe values within the root zone with an increase in water salinity at a constant drain depth. Similar significant (p-value <0.001) strong positive relationships were observed between soil Na^+ and ESP. In contrast, a significantly weak and moderate negative relationship is observed between EC_w and K^+, EC_w, and Mg^{+2} with correlation values of r= -0.25 and r= -0.53, respectively.

Generally, soil physiochemical properties indicated a strong relationship with the groundwater quality due to the shallow nature of the groundwater levels of the study area. For example, Xu et al. (2013) reported that high water tables favored capillary rise due to high climatic evaporative demands, resulting in the buildup of salts in the

root zone. These results indicate that the composition and physical properties of soil, the movement, and the quality of groundwater affect each other.

Soil porosity and permeability affect the water infiltration rate, and soil's chemical composition affects the chemical exchange rate with groundwater. Furthermore, soils absorb and adsorb contaminants, which can then be released into groundwater. As a result, changes to soil physicochemical properties can have a direct effect on the quality of groundwater. Additionally, aside from the direct influence of brackish water, shallow and saline groundwater tables in the low-lying areas of river floodplains allow upward movement of salt to the root zone through capillary action in the soil profile and rapid evaporation (Mahajan et al., 2015).

Results of multiple linear regression analysis to examine the relationship between ESP within the root zone and soil properties, sampling time, and site are shown in Table 8. The performance of the multiple linear regression model for predicting ESP across Site/Field was assessed through the coefficient estimates obtained from the generalized linear model. For Tonitaba, the coefficient estimate was 0.85 with a standard error of 0.28, resulting in a t-value of 3.031. The p-value of 0.0036 indicated a statistically significant relationship between Tonitaba and ESP, demonstrating that each unit increase in Tonitaba is associated with an 85 % increase in ESP (Table 4.4). On the other hand, the coefficient estimate for Kudang was -1.18, with a standard error of 0.41, leading to a t-value of -2.861. The p-value of 0.006 indicated a statistically significant relationship between Kudang and ESP, suggesting that each unit increase in Kudang is associated with a decrease of 1.18 in ESP. The significant coefficients for Tonitaba and Kudang indicate that these site/field locations substantially affect soil ESP. However, it is worth noting that the coefficient estimates for the two sites have opposite signs, indicating different effects on ESP.

Table 4. 3 Pearson's correlation matrix of physicochemical properties and groundwater in the floodplain of CRRS and LRR, The Gambia

G-Water	Soil	r	95 %	CI	t	p-value
EC_w	$pH(H_2O)$	-0.63	-0.75	-0.47	-6.93	< .001***
EC_w	EC_e	0.84	0.76	0.9	13.41	< .001***
EC_w	Na^+	0.6	0.43	0.73	6.38	< .001***
EC_w	ESP (%)	0.79	0.69	0.86	11.15	< .001***
EC_w	K^+	-0.25	-0.45	0.3	-2.23	0.028*
EC_w	Mg^{+2}	-0.53	-0.67	-0.34	-5.3	< .001***
Depth	Mg^{+2}	-0.53	-0.68	-0.35	-5.36	<.001***
Depth	ESP (%)	0.41	0.2	0.58	3.79	<.001***

G-W = Groundwater (mS/cm) , EC_w = EC Groundwater (mS/cm)

Tonitaba is associated with an increase in ESP, while Kudang is related to a decrease. These findings suggest that as one moves westward from Tonitaba towards the Atlantic Ocean, there is an expected increase in soil ESP.

Conversely, moving eastward beyond Kudang would decrease ESP by approximately 1.2 %, assuming all other site factors remain constant. The model's goodness of fit was strong, with an R-squared value of 0.98, which indicates that approximately 98.55 % of the variability in the ESP can be explained by the predictor variables in the model. The August coefficient estimate was -1.16, showing a statistically significant negative relationship with ESP. This means that, on average, each unit increase in sampling time during August is associated with a decrease of 1.16 in ESP. The t-value of -3.15 for August further confirms the statistical significance of this relationship, with a p-value of 0.0026, indicating strong evidence to reject the null hypothesis. Thus, ESP tends to decrease during August.

For September, the coefficient estimate was -0.95, suggesting a negative relationship with ESP. Still, with a p-value of 0.060, the t-value of -1.91 does not reach the conventional level of statistical significance ($p < 0.05$). This means that the relationship between ESP and sampling time in September is not statistically significant at the traditional level ($p < 0.05$).

Table 4. 4 Results of multiple linear regression for ESP prediction based on soil variables, sampling dates, and sites

Dep Variable	ESP		R-square		0.9855
Model	GLM		Adj. R-square		0.9855
Method	Least Squares		F-statistic:		245.9
No Observation	63		Prob (F-statistic):		245.9
Df. Residuals	58		p-value:		0.00002
Df. Model	16		R. std error		0.6317
Coefficients:	Estimate	Std. Err	t value	Pr(>|t|)	Sign
(Intercept)	11.79	1.11	10.57	0.004	***
Tonitaba	0.85	0.28	3.03	0.004	**
Kudang	-1.18	0.41	-2.86	0.006	**
August	-1.15	0.37	-3.15	0.001	**
pH_{soil}	-0.43	0.22	-1.93	0.058	.
EC_e dS/cm	0.36	0.16	2.26	0.027	*
Ca meq/100g	-0.23	0.07	-3.19	0.002	**
Na meq/100g	4.10	0.20	20.93	<0.001	***
K meq/100kg	-1.85	0.76	-2.37	0.021	*
Mg meq/100g	-0.50	0.05	-10.59	<0.001	***
Signif. codes:	0 '***' 0.001;	'**' 0.01;	'*' 0.05;	'.' 0.1'' 1	

However, it is still important to consider that the coefficient estimate is pessimistic, indicating a tendency for ESP to decrease during September, although this relationship requires further investigation and validation.

The relationship between ESP and various soil variables was examined to understand their association in the context of soil salinity. The results revealed significant associations, particularly highlighting the crucial role of Na meq/100g in influencing ESP. The Na meq/100g variable has a significant positive coefficient (4.10), with a highly significant p-value (0.00002), indicating the most substantial impact on ESP prediction among all predictor variables. This suggests that for each unit increase in Na^+ concentration, ESP increases by 4.1 meq/100g, assuming all other factors remain constant. Additionally, the coefficient estimate for ECe (Electrical Conductivity of the saturation extract) is 0.36, with a p-value of 0.03, indicating a positive association

between ECe and ESP. At the same time, this association is statistically significant but relatively weaker than Na meq/100g. Similarly, the coefficient estimates for pHsoil (soil pH) (-0.43) and Ca meq/100g (-0.23) also indicate negative associations with ESP, with the coefficient estimate for Ca having a highly significant p-value of 0.002.

The negative coefficient of Ca^{+2} meq/100g suggests that higher levels of exchangeable calcium are associated with decreased ESP. This is an essential aspect of managing sodic soil, as the application of calcium can replace sodium at the soil exchange complex, helping to disperse sodium ions and reduce soil sodicity. Proper management of Na+ and Ca+2 levels is critical in mitigating soil sodicity to enhance rice crop productivity in the study area.

Overall, the soil variables ECe (dS/m) and Na meq/100g exhibit the strongest associations with ESP. Exchangeable Na meq/100g demonstrates a significant positive association, while ECe shows a weaker positive association. On the other hand, pHsoil, Ca meq/10, K meq/100, and Mg meq/100 exhibit negative associations with ESP. The results emphasize the importance of these soil properties in influencing soil salinity and suggest that Tonitaba and Kudang play significant roles in determining ESP during the rice growing season.

4.5.3 Variability of Root-Zone Salinity on Growth and Yield of Rice

Figures 4.1a and 4.1b show the mean soil pH, EC_e, and Na^+ variability at different sites and rice growth stages during the season. The results indicated that the soils are mainly acidic, with pH values ranging from 4.0 to 5.8. Unlike saline soils with higher soil pH, coastal salt-affected soil had an acidic soil reaction, usually with a pH of $\leq$ 6.57 (Bandyapadhyay et al., 2003). Because saltwater intrusion causes an increase in the salinity level of coastal soils, saline soils with both high pH and acidic soils are distinctive characteristics of coastal saline soils (Bandyapadhyay et al., 2003; Mahajan et al., 2015).

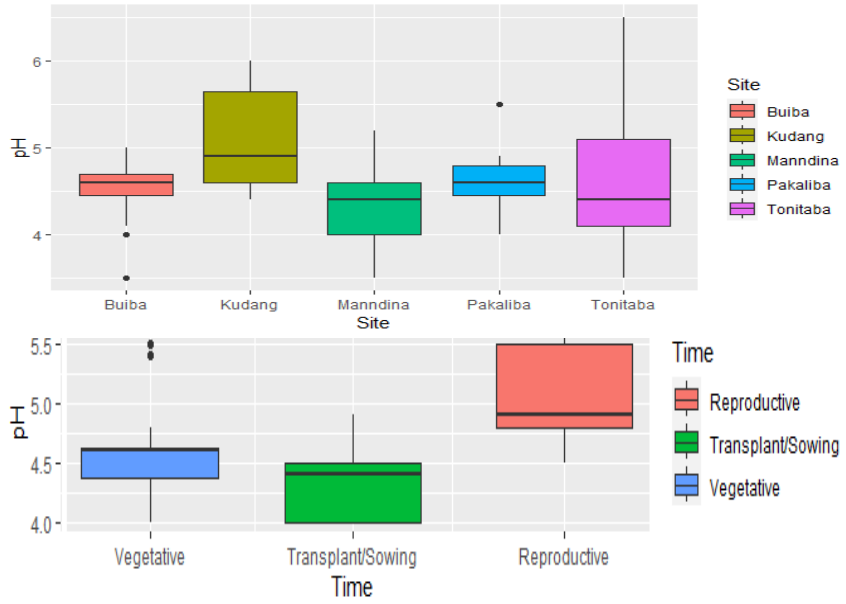

(a)

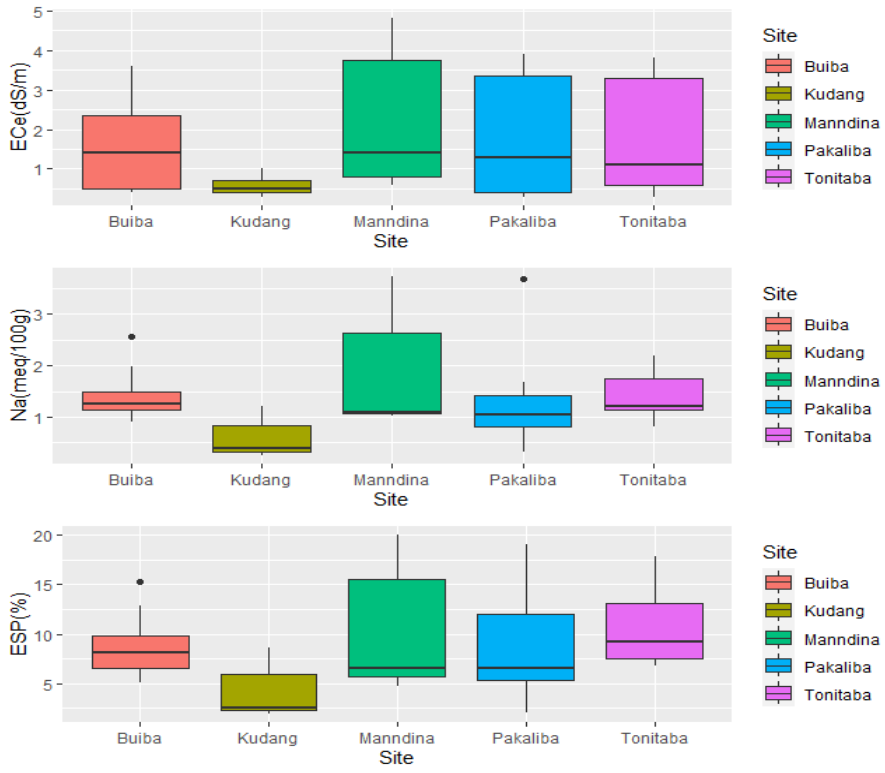

(b)

Figure 4. 1 Boxplot of mean soil pH, EC_e ESP across fields and stages of rice growth a) pH, b) EC_e, Na^+ and ESP, c) EC_e, Na^+ and ESP

Generally, alluvial soil manifests variability of acidity and approaches neutrality when submerged but becomes extremely acidic when drained and dry (Cakmak et al., 2008). The results indicate a variation of soil acidity with a decreasing trend as the season

progresses. After several rain showers, the soil's acidity decreases as the rainwater leaches out the acidity, and the soil pH becomes near neutral (7.0). This is in line with the findings of Sreelatha et al. (2022), who attributed the variation of soil pH in acid-saline soils of Kerala, India, to the freshwater influx by rainfall. Rice crops can be grown in slightly acidic or alkaline conditions, but a pH between 5.5 and 6.5 is recommended for optimal growth and yield. Kudang recorded the highest soil pH value across the study fields and during the various stages of rice production cycles. In contrast, the lowest value was observed in Mandina and Tonitaba throughout the season.

Table 4. 5 Mean soil salinity variability by field and growing season stage in LRR and CRRS

Site	Time	n	pH	ECe (dS/m)	Na^+ (meq/100g)	ESP (%)
Buiba	Reproductive	5	4.84	0.44	1.258	7.3
	Transplant/Sowing	5	4.1	3.04	1.652	11.72
	Vegetative	5	4.56	1.62	1.252	6.92
Kudang	Reproductive	5	5.8	0.46	0.37	2.36
	Transplant/Sowing	5	4.6	0.84	1.034	7.44
	Vegetative	5	4.98	0.38	0.32	2.48
Mandina	Reproductive	5	4.9	0.72	1.112	6.14
	Transplant/Sowing	5	4.08	4.332	3.104	17.92
	Vegetative	5	4.06	1.4	1.2	6.02
Pakaliba	Reproductive	5	4.94	0.36	0.62	4.04
	Transplant/Sowing	5	4.32	3.6	1.942	13.98
	Vegetative	5	4.62	1.38	1.065	7.04
Tonitaba	Reproductive	5	5.56	0.48	1.152	7.26
	Transplant/Sowing	5	3.9	3.5	1.126	14.86
	Vegetative	5	4.36	1.28	1.892	9.24

Soil EC_e indicated an opposite pattern as pH values show an eastward decrease with a high value in Mandina throughout the season (4.33 at planting/sowing, 3.89 at the vegetative stage, to 0.72 at harvesting) and lowest values recorded in Kudang respectively. The composition of sodium across the field shows high mean Na^+ and ESP values of 11.72, 17, 14.86, and 13.98 % in Buiba, Mandina, Tonitaba, and Pakaliba, respectively. Variability of soil salinity indicates a steady decrease in all sits as the season progresses.

This decrease is due to the dilution of soluble salts in the soil by rainwater. For example, Bandyapadhyay (et al., 2003) attributed the lower salinity level in different locations of coastal acid saline soils of Goa to the washing out of salt to rainfall during the monsoon months. As the rainwater infiltrates the soil, it dilutes and leaches the salinity, forming soluble salts, causing the salinity to decrease. This process usually takes place several weeks to a month after the onset of the rains, depending on the amount and the infiltration rate of the soil.

4.5.4 Relationship between groundwater, Soil Salinity, Growth, Yield, and Yield Components of Rice

Groundwater shows varying relationships with rice physiological growth and development, yield, and yield components. Water level depth correlates positively (r= 0.77) with plant height 4 Weeks After Transplanting (WAT). In contrast, groundwater's Total Dissolvable Salt (TDS) content indicated a significant moderate negative (r= -0.58) relationship with plant density 15 WAT.

Table 4. 6 Correlation analysis of biophysical properties on rice growth, yield, and yield components in farmers'

GW	Agronomic	r	95 %	CI	t	p-value
Depth (cm)	Height 4 WAT	0.77	0.42	0.92	4.3	<.001***
TDS(mg/l)	Density 15 WAT	-0.58	-0.84	0.9	-2.54	0.025*
Mg^{+}	Height 6 WAT	-0.52	-0.81	0	-2.17	0.049*
Mg^{+}	Tillers	0.59	0.12	0.85	2.65	0.020*
Mg^{+}	Grain wght	0.69	0.27	0.89	3.44	0.004**
Mg^{+}	Fill grain	0.63	0.17	0.86	2.91	0.012*
Grain weight	Fill grain	0.97	0.91	0.99	14.49	< .001***
1000grain(g)	Yield (kg/ha)	1	1.00	1	4814	< .001***

Note: GW = Groundwater

Significant positive correlations were observed between soil Mg compositions with the number of tillers (r= 0.59), grain weight (r= 0.69), and filled grain. Magnesium deficiency is commonly a limiting factor in crop production due to low levels of exchangeable Mg in acidic soil (Wang et al., 2020). Mg is closely related to leaf sugar production and is essential for biomass accumulation and grain development (Cakmak and Kirkby, 2008; Cakmak, 2013; Sadeghi, Rezeizad, and Rahimi, 2021).

Similarly, Ceylan et al. (2016) reported that Mg deficiency reduces grain weight and lower grain quality in wheat. Growth and yield parameters indicated varying significant correlations among themselves. For example, plant density 6 WAT and density 15 WAT show a meaningful, strong positive relationship with r= 0.99, whereas a perfect (r= 1) positive relationship exists between plant height 6 and 15 WAT.

Grain weight per meter square is highly significantly positively correlated with the filled grain ($p < 0.001$), and 1000 grain weight has a perfect relationship with Yield (kg/ha). This aligns with the findings of Huang et al. (2018), who reported a correlation between grain yield and filled grain. Similarly, Zhao et al. (2020) reported a significant positive correlation between grain yield and the filled-grain number per panicle, filled-grain percentage, and grain weight.

4.5.5 Effects of soil salinity on Growth and Yield of Rice

Plant heights were high in Buiba throughout the growth cycles of rice across all fields. Lower values of plant height were observed in Mandina at all times of sampling. Plant density across the areas shows Kudang recorded high mean plant density at all periods except during the 4 WAT, where Buiba and Mandina show relatively high values over Kudang. Similarly, plant density shows a steady decrease with time, as expected; however, the decline is lower in Kudang than in other sites. Figures 4.2a and b show the effect of soil salinity on the agronomic variables of rice in the different study fields.

The nonparametric multivariate one-way inference results, as shown in Table 4.12, reveal a highly significant global effect of the Field/Site on soil physicochemical properties, groundwater quality, and agronomic variables among the five study fields in the Lower (LRR) and Central River Region South (CRRS). All four of the statistical test criteria (ANOVA type test, LH Test, BNP Test, and Wilks Lambda) indicate significant results with very low p-values ($p < 0.001$). This suggests strong evidence against the null hypothesis, meaning statistically substantial differences exist between the different study fields.

These statistical tests, employing the F approximation and permutation (randomization) methods to assess the four multivariate distributions, consistently demonstrate the highly significant impact of the Field/Site factor on the soil physicochemical properties, groundwater quality, and agronomic variables in the

study. Further analysis of the relative treatment effects provides valuable insights into the contributions of specific soil variables to root zone salinity across the study fields (Table 4.7).

Table 4. 7 Nonparametric multivariate One-Way inference results: statistical test criteria

Statistic Type	Test Statistic	df1	df2	p-value	P.T. p-value
ANOVA type test	5.72	7.29	127.49	0.00	0.001
LH Test	3.57	16.00	128.12	0.00	0.000
BNP Test	3.13	17.24	297.75	0.00	0.000
Wilks Lambda	3.43	16.00	205.33	0.00	0.000

P.T. = Permutation Test p-value, LH= Lawley Hoteling; BNP= Bartlett-Nanda-Pillai

The relative treatment effects quantify the likelihood that a randomly chosen observation from a particular Site significantly differs from a randomly chosen observation from all the other Sites regarding each soil variable.

For example, in Kudang, soil pH exhibits a relatively high probability of being significantly different from the other fields, indicating notable variability in soil pH in this particular field. Soil pH affects the availability of essential nutrients to rice plants and can influence nutrient uptake. Acidic or alkaline soil conditions can limit nutrient absorption, leading to nutrient deficiencies that negatively impact rice yield (Chen et al., 2020).

On the other hand, Mandina shows distinctiveness in EC_e and Na^+, with higher probabilities of significant differences than in other fields. This suggests that soil salinity indicators, such as EC_e and Na^+, effectively discriminate Mandina from the rest of the study fields. High ECe values indicate elevated salt levels in the soil, which

can lead to osmotic stress in rice plants, affecting water uptake and nutrient absorption. This can ultimately reduce yield (Foulkes and Carvalho, 2020).

At the same time, sodium ions (Na^+) are one of the primary causes of saline soils. High sodium levels in the soil can disrupt the water balance in rice plants, leading to water stress and reduced growth (Kronzucker et al., 2008). Exchangeable sodium percentage (ESP) measures the proportion of sodium in the soil's cation exchange complex. Tonitaba stands out regarding ESP, displaying a highly pronounced effect that distinguishes it from all other sites.

The probabilities associated with ESP highlight its significant contribution to the unique characteristics of Tonitaba's soil properties. High ESP values can lead to soil dispersion and poor soil structure, adversely affecting rice root growth and nutrient uptake (Srivastava et al., 2021). Based on the results presented in Appendix 4.1 and 4.2, the study conducted an ANOVA-Type Statistic for the Subset Algorithm based on Factor Level (Site/Field) and Soil variables to compare multiple variables of soil properties, including pH, ECe, Na^+, and ESP, among the sites.

The hypothesis tested equality between the soil properties across these fields was rejected. From the table, it can be observed that there are significant differences in soil properties between Kudang and the other sites (Buiba, Mandina, Pakaliba, and Tonitaba). The study utilized a closed multiple-testing procedure to control the maximum overall type I error rate at alpha = 0.05, ensuring that the chances of making a type I error are minimized.

The rejection of the hypothesis of equality between the soil properties across the factor levels (Buiba, Kudang, Mandina, Pakaliba, and Tonitaba) implies that these sites have distinct soil characteristics. These differences are attributed to factors such as soil salinity, pH levels, Na^+ content, and ESP, which can significantly influence the growth and development of rice plants.

Table 4.9 presents the results of a one-way nonparametric MANOVA conducted to examine the effect of seasonal salinization on rice yield using response variables. The global hypothesis test indicates that there are significant differences ($p < 0.05$) among the factor levels (Buiba, Kudang, Mandina, Pakaliba, Tonitaba) for all test statistics except for the LH test (Lawley Hotelling).

This discrepancy implies that the dependent variables (pH, ECe, Density at 15WAT, Height at 15WAT, Number of Tillers, Unfilled Grain in kg/m, and Yield (kg/ha)) differ significantly among the distinct sites. Consequently, the null hypothesis of equal outcomes between these sites is refuted. A closer inspection of the effect size analysis highlights Mandina's significant influence on ECe (dS/m) and unfilled grain (0.83), with a comparatively lesser impact on yield (0.28). This points towards the interplay of elevated ECe and substantial unfilled grain contributing to a diminished yield (kg/ha) in Mandina.

Table 4. 8 Relative treatment effects of soil variables contributions to root zone salinity

Field	pH	ECe (dS/m)	Na^+ (meq/100g)	ESP (%)
Buiba	0.47	0.55	0.62	0.56
Kudang	0.71	0.25	0.20	0.22
Mandina	0.36	0.64	0.63	0.54
Pakaliba	0.52	0.52	0.44	0.49
Tonitaba	0.44	0.54	0.62	0.68

In contrast, Tonitaba's higher ECe and smaller effect size in pH and plant density result in a considerably smaller effect size on yield (kg/ha) than Kudang. Additionally, when contrasted with other sites, Kudang is highly likely to select measurements randomly for soil pH (0.71), filled grain, and yield in kg/ha (0.79). This could suggest reduced variability in Kudang's values for these variables.

The obtained outcomes further underscore the dissimilarities ($p < 0.05$) among sites concerning response variables, namely ECe (dS/m), plant density at 15WAT, Unfilled Grain (kg/m), and Yield (kg/ha). Based on the global multivariate inference tests shown in Table 4.9, the rejection of the null hypothesis concerning response variable equality is reinforced.

Moreover, nonparametric multiple comparison tests yield an overall quantile of 5.57 and a p-value of 0.06. The 5 % significance level fails to reject the null hypothesis for any individual assumption. Distinct variations in effect size across different variables within the site/field are evident. Noteworthy among these is Mandina's substantial effect size for ECe (dS/m) and unfilled grain (0.83), coupled with a minor effect size for yield (0.28). This supports the assertion that the amplified ECe and significant unfilled grain content in Mandina contribute to reduced yield (kg/ha).

Table 4. 9 Multivariate inference of Field/Site factor on salinity, yield, and yield components in LRR and CRRS, The Gambia

Test Type	Test Statistic	df1	df2	P-value	P.T. p-value
ANOVA type test	4.51	17.24	43.10	0.000	0.000
LH Test	7.37	23.00	2.55	0.085	0.115
BNP Test	2.50	45.49	31.84	0.004	0.001
Wilks Lambda	3.72	32.00	12.66	0.008	0.009

P.T. = Permutation Test p-value, LH= Lawley Hotelling; BNP= Bartlett-Nanda-Pillai

Recent research studies show that soil salinity substantially impacts rice yield, confirming that elevated ECe and significant unfilled grain content in Mandina contribute to reduced yield (kg/ha). Tian et al. (2022) revealed that salt stress had a notable effect on various yield-related parameters, including panicle number, grain number per panicle, seed setting rate, 1000-grain weight, and rice yield.

Contrarily, Tonitaba's high ECe and modest effect size in pH and plant density lead to a markedly smaller effect size on rice yield (kg/ha) compared to Kudang. Additionally, Kudang's tendency to randomly select measurements for soil pH (0.71), filled grain, and yield in kg/ha (0.79) distinguishes it from other sites, potentially indicating less variability in its data. Statistical comparisons between Kudang and other fields/sites reveal significant effects at a 5 % significance level, except for Mandina and Tonitaba, which exhibit p-values of 0.05 and 0.02, respectively.

Table 4. 10 Mean comparisons of rice yield (kg/ha) between Kudang and other fields/sites

Comparison	Est.	df	Statistic	P-value	Rejected
Buiba-Kudang	-0.38	2.32	-1.28	0.31	FALSE
Mandina-Kudang	-0.51	3.11	-3.07	0.05	TRUE
Pakaliba-Kudang	-0.16	3.79	-1.20	0.30	FALSE
Tonitaba-Kudang	-0.40	3.67	-4.02	0.02	TRUE

Specifically, the mean comparison detailed in Table 4.11 demonstrates a significant difference ($p < 0.05$) between Mandina and Kudang, with Mandina yielding less (mean value of 213.8 kg/ha) compared to Kudang (mean value of 254 kg/ha). Similarly, a significant disparity ($p < 0.05$) emerges between Tonitaba and Kudang, with Tonitaba recording a lower yield (mean value of 221.9 kg/ha) than Kudang.

This outcome reinforces the notion that Kudang exhibits higher yield potential than Tonitaba. The results align with those of Zheng et al. (2023), who conducted a meta-analysis examining salinity stress's impact on rice yield and grain quality. Their findings indicated that grain yield exhibited a linear reduction with increasing soil electrical conductivity (EC), with a 50 % reduction observed at an EC of 6.5 dS/m.

4.6 SUMMARY

The study revealed that the soil in these areas predominantly exhibits clay texture, characterized by high acidity levels (with pH ranging from 4.1 to 4.3) and elevated electrical conductivity (ECe), indicating salinity concerns. Furthermore, the exchangeable sodium percentage (ESP) values were relatively high, indicating the presence of sodic soils. The result of correlation analysis established significant relationships among soil pH, ECe, Na^{+}, and ESP, underscoring the profound influence of these factors on soil salinity dynamics.

The analysis of linear regression indicated that increased soil calcium (Ca^{+2}) levels could effectively reduce soil sodium (Na^{+}) composition by 0.2 meq/100g, suggesting the potential benefits of adding calcium-containing amendments such as gypsum and lime biochar to manage sodic soils effectively. Similarly, seasonal variability soil salinity highlighted a notable decline in ESP values of 1.2 % during August and 0.95 % in September, indicating seasonality in salinity conditions.

Analysis of relative treatment effects of soil variable contributions to root zone salinity on the yield and yield components of rice show high ECe and small effect size in pH and plant density lead to a markedly smaller effect size on rice yield of 0.36 and 0.44 in Mandina and Tonitaba, respectively.

Results of MANOVA Multiple tests for many-to-one mean comparisons indicated notably higher rice yields in Kudang (254 kg/ha) than in Mandina (213.8 kg/ha),

emphasizing the potential impact of specific interventions or management practices on enhancing rice production.

CHAPTER FIVE

ASSESSING THE VULNERABILITY OF RICE PRODUCTION TO CLIMATE CHANGE IN THE LOWER CENTRAL REGIONS OF THE GAMBIA[3]

ABSTRACT

Rice production in The Gambia's Lower River Region (LRR) and Central River Region South (CRRS) is carried out under diverse ecologies. Changes in global warming temperature, carbon dioxide levels, and rainfall variability are anticipated to impact rice production in LRR and CRRS. The study aims to assess the vulnerability of rice cultivation in LRR and CRRS. The non-parametric Mann-Kendall (M.K.) and Seasonal Kendell (SMK) tests were used to determine trends in climate variables. The linear regression model evaluated the relationship between climate variables and rice production (yield), and the random forest model was used to predict rice yield based on historical climate trends. The results show that monthly rainfall patterns peaked in August in both regions, with a maximum of 486 mm during the study period. M.K. trend analysis indicated a significant positive increase in annual rainfall in both areas, whether accounting for autocorrelation or not, albeit with an eastward decrease in yearly rain. Maximum temperature exhibited a strong negative correlation with precipitation, while minimum temperature showed a moderate to strong positive relationship with rainfall in both regions. Linear regression models explained a substantial portion of rice yield variability, with 67% for LRR and 64% for CRRS. The random forest model shows the significance of maximum temperature as the most influential predictor, with an importance score of 1968993, followed by rainfall with a score of 1647426, showcasing their substantial contribution to predictive performance. Minimum temperature had the most negligible influence (1437471), highlighting that alterations in maximum temperature have the most profound effect on historical yield prediction. The findings underscore the necessity of region-specific strategies to enhance rice production resilience in the face of climate change. The study recommends adapting agricultural practices, optimizing irrigation systems, and adopting climate-resilient rice varieties.

[3] A manuscript has been developed from this chapter to be publish in a journal

5.1 Introduction

Globally, rice is the second-most widely grown cereal crop, the staple food for more than 50 % of the world's population (Ibrahim and Saito, 2022). Rice-based systems play a crucial role in the livelihoods of approximately one billion households across Africa, the Americas, and Asia (Van Nguyen et al., 2006). The centrality of rice as a staple food makes it a key player in the fight against hunger and poverty worldwide. In the 2019/20 season, global rice production was projected to reach 497.8 million tonnes, with utilization reaching a record 494.5 million tons (USDA, 2019). As we look into the future, there is an anticipated increase in rice consumption, with global utilization expected to rise by 1.1 % annually, mainly driven by population growth, especially in developing countries such as Asia and Africa (OECD-FAO, 2019).

Sub-Saharan Africa (SSA) heavily relies on rice for food security. However, despite its importance, rice production in SSA faces challenges. The region experienced a decrease in rice self-sufficiency from 61 % to 52 % between 2008 and 2018, as rice consumption expanded faster than production growth (AfricaRice, 2018). The average annual growth rate of rice production in SSA is 4.6 %, while the annual consumption growth rate is 6.2 %. By 2025, rice consumption is projected to reach 49.25 million tonnes, highlighting the growing demand and need for increased production in the region (AfricaRice, 2018).

The Gambia, located in West Africa, is one of the SSA countries that is heavily reliant on rice consumption. In 2019, per capita rice consumption in The Gambia was estimated to be 117 kg, significantly higher than the global average of 56.9 kilograms (Fahad et al., 2019; OECD-FAO, 2019). The country's population growth rate of 3.1 % per year is expected to drive a considerable increase in rice demand, with projected estimates reaching 319,746 metric tonnes by 2030 and 443,902 metric tonnes in 2040, compared to 221,661 metric tonnes in 2018 (Mungai et al., 2019). Rapid population growth demands a substantial increase in domestic rice production, currently at 38,000 metric tonnes as of 2018, necessitating significant efforts to boost production and enhance food security.

Rice production in the Lower River Region (LRR) and Central River Region South (CRRS) of The Gambia is carried out under diverse ecologies, such as tidal or pump-irrigated, rain-fed, upland, and flood-prone conditions (Ceesay, 2014). However,

future changes in global warming temperature, carbon dioxide levels, and rainfall variability are anticipated to impact rice production in LRR and CRRS. Studies have shown that such changes can adversely affect productivity and impose limitations on suitable ecologies for rice cultivation (Lobell and Field, 2007; Kamali et al., 2018). Welch et al. (2010) reported future reductions in rice yields based on the growing season and environmental conditions in many rice-growing areas.

Rice crops are sensitive to temperature extremes during different growth stages, with high temperatures (>32°C) and low temperatures (<18°C) causing significant reductions in yield (Sánchez et al., 2013; Promchote et al., 2022; Chandio et al., 2020). As projected, The Gambia is expected to experience an increase in annual mean temperatures of 1.7 to 2.1°C by 2050 and 3.1 to 3.9 °C by 2100 relative to 2000 (McConnell & Jallow, 2020). Such a temperature rise could have substantial implications for rice production in these significant hubs of LRR and CRRS.

Given the potential impact of climate change on rice production, it is crucial to assess the vulnerability of rice cultivation in LRR and CRRS. The study aims to investigate the prospects of rice production in the context of climate change to inform policy decisions and develop strategies for enhancing rice productivity in the country's major hubs. The outcomes of this research are expected to be valuable to farmers, agronomists, scientists, planners, policymakers, and investors, aiding the development of effective strategies to ensure sustainable rice production and productivity in The Gambia's changing climate in these major hubs.

5.2 Materials and Methods

5.2.1 Data Collection and Analysis

Historical monthly data (1981 - 2020) of minimum temperature (Tmin), maximum temperature (Tmax), and rainfall were collected for two metrological stations, viz. Sapu, Central River Region South (CRRS), and Junior, Lower River Region (LRR), from the Department of Water Resources (DWR), The Gambia. Historical data for lowland/swamp rice production were collected for (LRR) and CRRS of The Gambia from the Department of Planning Services of Agriculture (DOA) for the period under review (1981-2020). To obtain the annual climate data, a re-sampling approach was used to compute the sum and mean of all the grouped values by region and date for the monthly climate variables (i.e., temperature and rainfall) (Ragatoa et al., 2018).

5.2.2 Exploratory Data Analysis (EDA)

Exploratory data analysis was carried out to check the general characteristics of the variables, including the variations in the summary statistics, trends, and variations at the different time scales of the data. Commonly, EDA is considered the first important step in data analysis to identify potential flaws in data collection and evaluate the need for handling imbalanced data (Davydenko & Charith, 2020). EDA was done using descriptive statistics (mean, maximum, median, minimum, standard deviation, coefficient of variation (CV), skewness, and kurtosis summarized), which were calculated for annual climate variables. These statistics provided insights into the characteristics of climate variables.

5.2.3 Mann-Kendall Test (M.K.) Trend Analysis

Non-parametric tests, such as the Mann-Kendall (M.K.) and Seasonal Kendall (SMK) tests, offer robustness compared to parametric alternatives. While parametric measures provide an overall perspective on trends, non-parametric tests like M.K. and SMK excel in detecting trends with seasonal variations. The M.K. test is widely used in hydrological and climate trend detection studies and recommended by the World Meteorological Organization (WMO) for climatological trend analysis due to its ability to identify monotonic increases or decreases (Tabari and Talaee, 2011; Jaiswal et al., 2015). The M.K. test assesses the significance of a trend, while the non-parametric Sen's method estimates its magnitude, making it a valuable tool in trend

analysis. The test does not require that the data series follow a specific probability normal distribution (Gedefaw et al., 2018).

The statistic S is calculated according to equation 1:

$$S=\sum_{k=1}^{n-1}\sum_{j=k+1}^{n} \operatorname{sgn}(X - X_k) \quad \text{... equation(5.1)}$$

$$\text{signs}=\begin{cases}1 \text{ if } x>0\\0 \text{ if } x=0\\-1 \text{ if } x<0\end{cases} \quad \text{... equation(5.2)}$$

Mann (1945) and Kendall (1975) have demonstrated that when $n \geq 8$, the statistic S is approximately normally distributed with the mean E(s) = 0 and variance Var(S) as follows.

$$\text{Var}(S)=\frac{n(n-1)(n2+5)-\sum_{j=1}^{p} t_j(t_j-1)(2t_j+5)}{18} \quad \text{... equation(5.3)}$$

Where p is the number of the tied groups in the data set, and *tj* is the number of data points in the jth tied group. The statistic S is approximately normally distributed provided the following Z-transformation (Pohlert, 2020).

$$Z=\begin{cases}\frac{s-1}{\delta} \; if \; S>0\\0 \quad if \; S=0\\\frac{s-1}{\delta} \; if \; S<0\end{cases} \quad \text{... equation(5.4)}$$

The Mann-Kendall (M.K.) test is a statistical method used to assess changes in a time series' central value or median over time. It calculates a Z value to determine the significance of a trend, where a positive Z indicates an upward trend and a negative Z suggests a decreasing trend. The test involves a null hypothesis (H_0), assuming data come from a population with independently distributed random variables, and an alternative hypothesis (H_1) suggesting the presence of a monotonic trend.

This two-tailed test is conducted at a significance level of $\alpha = 0.05$, allowing it to assess increasing and decreasing monotone trends. The null hypothesis (H0) is rejected if the absolute value of the computed Z exceeds a critical value ($Z_{1-\alpha/2}$) obtained from the standard distribution table. However, although robust, the standard M.K. test may produce misleading results when a seasonal serial correlation is present and does not distinguish between linear and nonlinear trends.

On the other hand, the Seasonal Mann-Kendall Test (SM-K) offers a more realistic assessment of significance but is less robust. The choice between the two tests, especially when dealing with seasonal data and autocorrelation, involves a trade-off. The positive serial correlation increases the likelihood of rejecting the null hypothesis, while negative serial correlation reduces the rejection rate, particularly in small sample sizes (Merabtene et al., 2016). Hirsch et al. (1982) proposed the Seasonal Mann-Kendall (SM-K) test for the trend insensitive to seasonality. The Mann-Kendall statistic for the gth season is calculated as:

$$S_g = \sum_{i=1}^{n-1} \sum_{j=i+1}^{n} \text{sgn}\,(X_{jg} - X_{ig}) \qquad (1 \le g \le m) \qquad \ldots \text{equation}(5.5)$$

The mean of Sg is μg = 0. The variance, including the correction term for ties, is

$$\delta_g^2 = \left\{ n\,(n-1)(n2+5) - \sum_{j=1}^{p} t_{jg}\left(t_{jg}-1\right)\left(2t_{jg}+5\right) \right\} /18 \quad (1 \le g \le m \quad \ldots \text{equation}(5.6)$$

The seasonal Mann-Kendall statistic, $\hat{S}$, for the entire series, is calculated according to (Hirsch et al. 1982)

$$\hat{S} = \sum_{i=1}^{n-1} S_g \qquad \sigma^{\wedge 2}_{g} = \sum_{g=1}^{m} \sigma_g^2 \qquad \ldots \text{equation}(5.7)$$

The statistic S_g is approximately normally distributed, with variance

$$Z_g = S_g / \sigma_g \qquad (5.8)$$

The variance, including the correction term for ties, is

$$z = sgn(S_g)\,(|S_g| - 1)\,/\sigma_g \qquad \ldots \text{equation (5.9)}$$

The seasonal Kendall slope estimator is a trend magnitude estimator. It is an unbiased estimate of the linear trend's slope. It has far greater precision than regression when the data is heavily skewed but somewhat poorer accuracy when normal. The null hypothesis H_0 for the seasonal Kendall test is that x is a sample of independent random variables xij and xi is a subsample of independent and identically distributed random variables i = 1,2,....12. The alternative hypothesis is that for one or more months of the subsample is not identically distributed.

5.2.4 Serial correlation

The study assessed serial correlation in climate variables, specifically Tmax (maximum temperature), Tmin (minimum temperature), and Rainfall. This assessment employed established methodologies outlined by Hirsch et al. (1982), known as whitening methods. In both approaches, the serial correlation coefficient (autoregressive process at lag-1) was estimated, and significance testing was performed using the Kendall test at a significance level of 0.05. This rigorous examination accounted for serial correlation when analyzing temperature and rainfall data trends, ensuring that the M.K. test's results are robust and accurate (Hirsch et al., 1982; Pohlert, 2020).

5.2.5 Prediction of Climate Change and Rice Production LRR and CRRS

5.2.5.1 ARIMA Model

Time series analysis involves analyzing sequential data to derive meaningful statistics. In climatological and hydrologic studies, the main goal is understanding and quantifying the generating process and making predictions based on historical data. The ARIMA (Auto-Regressive Integrated Moving Average) model is commonly used

in such studies and is recognized for its flexibility and potency. This modeling approach encompasses autoregression (A.R.), which uses past observations' dependence, integration (I), involving differencing to achieve stationarity, and moving average (M.A.), which relates an observation to residuals from a lagged moving average model. These components are represented as parameters in the ARIMA (p; d; q) notation, where integers replace the parameters according to the specific ARIMA model.

The formulation for non-seasonal ARIMA is as follows.

$$\left(1 - \phi_1 - \cdots - \phi_p B^p\right)(y_t' - \mu) = \left(1 + \theta_1 B + \cdots + \theta_q B^q\right) \quad \ldots \text{equation}(5.10)$$

Where:

y'_t is the differenced series (it may have been differenced more than once). The "predictors" on the right-hand side include both lagged values of y^t and lagged errors.

Where:

$y'_t = (1\text{-}B)^d y'_t$ and μ is the mean

Box and Jenkins propose a three-stage process for assessing an ARIMA model involving model identification, parameter estimation, diagnostic checking, and forecasting (Findley et al., 2014). Model identification includes assessing normality, stationarity, and seasonality and selecting model specifications. Parameter estimation finds coefficients using maximum likelihood or least-squares methods.

Diagnostics evaluate model assumptions and error conformity for a stationary univariate process. This study applied these steps for climate variable modeling and forecasting in two regions using training (1981-2000) and testing (2001-2020) data sets. ARIMA model parameters were determined from significant and PACF charts, selecting 'p' and 'q' values where the charts cross upper confidence intervals. Five out of six tentative ARIMA models for annual climate variables were chosen based on AIC and BIC criteria. The selected model's diagnostic analysis focused on autocorrelation and residual normality using Ljung-Box tests.

5.2.5.2 Ordinary Least Squares Regression (OLS)

Ordinary Least Squares regression (OLS) is a common technique for estimating coefficients of linear regression equations, which describe the relationship between one or more independent quantitative variables and a dependent variable (Sonko et al.,

2019). Before conducting OLS regression analysis, Multicollinearity tests used the variance inflation factor (VIF). Multicollinearity is the proportion of variance in one independent variable not explained by the remaining independent variables (Hair et al., 1995; Haitham, 2018). The test aims to determine whether there is a strong correlation between the independent variables to enable building an unbiased model. The VIF measures collinearity among predictor variables within a multiple regression (Hair et al., 1995; Ringle et al., 2015). VIFs identify the severity of any multicollinearity and allow a quick measure of how much a variable contributes to the standard error in the regression (Zenati, 2015).

The analysis aims to predict rice yield based on climate variables (rainfall and temperature). The regression coefficients (β0, β1…, βk) were estimated from the historical rice yield for each region (CRRS and LRR). For each model, the yield was used as the dependent variable, whereas the climate variables were used as the independent variables.

Multiple independent variables predict the dependent or Y predictor.

$$Y_i = \beta_0 + \beta_1 X_{1i} + \cdots + \beta_k X_k + ui, i = 1, \ldots, n. \quad \ldots \text{equation}(5.11)$$

Where:

Y_i…, Xk: The independent variables (Tmax, Tmin, and RF) for the ith observation.

β_1,…, β_k: The coefficients associated with each independent variable (X_1, X_2, ..., X_k), representing the change in the dependent variable for a one-unit change in the corresponding independent variable, holding other variables constant.

X_{1i}…., X_k: The independent variables (climate variables) for the ith observation.

ui: The error term represents the unobserved factors that affect the dependent variable but are not explicitly included in the model.

5.2.5.3 Random Forest Model Prediction of Rice Yield

The study employed the Random Forest algorithm to predict rice yield using historical climate and yield data. The historical climate data included parameters like minimum temperature (Tmin), maximum temperature (Tmax), and rainfall (RF), spanning the years 1980 to 2020. The historical yield data encompassed the same time frame. Using

historical climate data, separate Random Forest models were built to predict Tmin, Tmax, and RF.

The model was trained using historical yield and the predicted climate variables to capture the interplay between climatic conditions and yield outcomes. The model predicted based on the climate variables for the same period. This step involved utilizing the previously trained model to simulate how climate changes might impact yield outcomes.

The percentage change between predicted and actual historical yield was computed, offering an aggregate view of the deviation between the two. Feature importance scores were extracted from the relationship model to ascertain the significance of each climate variable in predicting yield. These scores were based on the IncNodePurity metric, with the higher scores indicating greater importance in yield prediction. The coefficient of determination (R-squared) was calculated to evaluate model performance, reflecting the goodness of fit between predicted and actual historical yield.

5.3 RESULTS AND DISCUSSION

5.3.1 Exploratory Data Analysis

Summary statistics of the annual climate variables and rice production data are shown in Tables 1 and Figure, respectively. Both regions have similar mean temperatures, with CRRS South having a slightly higher mean Tmax of 36.0°C than LRR's mean Tmax of 35.82°C. In terms of variability, the standard deviation (SD) of Tmax and Tmin is slightly lower in LRR (2.70 and 3.70°C, respectively) than in CRRS South (2.80 and 3.06°C, respectively).

The coefficient of variation (CV), which measures the relative variability, indicates that Tmax and Tmin are slightly more variable in LRR (CV of 0.08 and 0.18, respectively) compared to CRRS South (CV of 0.07 and 0.16, respectively). The skewness values for both Tmax and Tmin are positive in both regions, suggesting a slight right-skewed distribution, but the skewness is more pronounced in LRR. This indicates that LRR might experience higher temperatures than CRRS South. The LRR has a slightly higher mean annual rainfall (809.16 mm) than CRRS South (768.93 mm).

The maximum seasonal rain was observed in both regions (1571 mm). Both parts have the same median and minimum monthly rainfall of 0.00 mm, and some months experienced very little or no rain in both areas, suggesting an unimodal rainfall pattern.

Table 5. 1 Summary statistics of annual climate variables for CRRS and LRR from 1980 -2020

Variables	Tmax (°C)		Tmin (°C)		Rainfall (mm)	
Region	CRRS	LRR	CRRS	LRR	CRRS	LRR
Mean	36.0	35.8	20.8	20.3	768.9	809.2
Max	43.1	43.1	26.8	25.2	1571	1571
Median	36.0	35.4	21.6	21.6	0.00	0.00
Min	29.2	30.6	9.50	9.2	0.00	0.00
SD	2.80	2.70	3.06	3.70	107	105
CV	0.07	0.08	0.16	0.18	1.62	1.56
Skewness	0.14	0.32	-0.88	-0.61	1.76	1.52
Kurtosis	-1.0	0.98	0.28	-0.88	2.53	1.30

The standard deviation of rainfall is slightly lower in LRR (105.2 mm) than in CRRS South (107.4 mm), indicating less variability in annual rainfall in LRR. The coefficient of variation for rain is similar in both regions, with LRR having a slightly lower value (CV of 1.56) compared to CRRS South (CV of 1.62).

The skewness and kurtosis values for rainfall suggest that the distribution is positively skewed and leptokurtic (more peaked) in both regions. LRR has a slightly higher skewness and kurtosis, indicating more frequent occurrences of extreme rainfall events.

Figures 5.1a and b show the average monthly climate variables over 40 years (1980 – 2020) for CRRS and LRR across different years and months, respectively. The average temperatures in CRRS vary from 25.4°C in January to 31.2°C in May, with the highest in May and June. Conversely, the lowest average temperature occurs in December, with a value of 25.9°C. In comparison, LRR exhibits a temperature range from 24.7°C in January to 30.8°C in May, with May being the warmest month. December is the most incredible month in LRR, with an average temperature of 25°C. Throughout the year, LRR generally experiences slightly lower temperatures than CRRS.

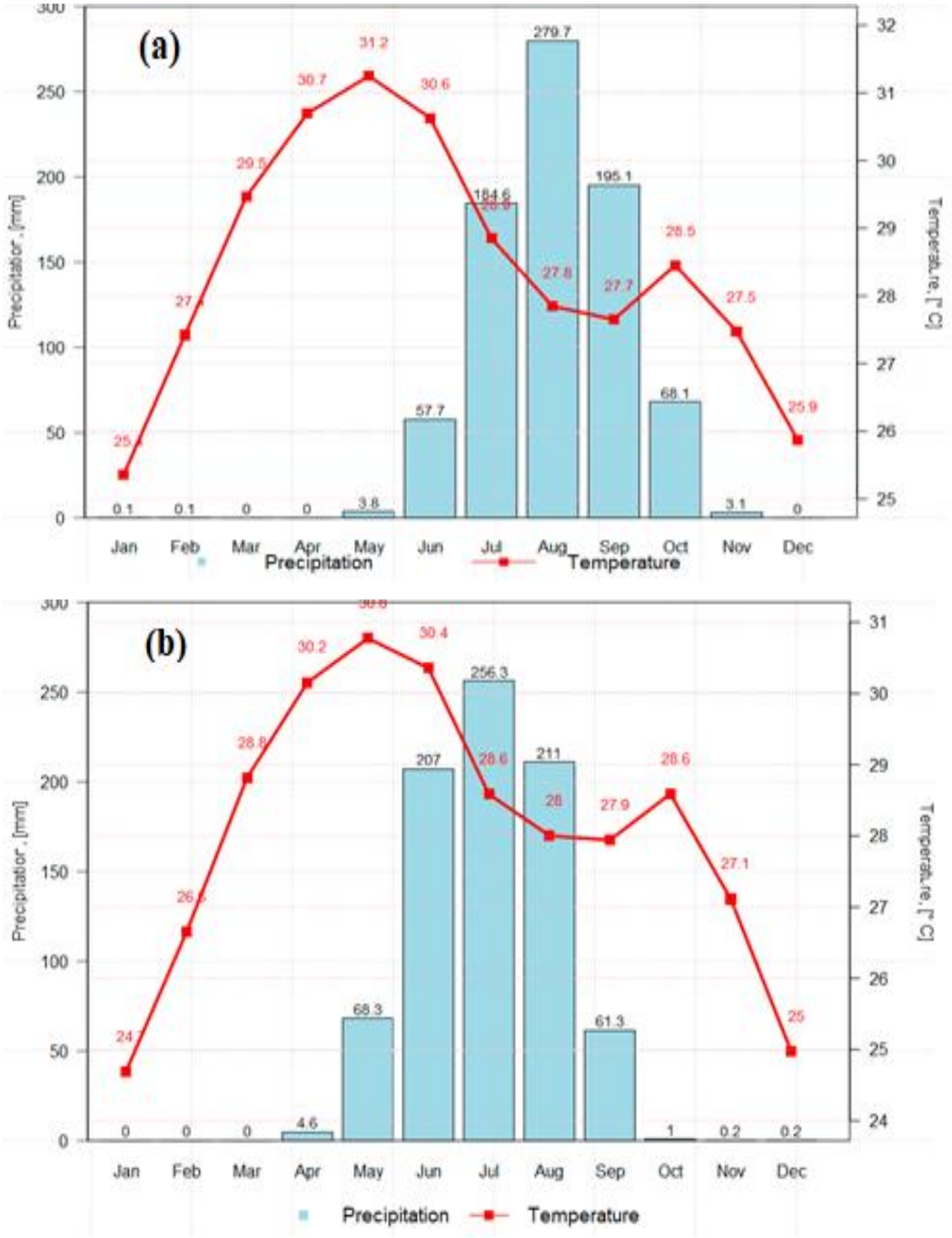

Figure 5. 1 Average monthly temperature and precipitation from 1980 -2020 a) CRRS b) LRR

CRRS and LRR experienced no rainfall from January to March, the season starting in April, and the two regions exhibit unimodal rainfall patterns. In CRRS, precipitation gradually increases in April (3.8 mm) and reaches its highest levels in August (279.7 mm) and July (184.6 mm). After that, the rainfall gradually diminishes until December (0 mm). Similarly, LRR follows a similar pattern with no rain from January to March. Still, precipitation starts to increase in April (4.6 mm) and reaches its peak in July

(266.3 mm) and August (211 mm). Like CRRS, LRR experiences reduced rainfall after August, but some precipitation persists in September, October, and November, tapering off in December (0.2 mm).

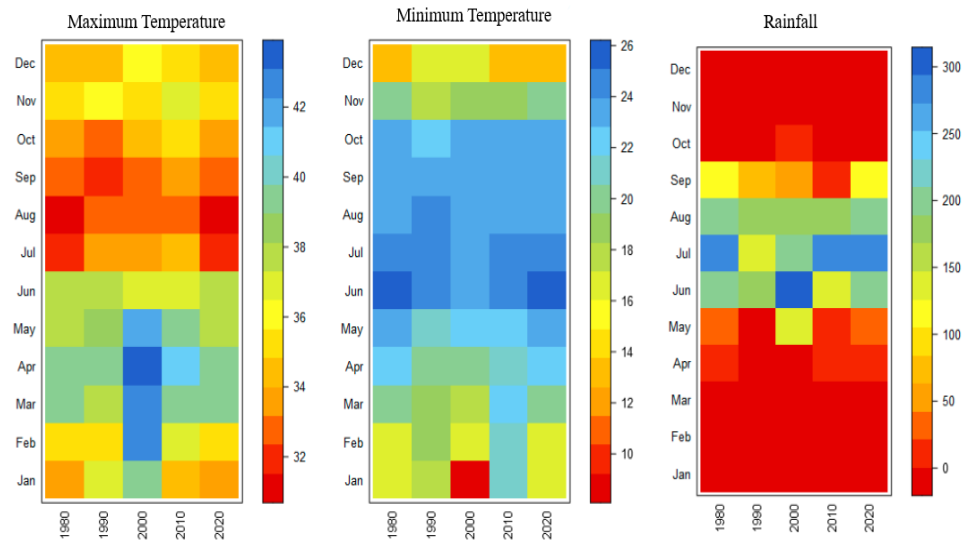

(a)

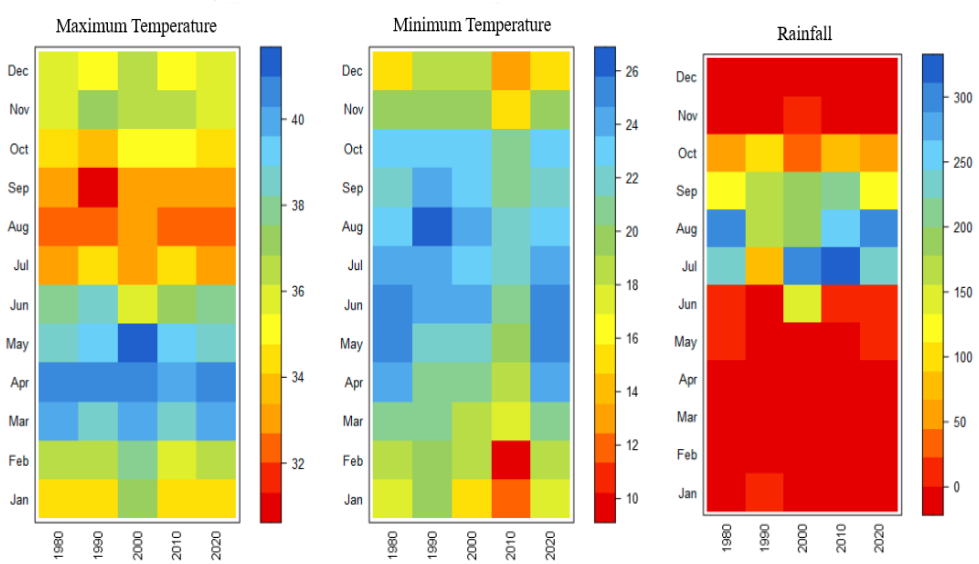

(b)

Figure 5. 2 Decadal seasonal climate variable from 1980 -2020 a) LRR b) CRRS

Comparatively, LRR generally receives more rainfall than CRRS during the wet months. This is in line with several previous studies that show an eastward decrease in rainfall and an increase in temperature (Amuzu et al., 2018).

5.3.2 Correlation analysis of Climate variables

Pearson correlation between the results of the climate variables indicates a higher correlation value for LRR than CRRS. The relation between seasonal Rainfall (RF) and Maximum Temperature (Tmax) shows a strong negative correlation of -0.61 and a moderate positive relationship for minimum temperature (0.45) in CRRS. Strong positive correlations were observed between Tmin and RF in LRR, whereas a weak association was observed between Tmin and Tmax in both regions.

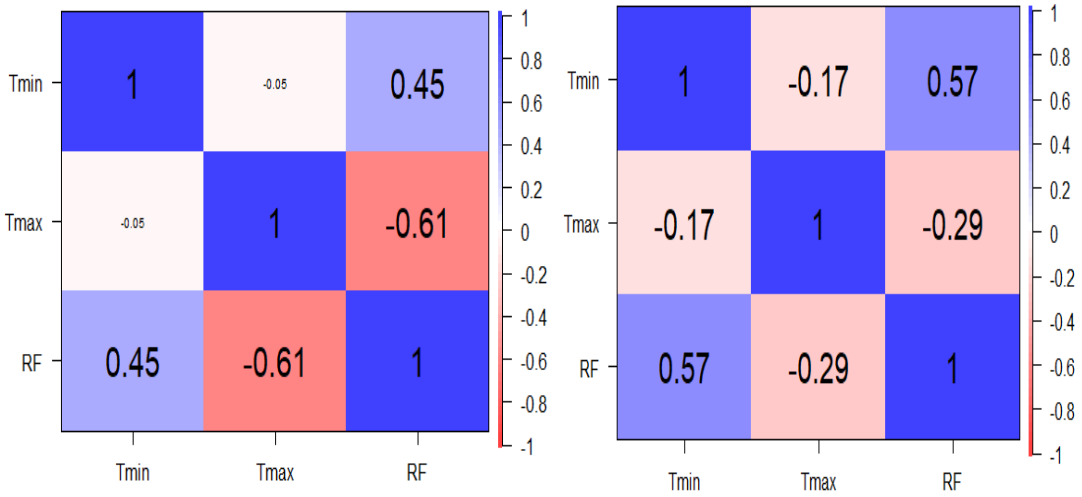

Figure 5. 3 Correlation heat map between seasonal climate variable a) CRRS b) LRR

The general correlation between seasonal climate variables was stronger in LRR than in CRRS. The correlation between rice production (yield and annual climate variables shows a weak regional relationship.

5.3.3 Trend Analysis

Statistical trends were measured using the non-parametric Mann-Kendall trend test for detecting monotonic tendencies in climate variables. The Mann-Kendall test is based on the null hypothesis (H0) that there is no trend against the alternative hypothesis H_1 of a monotonic trend for a chosen significance level of 0.05 %. In this study, the standard M.K. (1945) and Seasonal M.K. (S-MK) insensitive to serial correlation (Hirsch et al. 1982) and prewhitening (P.W.) method to eradicate the effects of the serial correlation on the statistical testing for the Mann-Kendall test were used (Zhang et al., 2001; Yue et al., 2002). Appendix 5.1 shows the annual and seasonal trend of

climate variables using M.K. statistics (one-tailed with a 5 % significance interval) with or without autocorrelation.

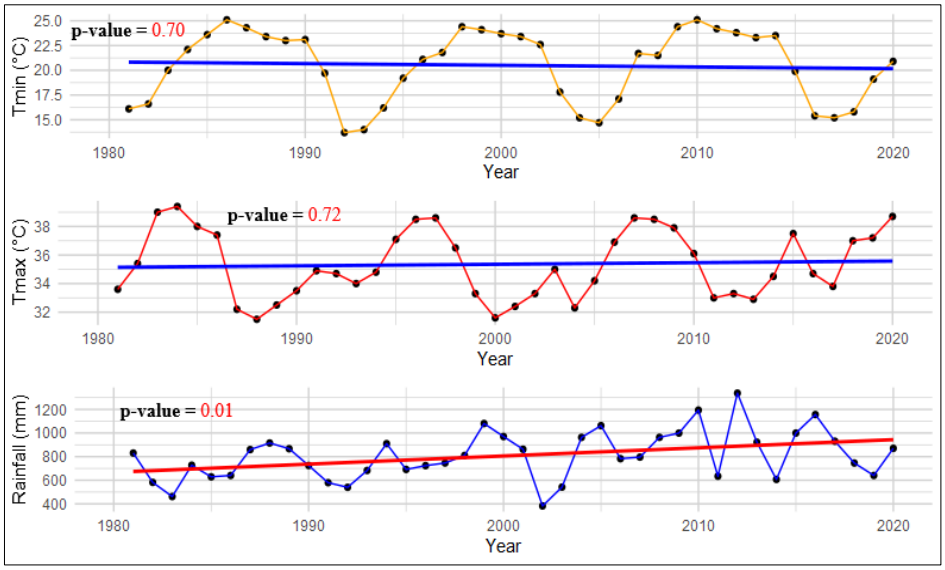

(a)

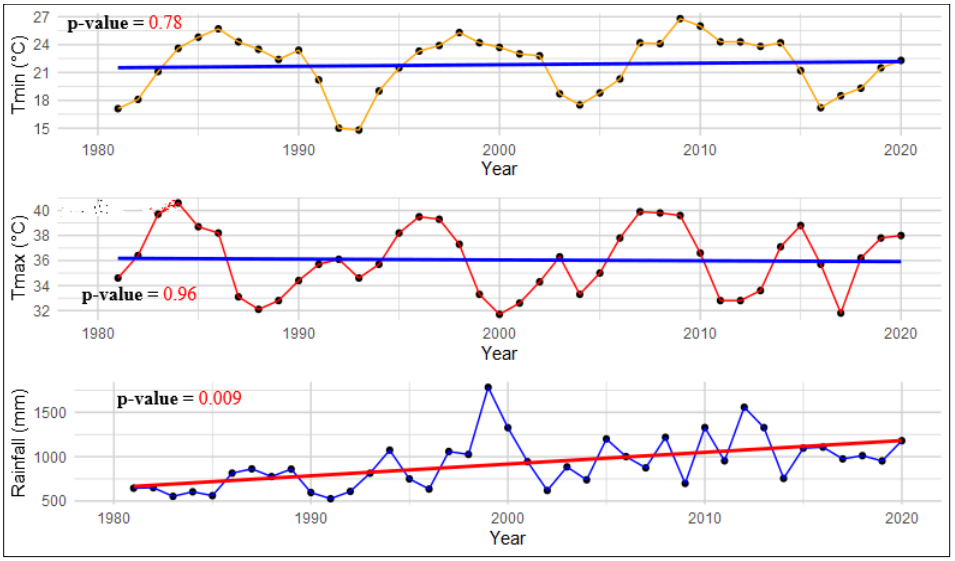

(b)

Figure 5. 4 Mann-Kendall trend of climate variability from 1980 -2020 a) LRR b) CRRS

The standard Mann-Kendall test was employed to analyze the annual climate variables, revealing distinct trends in the Central River South (CRRS) and Lower River Region (LRR) regions (Figure 5.4). For maximum temperature, CRRS displayed a negative trend with a Sen's Slope (S.S.) of -4.0, indicative of a slight decline. In contrast, LRR showcased a positive direction with a substantial S.S. of 3.40, signifying an upward shift in maximum temperatures. For the annual climate variables, CRRS exhibited predominantly positive trends. Notably, rainfall revealed a

significant positive trend in CRRS, supported by a substantial Sen's Slope (S.S.) of 224 and a low p-value (<0.05), denoting statistical significance. Similarly, LRR displayed comparable positive and statistically significant trends in rainfall, with a S.S. of 222 and a p-value below the threshold of 0.05.

Interestingly, both CRRS and LRR revealed significant and positive trends in annual rainfall when accounting for serial correlation. The p-values of 0.015 for CRRS and 0.011 for LRR underscore the statistical significance of these trends. This suggests a consistent increase in annual rainfall over time in both regions, with the trends retaining their value even when considering serial correlation. This aligns with Barry et al. (2018), who reported increased rainfall in eastern Gambia. Their study also indicated changes in average rainfall intensity in east Gambia, central Senegal, eastern Guinea Bissau, western Mauritania, central Ghana, southern Benin, central Togo, and north-eastern and south Nigeria (Barry et al., 2018).

The Seasonal Mann-Kendall (S-MK) test on seasonal climate variables for the two regions shows similar positive trends for Tmax using the Standard MK test. However, the Z and S.S. values for the S-MK test indicated a relatively low direction in LRR compared to CRRS. S-MK shows a significant ($p < 0.001$) positive trend for seasonal Tmax in CRRS, whereas, in LRR, the trend for Tmax was not significant either with or without serial correlation. In both regions, Tmin shows a significant ($p < 0.05$) negative seasonal trend SS= -11.07 and -4.3 with a p-value of < 2.200 and <0.001 for CRRS and LRR, respectively (Appendix 5.1).

While both regions indicated a negative trend of Tmin using S-MK, the trend was only significant for CRRS using the Prewhitening procedure. Seasonal rainfall using S-MK shows a similar trend in both regions with no significant ($p > 0.05$) trend. The trend-free pre-whitening (TFPW) method using Yue (2002) to determine trends in climate data indicated fewer significant trends in seasonal climate variables for both regions than the S-MK method. In the TFPW approach, the trend was computed using the Theil-Sen approach (TSA), and if it differs from zero, then it is assumed to be linear, the data are detrended, and the AR (1) is computed for the detrended series (Zhang et al., 2019). Collaud et al. (2020) recommend a prewhitening method on time series when lag-1 autocorrelation is statistically significant. The prewhithnenig of the annual rainfall series indicated a significant ($p < 0.05$) positive trend for both regions.

5.3.4 Climate Change Prediction and Rice Production in LRR and CRRS

Autocorrelations indicate that an autoregressive integrated moving average (ARIMA) model could model the time series. The ACF and PACF of the annual climate variables (Tmin and Tmax) are shown in Appendix 5.3. The autocorrelations for small lags tend to be significant and positive since observations nearby in time are also nearby in size. Appendix 5.3 shows significant autocorrelations at lag 1 for almost all the climate variables (Tmin and Tmax), suggesting the estimated ARIMA model requires one MA (1). The partial autocorrelation at lag k quantifies the correlation between data points separated by k steps. This calculation considers their correlation with the data between those k steps (Jenkins et al., 2018). Lag values whose lines cross above the dotted line are statistically significant.

Appendix 5.3 a, b, and c shows two such values, at k = 1 and k = 2, for PCA of all the annual climate variables, suggesting an ARIMA model with one or two A.R. coefficients AR (1; 1; 1). However, this will depend on the model with the lowest AIC and forecast error evaluation (Delima & Lumintac, 2019). To estimate an optimal ARIMA (p,d,q) model to be used for forecasting climate, the ACF and PACF and the stationarity of the data were observed. The letter "p" corresponds to the lag value where the PACF chart initially crosses the upper confidence interval. Additionally, the letter "q" corresponds to the lag value where the ACF chart initially crosses the upper confidence interval. The ACF and PACF suggest an AR (1) and MA (1) model. So, the initial candidate models are ARIMA (0, 1, 0) and ARIMA (0, 1, 1). The order of p and q was determined based on the ACF and PACF plots for creating five preliminary ARIMA models for the yearly climatic variables in CRRS and LRR. Out of the five models, ARIMA, with the lowest AICc and RMSE, was selected for diagnostic analysis (Patel et al., 2014; Bagbuhouna et al., 2018). A better model for predicting climate variables was created using the normalized root mean squared error (NRMSE) performance measures.

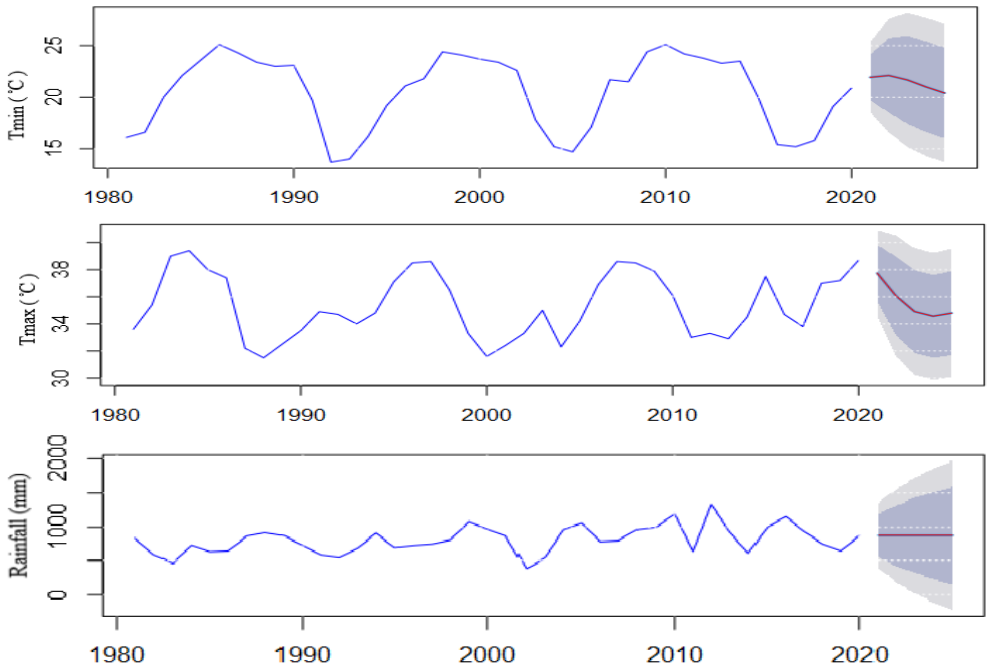

Figure 5. 5 ARIMA Model predicted values for climate variables for LRR (2020-2025)

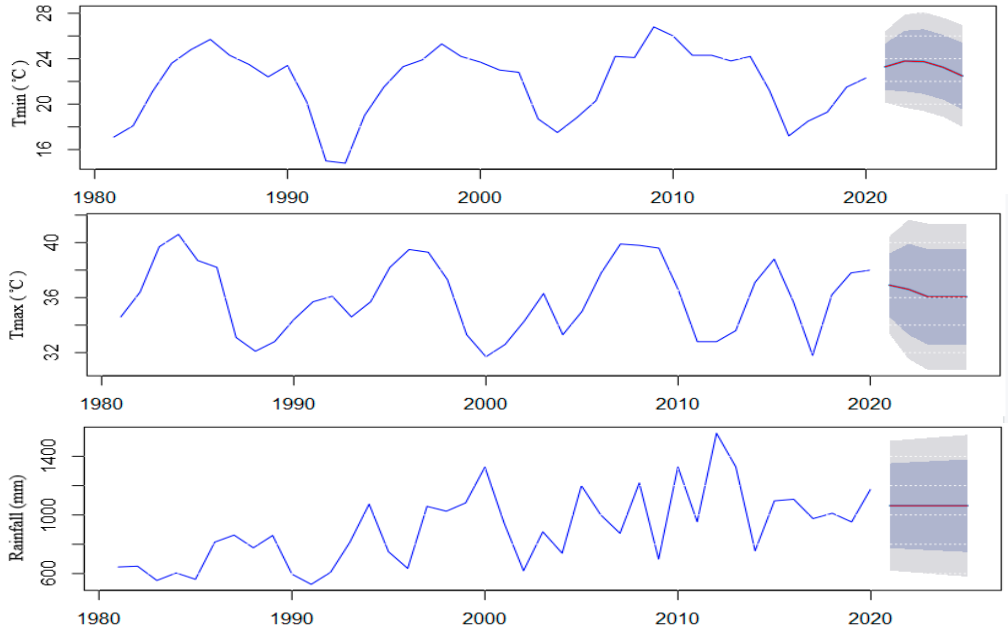

Figure 5.6: ARIMA Model Predictions for Climate Variables in CRRS (2020-2025)

Different models were chosen for the maximum temperature for the two regions (ARIMA 0, 1, 0, CRRS, and 0, 1, 0 for LRR). The minimum temperature shows a similar behavior where ARIMA 0,1,0 shows the lowest AIC and RMSE value as opposed to the maximum temperature in CRRS, ARIMA 0,1,0 indicated the lowest AIC (157.63) and RMSE (1.42) for LRR respectively. The best-performing model

according to AIC and RMSE values for rainfall in the two regions is the same (ARIMA 0,1,1); even though they are high for LRR compared to CRRS, the model recorded the lowest values over all models. Contrarily, rainfall shows ARIMA 0, 1, 1 as the better-performing model.

Diagnostic checking of the models using Jlung-Box chi-square statistics and autocorrelation of residuals was done to analyze ARIMA results and determine if the model meets the assumptions. A plot of the standardized residuals, the ACF, a boxplot of the standardized residuals, the p-values associated with the Q-statistic, and a Q-Q plot are shown in Appendix 5.4 a, b, and c. When the model fits effectively, the standardized residuals should exhibit the characteristics of a white noise sequence, featuring an average of zero and a variance of one. Examination of the time plot of the standardized residuals in Appendix 5.4, a, b, and c shows no apparent patterns. There may be outliers, with a few values surpassing three standard deviations in magnitude. The standardized residuals' ACF offers no evident departure from the model assumptions, and the Q-statistic is never significant at the delays given. Except for the likely outliers, the usual Q-Q plot of the residuals reveals that the normality assumption is valid. The model is a good match.

Table 5.2 provides changes in the historical data based on ARIMA-predicted climate variables for two distinct regions, LRR and CRRS, with a particular focus on Tmin (Minimum Temperature), Tmax (Maximum Temperature), and Rainfall for the next five years (2021–2025). In the LRR region, there are notable variations in the predicted values compared to historical records. Tmin is projected to decrease by approximately -6.36%, indicating a cooling trend in minimum temperatures.

Conversely, Tmax demonstrates a more marginal decline of -0.75%, implying relatively stable maximum temperatures. However, Rainfall is expected to experience a substantial increase of 34.84% in predicted values relative to historical data, suggesting a significant uptick in precipitation levels. For the CRRS region, the trends are somewhat different.

Tmin is anticipated to increase notably by 5.63%, signaling a significant warming trend in minimum temperatures. Tmax remains relatively stable with a minor -0.75 and 0.39% decrease in predicted values compared to historical records for LRR and

CRRS, respectively. Rainfall is projected to rise by 25.73%, indicating a considerable increase in precipitation levels.

Table 5. 2 Projected climate variable changes for LRR and CRRS Regions (2021–2025

Region	Variable	Historical	Predicted	% Change
LRR	Tmin	25.20	23.60	-6.36
	Tmax	35.82	35.55	-0.75
	Rainfall	809.16	1091.04	34.84
CRRS	Tmin	20.80	21.97	5.63
	Tmax	36.05	35.90	-0.39
	Rainfall	768.90	966.72	25.73

These findings highlight the distinct climate patterns in each region. In the LRR region, the anticipated decrease in Tmin and relatively stable Tmax could signify a shift towards cooler nights while maintaining daytime temperature stability. Meanwhile, the substantial increase in rainfall suggests potential impacts on local ecosystems and water resources. In contrast, CRRS is expected to experience warming in minimum temperatures, which can have various ecological and agricultural consequences. The slight decrease in Tmax implies relatively stable maximum temperatures, and the increased rainfall could benefit the region's water supply and agriculture.

5.3.5 Rice Production Trend in LRR and CRRS of The Gambia

Rice yields in CRRS and LRR were analyzed using a linear regression model for the rice yield data from 1982 to 2020. The model aimed to establish a relationship between year and rice yield by explaining the proportion of the variance in rice yield as the year changes. The R^2 value of 0.67 indicates that around 67 % of the variability in rice yield can be explained by the differences in the year. Similarly, for the CRRS, the R^2 value of 0.64 indicates that around 64 % of the variability in rice yield can be explained by the changes in the year in the lowland rice production.

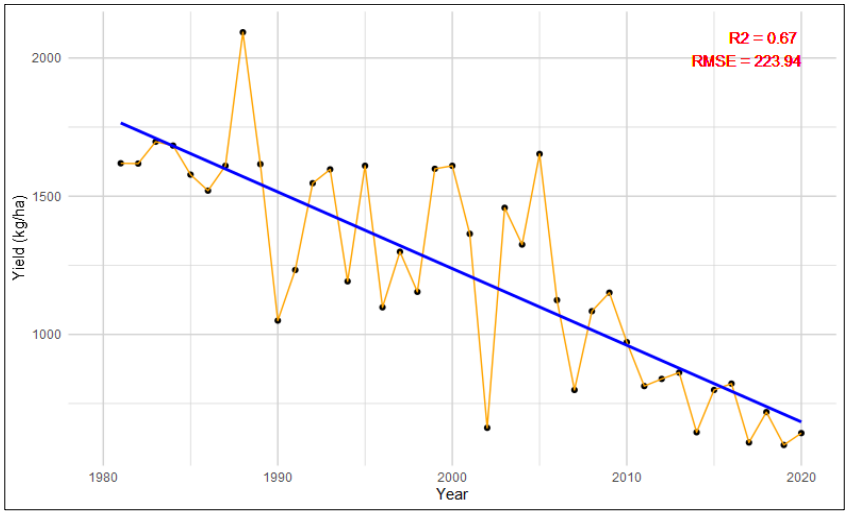

(a)

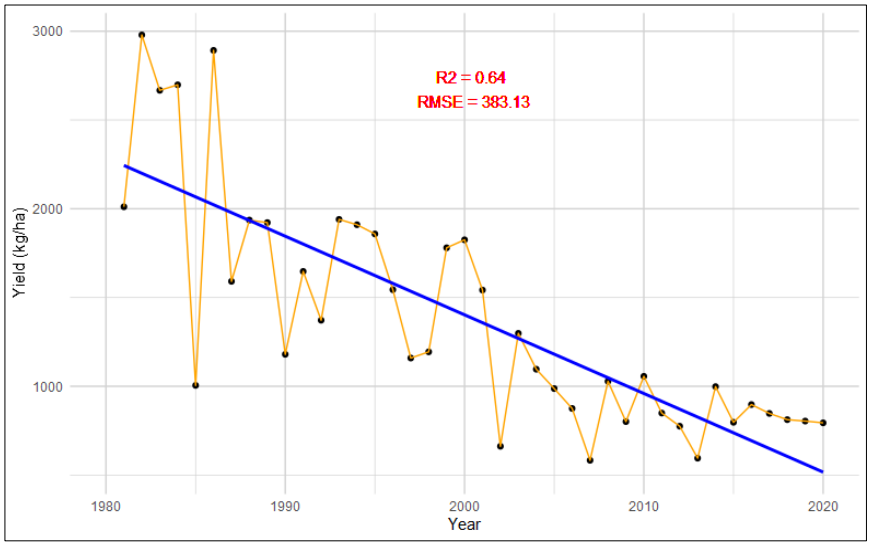

(b)

Figure 5. 5 Historical rice yield (kg/ha) trend from 1980 -2020 a) LRR b) CRRS, The Gambia

The RMSE value of 223.94 for LRR and 383.13 for CRRS suggest that the predicted rice yield values from the linear regression model are, on average, closer to the actual values in the LRR compared to the CRRS. This means that the model's predictions in the LRR have less deviation from the actual data points than the CRRS. The coefficient of determination indicates an R^2 value of 0.64, suggesting that approximately 64 % of the variability observed in rice yield can be attributed to the linear relationship with year. Rice yield values in LRR show a high range of variability with a minimum of 600 kg/ha and a maximum of 2093.0 kg/ha of rice.

The mean yield recorded in LRR averages 1224.2 kg/ha. Comparatively, rice yield in CRRS shows some exciting patterns similar to LRR; the dataset for CRRS spans from

1981 to 2020. The minimum result observed in CRRS is 583.0 kg/ha, slightly lower than LRR. The quartile values indicate that CRRS has a higher median yield (1169.5 kg/ha) than LRR. The mean yield for CRRS is also higher at 1380.2 kg/ha, with a maximum recorded yield of 2979.0 kg/ha in CRRS, significantly higher than in LRR, suggesting a relatively higher average yield in this region.

Ordinary least square regression (OLS) analysis was conducted to determine the effect of climate on rice yield in the two regions. Each model yield was used as the dependent variable, whereas the climate variables were used as the independent variables.

Table 5.3 OLS regression analysis for historical climate variables as predictors of rice Yield in the Lower River Region (LRR)

	Dependent variable: Yield			
Predictors	Estimates	S.E.	t.val.	p-value
(Intercept)	3304.57	685.38	4.82	<0.001
Tmin	17.28	11.29	1.53	0.150
Tmax	-49.32	17.47	-2.82	0.014
RF	-0.07	0.04	-1.62	0.129
Observations	18		F(4,34) = 7.71	
R^2 0.70	Adj. R^2 0.61			p = <0.001

In the LRR region, the OLS regression analysis uncovered a robust model with an adjusted R-squared of 0.61, indicating a well-fitted relationship between climate variables and rice yield. Specifically, Tmax demonstrated a significant negative relationship (-49.32) with yield, suggesting that increasing maximum temperature is linked to decreasing rice yield. However, Tmin and RF exhibited no statistically significant associations. The coefficient of determination R^2 value indicated that 70 % of yield variation in rice yield is a climatic effect. This underscores the significance of considering maximum temperature in comprehending and predicting rice yield fluctuations in the LRR region. In CRRS, the OLS model is statistically significant (t-value = 3.39, p = 0.008), indicating a baseline yield without climate variables. Examining individual climate predictors, Tmin exhibited a non-significant coefficient of 1.01, while Tmax showed a non-significant coefficient of -44.09.

Table 3.4 OLS regression analysis for historical climate variables as predictors of rice Yield in the Lower River Region (LRR)

		Dependent variable: Yield		
Predictors	Estimates	S.E.	t. val.	p-value
(Intercept)	4329.89	127.97	3.39	**0.008**
Tmin	1.01	31.32	0.03	0.975
Tmax	-44.09	29.06	-1.52	0.164
RF	-0.14	0.07	-2.17	0.051
Observations	14		F(4,34) = 4.48	
R^2 0.67	Adj. R^2 0.52			p = 0.03

Rainfall (RF) displayed a marginally significant negative coefficient of -0.14, suggesting a potential impact on rice yield in the CRRS region. The overall model was statistically significant (F(4,34) = 4.48, p = 0.03), indicating at least one predictor's significant relationship with rice yield. The R2 value of 0.67 denoted that the model explained approximately 67% of the variability in rice yield. At the same time, the adjusted R-squared (0.52) provided a more conservative measure, considering the number of predictors and observations.

The random forest model shows that maximum temperature is the most influential predictor, with an importance score of 1968993, following rainfall with a score of 1647426, showcasing its substantial contribution to the predictive performance.

Table 5. 5 Comparison of IncNodePurity values for Tmin, Tmax, and RF for LRR and CRRS

Region	LRR	CRRS
Tmin	1437471	3663804
Tmax	1968993	4475451
RF	1647426	5258378

This indicates that fluctuations in maximum temperature also significantly impact rice yield. Higher maximum temperatures may accelerate crop maturation, affecting the duration of growth stages and yield. The least essential climate variable is the minimum temperature (1437471). This ranking of importance suggests that alterations in maximum exhibit the most profound effect on historical yield prediction, followed by rainfall and, subsequently, minimum temperature.

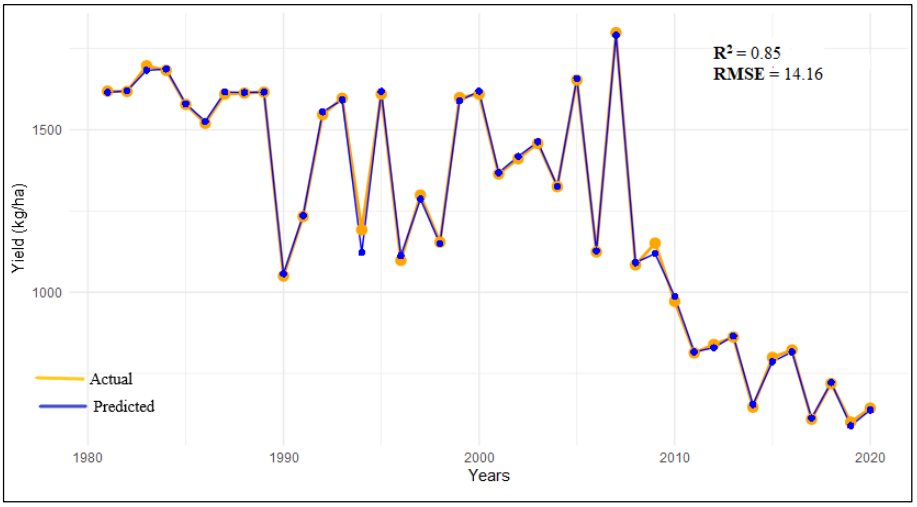

(a)

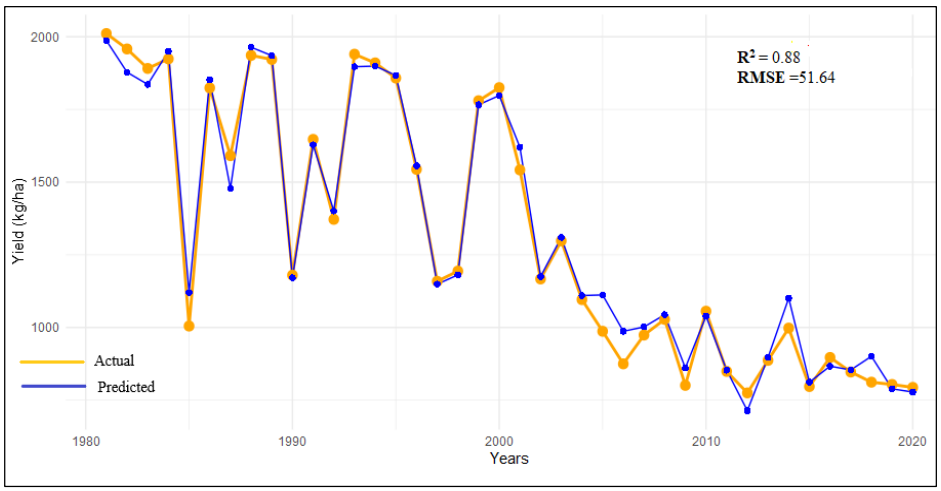

(b)

Figure 5. 6 Random Forest prediction of rice yield due to annual trends in historical rainfall, minimum and maximum temperatures from 1980 -2020 a) LRR b) CRRS

Temperature and rainfall are important factors affecting rice yield in the Sudano-Sahelian part of West Africa. For example, Roudier et al. (2011) reported that cultivated regions within the Sudano-Sahelian zone are expected to experience a more significant impact from climate change than those in the Guinean zone. Sultan and Gaetani (2016) indicated more substantial warming in the Sahel and Sahara compared to temperatures in the Guinean zone influenced by the Atlantic Ocean and are expected to increase more slowly.

Sultan et al. (2019) affirmed that rising temperatures lead to crop yield losses, regardless of rainfall pattern, due to the shortening of crop duration and increasing evapotranspiration demand, thus reducing crop yields in West Africa. However, the

results must be interpreted cautiously, especially in the case of CRRS. Because of the year-round availability of freshwater from the river Gambia in CRRS, rice production is done during the dry season (March to June) and the late part of the regular cropping season (Sept to Dec) depending almost entirely on river Gambia as the source of irrigation.

The practice is done to avoid periods of high levels of surface water induced by torrential rains and amplified high tidal levels. Similarly, CRRS South and North serve as the country's rice production hub. Thus, several land development programs were conducted in the rice cultivation field through government projects and programs in the form of water control structures. These programs are usually designed in a manner that tends to restrict drainage into the river for effective water retention in the cultivated field. These prevent the conveyance/discharge of flooded rainwater from the upper slopes (upland) into the river during the rainy season.

This means that any further increase in water levels by rainfall results in inundations/flooding of rice fields, rendering them temporarily unsuitable for production. Another critical factor to this end is farmers' cultural /agronomic practices. Rice production in the lowland ecosystems is mainly based on transplanting 4- to 6-week-old seedlings grown in nurseries.

Seed rates in nursery beds are usually high, thus producing tiny seedlings due to competition for solar radiation and other essential nutrients. Due to the minor nature of seedlings at transplanting, farmers tend to increase the rate of seedlings per transplanting hill above the recommended rate of 3-4. This promotes excessive vegetative growth and increases competition, which can reduce the yield. Similarly, fertilizer applications are usually made under normal flooded conditions. However, this usually reduces fertilizer use efficiency if the application coincides with high tides and intensive rainfall, resulting in overflooding above the bund, washing away the fertilizer.

5.3.6 Summary

The study analysis of climate variables in the Lower River Region (LRR) and Central River Region South (CRRS) reveals notable trends and implications for agriculture

and climate resilience. While both regions exhibit similar monthly climate variables, such as temperature and rainfall, distinct trends emerge.

In terms of temperature, there is an eastward increase in maximum temperature from LRR to CRRS and a corresponding westward decrease in minimum temperature from CRRS to LRR. A significant positive trend in seasonal maximum temperatures is observed in CRRS, while LRR shows a non-significant trend, regardless of autocorrelation considerations. These findings align with The Gambia's projected climate change trends, which anticipate rising temperatures and increased evapotranspiration (Gibba & Jallow, 2020).

Monthly rainfall patterns in both regions peak in August, with a maximum of 486 mm during the study period (1980 – 2020). Trend analysis indicates a significant positive increase in annual rainfall in both areas, whether considering autocorrelation or not. However, there is an eastward decrease in yearly rainfall, with LRR recording annual values of 809.16 mm and CRRS at 758.93 mm.

The analysis's linear regression models reveal that a substantial portion of rice yield variability in LRR (67%) and CRRS (64%) can be explained by annual changes. The model's accuracy in reflecting observed trends is more pronounced in LRR, highlighting its utility for understanding and predicting climate-induced impacts on rice production.

CHAPTER SIX
CONCLUSIONS AND RECOMMENDATIONS

6.1 CONCLUSIONS

This study has investigated the complex relationship between soil salinity and climate change and their combined impact on rice cultivation within the floodplain regions of the Lower River Region (LRR) and Central River Region South (CRRS) of The Gambia. The study employed advanced machine learning methods to predict and map the extent of soil salinity, assess the seasonal variability of soil salinity, and assess climate trends to elucidate the effects of these factors on rice production dynamics. The following conclusions can be drawn from the study in line with the specific objectives set:

The spatio-temporal dynamics of soil salinity in the tidal swamp rice production zones of the River Gambia floodplain revealed significant insights. The western part, influenced by seawater intrusion, exhibited higher salinity levels. Integration of correlation, regression models, and remote sensing data provided a comprehensive understanding of soil salinity variations. The Random Forest (RF) model emerged as a robust predictor with high accuracy and reliability, showcasing R2 values of 0.93 for LRR and 0.89 for CRRS. Historical trend analysis indicated a 9.56% increase in salt-affected areas in LRR and a 13.94% reduction in CRRS. LRR witnessed a decline in non-saline regions and slightly increased saline soils (26.62%). In contrast, CRRS experienced contractions in slightly saline (-8.92%) and moderately saline (-21.26%) areas. These findings emphasize the need for tailored strategies to manage expanding salinity-affected areas in LRR and reduce salinity in CRRS for sustainable land use and ecosystem health.

Investigating the seasonal variability of root-zone salinity and its impact on rice yield provided valuable insights. Notable variations in soil physicochemical properties influenced rice growth and productivity. Correlation and regression analyses highlighted the significant effect of soil salinity on rice crop performance—field-specific dynamics shaped salinity conditions, including soil pH, sodium composition, and groundwater quality. The Multiple Linear Regression models showcased robust fits with R^2 values of 0.98, indicating a remarkable 98.55% variability in soil and water salinity conditions in the study area. Distinctiveness in soil properties translated into significant differences in rice yield among study fields. Kudang, with lower soil

salinity levels, exhibited more favorable conditions for rice cultivation, resulting in higher yields (254 kg/ha) compared to Mandina (213.8 kg/ha) and Tonitaba (221.9 kg/ha). These varying soil salinity conditions pose challenges and opportunities for site-specific salinity management options and practices to optimize rice productivity.

Assessing climate trends in LRR and CRRS highlighted significant changes with implications for rice production. OLS regression models elucidated the relationships between climate variables and rice yield. In the LRR region, the OLS regression analysis uncovered a robust model with an adjusted R^2 value 0.61, emphasizing the well-fitted relationship between climate variables and rice yield. Maximum temperature demonstrated a significant negative relationship (-49.32) with yield, suggesting the need to address the impact of temperature fluctuations. The CRRS model showed statistically significant results (t-value = 3.39, p = 0.008), indicating a baseline yield without climate variables. Minimum and maximum temperatures showed a non-significant coefficient of 1.01 and -44.09, respectively. Rainfall (RF) displayed a marginally significant negative coefficient of -0.14, suggesting a potential impact on rice yield in the CRRS region. The overall model was statistically significant (p = 0.03) with an R^2 value of 0.67, indicating that climate variables significantly impacted rice yield. The random forest models highlighted the substantial influence of maximum temperature and rainfall on rice yields, emphasizing the vulnerability of rice production to climate change in both regions. These findings underscore the urgency of climate-resilient agricultural practices to mitigate the impact of changing climate conditions on rice production in both regions.

6.2 RECOMMENDATIONS

6.2.1 Recommendations for policy

Based on the study's findings, it is recommended that region-specific soil salinity management strategies be implemented, considering the distinct challenges in LRR and CRRS. Through relevant state departments, the government should introduce measures to reduce salinity in CRRS and manage the salinity-affected areas in LRR.

The study recommended promoting site-specific agricultural practices and provided farmers with information on optimal cultivation practices based on soil salinity levels.

There is also the need to support the adoption of rice varieties that exhibit resilience to specific soil conditions.

Furthermore, stakeholder collaboration is recommended to develop and implement climate-resilient agricultural policies that address the challenges of changing climate conditions in LRR and CRRS. These should include integrating climate-smart agricultural practices to enhance the adaptive capacity of rice production systems.

6.2.2 Recommendations for further research

The study recommended longitudinal studies to monitor the effectiveness of implemented salinity management strategies. Further research should explore the impact of climate change on soil salinity dynamics and assess the adaptability of different rice varieties to varying salinity levels.

To promote rice production in the study area, an in-depth study on the genetic characteristics of rice varieties to identify traits associated with resilience to varying soil salinity levels is required. These should include investigating the long-term effects of site-specific management practices on soil health and rice productivity.

The study suggests additional research to monitor climate trends and their effects on rice production, informing adaptive strategies. This research should investigate the interaction between climate variables and rice yield at a more detailed spatial and temporal scale, improving predictive models. Additionally, further investigations are needed to assess the efficacy of climate-resilient agricultural practices in reducing the impact of temperature and rainfall fluctuations on rice yields.

6.2.3 Contribution to Knowledge

The study contributes to the knowledge of integrating remote sensing, soil data, and statistical models to estimate soil salinity. Furthermore, the study's findings contribute significantly to understanding soil salinity dynamics in the Lower and Central River Region South of The Gambia.

These findings are relevant for promoting sustainable land management and climate-resilient practices within the floodplains of The Gambia River Basin, aligning with the UNCCD's Land Degradation Neutrality (LDN) goal by 2030. The study offers a wealth of evidence-based insights into the complexities of sustainable rice production in the distinctive agricultural landscape of mangrove swamp areas in The Gambia.

REFERENCES

Abd-elwahed, M. S. (2014). Assessment of soil salinity problems in agricultural areas through spatial and temporal remote sensing assessment of soil salinity problems of farm areas through spatial and temporal In the Graduate College. December 2005. Approach Paper. (2015).

Abuelgasim, A.; Ammad, R. (2018). Mapping Soil Salinity in Western United Arab Emirates (UAE) Using Satellite Data. Preprints, 2018040203. https://doi.org/10.20944/preprints201804.0203.v1.

Acion L, Peterson JJ, Temple S, Arndt S (2006). "Probabilistic Index: An Intuitive Nonparametric Approach to Measuring the Size of Treatment Effects." Statistics in Medicine, 25(4), 591–602. https://doi:10.1002/sim.2256.

Acion, L., Peterson, J. J., Temple, S., & Arndt, S. (2005). Probabilistic index: an intuitive non-parametric approach to measuring the size of treatment effects. Statistics in Medicine, 24(15), 2441-2449. https://doi.org/10.1002/sim.2256.

Adefurin, O., & Zwart, S. (2017). A detailed map of rice production areas in mangrove ecosystems in West Africa in 2013 – Mapping of mangrove rice systems using Landsat 8 satellite imagery and secondary data. AfricaRice GIS Report – 2. Africa Rice Center, Cotonou, Benin. https://doi.org/10.13140/RG.2.2.32544.58889.

Adesina, A. J., Kumar, K. R., & Sivakumar, V. (2016). Aerosol-Cloud-Precipitation Interactions over Major Cities in South Africa: Impact on Regional Environment and Climate Change. Aerosol and Air Quality Research, 16, 195–211. https://doi.org/10.4209/aaqr.2015.03.0185.

Adger, W. N., Brown, K., Nelson, D. R., Berkes, F., Eakin, H., Folke, C. Tompkins, E. L. (2011). Resilience implications of policy responses to climate change. Wiley Interdisciplinary Reviews: Climate Change, 2(5), 757–766. https://doi.org/10.1002/wcc.133.

Akbarzadeh, A., & Mehrijardi, R. T. (2010). Distribuţia Spaţială a unor Proprietăţi ale Solului prin Utilizarea Metodelor Geostatistice în Regiunea Khezrabad (Yazd) din Iran. ProEnvironment Promediu, 3(5).

Akça, E., Aydin, M., Kapur, S., Kume, T., Nagano, T., Watanabe, T., & Zorlu, K. (2020). Long-term monitoring of soil salinity in a semi-arid environment of Turkey. Catena, 193, 104614.

Akritas, M. G. (2015). Probability and Statistics with R for Engineers and Scientists (1st ed.). New York: Pearson.

Allbed, A., & Kumar, L. (2013). Soil Salinity Mapping and Monitoring in Arid and Semi-Arid Regions Using Remote Sensing Technology: A Review. Advances in Remote Sensing, 02(04), 373–385. https://doi.org/10.4236/ars.2013.24040.

Allbed, A., Kumar, L., & Sinha, P. (2014). Mapping and modeling spatial variation in soil salinity in the Al Hassa Oasis based on remote sensing indicators and regression techniques. Remote Sensing, 6(2), 1137–1157. https://doi.org/10.3390/rs6021137

Allen, R.G., Pereira, L.S., Raes, D., Smith, M., (1998). Crop evapotranspiration. Guidelines for Computing Crop Water Requirements. FAO Irrigation and Drainage Paper 56. Food and Agriculture Organization of the United Nations, Rome.

Amuzu, J., Jallow, B.P., Kabo-Bah, A.T., & Yaffa, S. (2018). The Socio-economic Impact of Climate Change on the Coastal Zone of The Gambia. Natural Resources and Conservation, 6(1), 13-26. http://doi.org/10.13189/nrc.2018.060102.

Anderson, M. J. (2001). A new method for nonparametric multivariate analysis of variance. Austral Ecology, 26(1):32–46.

Angulo, C., Becker, M., & Wassmann, R. (2012). Yield gap analysis and assessment of climate-induced yield trends of irrigated rice in selected provinces of the Philippines. Journal of Agriculture and Rural Development in the Tropics and Subtropics, 113, 61–68.

Anwar, M. R., Liu, D. L., Macadam, I., & Kelly, G. (2013). Adapting agriculture to climate change: a review. Theoretical and applied climatology, 113, 225-245.

Aredehey, G., Libsekal, H., Brhane, M., Welde, K., Giday, A., & Tigray, S. (2018). Top-soil salinity mapping using the geostatistical approach in the agricultural landscape of Timuga irrigation scheme, South Tigray, Ethiopia Top-soil salinity mapping using the geostatistical approach in the agricultural landscape of Timuga. Cogent Food & Agriculture, 4(1), 1–13. https://doi.org/10.1080/23311932.2018.1514959.

Arslan, H., & Demir, Y. (2013). Impacts of seawater intrusion on soil salinity and alkalinity in Bafra Plain, Turkey. Environmental Monitoring and Assessment, 185(2), 1027–1040. https://doi.org/10.1007/s10661-012-2611-3.

Asch, F., & Wopereis, M. C. (2001). Responses of field-grown irrigated rice cultivars to varying levels of floodwater salinity in a semi-arid environment. Field Crops Research, 70(2), 127-137.

Awal, R., Bayabil, H. K., & Fares, A. (2016). Analysis of potential future climate and climate extremes in the Brazos headwaters Basin, Texas. Water (Switzerland), 8(12), 1–18. https://doi.org/10.3390/w8120603.

Bado, S., Forster, B. P., Nielen, S., Ali, A. M., Lagoda, P. J. L., Till, B. J., & Laimer, M. (2015). Plant Mutation Breeding: Current Progress and Future Assessment. In J. Janick (Ed.), Advances in Plant Breeding Strategies: Breeding, Biotechnology and Molecular Tools (pp. 13-41). John Wiley & Sons. https://doi.org/10.1002/9781119107743.ch02.

Badreldin, N., & Goossens, R. (2014). Monitoring land use/land cover change using multi-temporal Landsat satellite images in an arid environment: a case study of El-Arish, Egypt. Arabian Journal of Geosciences, 7, 1671-1681.

Bagbuhouna, M., Yaffa, S., Sogbedji, J. M., Bah, & Koglo, Y. S. (2018). Knowledge and adaptive responses of rice farmers to saline-water intrusion on swamp rice-growing fields in the Gamba lower river region. Journal of Environment and Earth Science, 8 (3), 63-76.

Baggie, I., Sumah, F., Zwart, S. J., Sawyerr, P., Bandabla, T., & Kamara, C. S. (2018). Characterization of the mangrove swamp rice soils along the Great Scarcies River in Sierra Leone using principal component analysis. CATENA, 163, 54–62. https://doi.org/10.1016/j.catena.2017.11.026.

Balasubramanian, V., Sie, M., Hijmans, R.J., Otsuka, K. (2007). "Increasing Rice Production in Sub-Saharan Africa: Challenges and Opportunities." In D.L. Sparks (Ed.), Advances in Agronomy, Volume 94, Pages 55-133. Academic Press. ISSN 0065-2113. ISBN 9780123741073. https://doi.org/10.1016/S0065-2113(06)94002-4.

Bandyapadhyay, B.K., Maji, B., Sen, H.S. and Tyagi, N.K. (2003) Coastal soils of West Bengal – their nature, distribution, and characteristics. Bulletin No. 1/2003. Central Soil Salinity Research Institute, Regional Research Station, Canning Town, West Bengal, pp. 1-62.

Bannari, A., Rhinane, H., Shahid, S. A., & Hameid, N. (2021). Validation and Comparison of Physical Models for Soil Salinity Mapping over an Arid Landscape Using Spectral Reflectance Measurements and Landsat-OLI Data.

Barrett-Lennard, E. G., Bennett, S. J., & Colmer, T. D. (2008, March). Standardizing terminology for describing the level of salinity in soils in Australia. In 2nd International Salinity Forum. Salinity, Water, and Society: Global Issues, Local Action (Vol. 30).

Barry, A. A., Caesar, J., Klein Tank, A. M. G., Aguilar, E., McSweeney, C., Cyrille, A. M., Nikiema, M. P., Narcisse, K. B., Sima, F., Stafford, G., Touray, L. M., Ayilari-Naa, J. A., Mendes, C. L., Tounkara, M., Gar-Glahn, E. V. S., Coulibaly, M. S., Dieh, M. F., Mouhaimouni, M., Oyegade, J. A., Sambou, E., & Laogbessi, E. T. (2018). West Africa climate extremes and climate change indices. International Journal of Climatology, 38(1), 428-442. https://doi.org/10.1002/joc.5420.

Basak, N., Shit, P.K., Adhikary, P.P., Bhunia, G.S., Sengupta, D. (2022). Salt Affected Soils: Global Perspectives. In: Shit Soil Health and Environmental Sustainability. Environmental Science and Engineering. Springer, Cham. https://doi.org/10.1007/978-3-031-09270-1_6.

Basso, D., & Salmaso, L. (2009). A permutation test for umbrella alternatives. Statistics and Computing, 21(1), 45–54. https://doi.ogr/10.1007/s11222-009-9145-8.

Basso, D., & Salmaso, L. (2011). A permutation test for umbrella alternatives. Statistical Computing, 21(1), 45–54. https://doi.org/10.1007/s11222-009-9145-8.

Bathiany, S., Dakos, V., Scheffer, M., & Lenton, T. M. (2018). Climate models predict increasing temperature variability in poor countries. Climatology, 1. https://doi.org/10.1126/climatology.aav8220.

Bathke, A., Friedrich, S., Konietschke, F., Pauly, M., Staffen, W., Strobl, N., and H¨oller, Y. (2016). Using EEG, SPECT, and multivariate resampling methods to differentiate between Alzheimer's and other cognitive impairments. arXiv preprint arXiv:1606.09004.

Bayabil, H. K., Li, Y., Tong, Z., & Gao, B. (2021). Potential management practices of saltwater intrusion impact soil health and water quality: a review. Journal of Water and Climate Change, 12(5), 1327-1343.

Bell, J. E., Brown, C. L., Conlon, K., Herring, S., Kunkel, K. E., Lawrimore, J., ... & Uejio, C. (2018). Changes in extreme events and the potential impacts on human health. Journal of the Air & Waste Management Association, 68(4), 265-287.

Belle E.M.S., Burgess N.D., Misrachi M., Arnell A., Masumbuko B., Somda J., Hartley A., Jones R., Janes T., McSweeney C., Mathison C., Buontempo C., Butchart S., Willis S.G., Baker D.J., Carr J., Hughes A., Foden W., Smith R.J., Smith J., Stolton S., Dudley N., Hockings M., Mulongoy J., Kingston N. (2016). Climate Change Impacts on Biodiversity and Protected Areas in West Africa, Summary of the main outputs of the PARCC project, Protected Areas Resilient to Climate Change in West Africa. UNEP-WCMC, Cambridge, UK.Berners-Lee, M., Kennelly, C., Watson, R., & Hewitt, C. N. (2018). Global food production is sufficient to meet human nutritional needs in 2050, provided radical societal adaptation exists. Elem Sci Anth, 6, 52.

Berrar, D. (2019). Cross-Validation. *Encyclopedia of Bioinformatics and Computational Biology*, pp. 542–545. https://doi.org/10.1016/B978-0-12-809633-8.20349-X.

Beveridge, L., Whitfield, S., Challinor, A. (2018). Crop modeling: towards locally relevant and climate-informed adaptation. Climatic Change 147, 475–489. https://doi.org/10.1007/s10584-018-2160-z.

Bhavnani, R., Vordzorgbe, S., Owor, M., & Bousquet, F. (2008). Report on the status of disaster risk reduction in the Sub-Saharan Africa region. Commission of the African Union, World Bank, UNISDR, Nairobi.

Biasutti, M. (2019). Rainfall trends in the African Sahel: Characteristics, processes, and causes. Wiley Interdisciplinary Reviews: Climate Change, e591. https://doi.org/10.1002/wcc.591.

Bodian, A., Dezetter, A., Diop, L., Deme, A., Djaman, K., & Diop, A. (2018). Future Climate Change Impacts on Streamflows of Two Main West Africa River Basins : Senegal and Gambia. March. https://doi.org/10.3390/hydrology5010021

Bruckner M.Z., (2012), Water and Soil Characterization- pH and Electrical Conductivity, Microbial Life Educational Resources. Montana State University Bozeman, 2012.

Burchett, W. W., Ellis, A. R., Harrar, S. W., & Bathke, A. C. (2017). Nonparametric Inference for Multivariate Data: The R Package npmv. Journal of Statistical Software, 76(4), 1–18. https://doi.org/10.18637/jss.v076.i04.

Cakmak, I. (2013). Magnesium in crop production, food quality, and human health. Plant Soil 368, 1–4. at https//doi.org/10.1007/s11104-013-1781-2.

Cakmak, I., and Kirkby, E. A. (2008). Role of magnesium in carbon partitioning and alleviating photooxidative damage. Physiol. Plantarum 133, 692–704. At: https://doi.org/10.1111/j.1399-3054.2007.01042.x.

Calanca, P. (2007). Climate change and drought occurrence in the Alpine region: How severe are becoming the extremes? Global and Planetary Change, 57(1-2), 151–160. https://doi.org/10.1016/j.gloplacha.2006.11.0.

Carating, R.B. and Division, S.S. (2008) 'Soil fertility mapping,' (1).

Carney, J. (2017). Converting the wetlands, engendering the environment: the intersection of gender with agrarian change in the Gambia. In Development (pp. 133-152). Routledge.

Cavallaro, V., & Dansero, E. (1998). Sustainable development: global or local? GeoJournal, 45(1/2), 33–40. http://www.jstor.org/stable/41147216.

Ceesay, M. M. (2004). Management of rice production systems to increase productivity in The Gambia, West Africa (Doctoral dissertation). Cornell University.

Ceylan, Y., Kutman, U. B., Mengutay, M., and Cakmak, I. (2016). Magnesium applications to growth medium and foliage affect the starch distribution, increase the grain size, and improve seed germination in wheat. Plant Soil 406, 145–156. https//:doi:10.1007/s11104-016-2871-8.

Chakroff, M. S., & DuBois, R. (1982). Marine Fisheries - Case Studies. Published for Peace Corps by Trans-Century Corporation, Washington, D.C. Peace Corps Information Collection and Exchange, Case Studies C 1. March 1981 - April 1982. Marine Fisheries Programming Guide, October 1980. Prepared for the Peace Corps by Trans-Century Corporation under Contract No. 79-043-1029. Available through Peace Corps, ICE, 806 Connecticut Avenue, N.W.,

Washington, D.C. 20525. PEACE CORPS Office of Training and Program Support. Training Manual T0057.
Chandio, A. A., Gokmenoglu, K. K., Ahmad, M., et al. (2022). Towards Sustainable Rice Production in Asia: The Role of Climatic Factors. Earth System and Environment, 6(1), 1–14. https://doi.org/10.1007/s41748-021-00210-z.
Chandra, P., Enespa, & Singh, R. (2020). Soil salinity and its alleviation using Plant Promoting Fungi. Agriculturally Important Fungi for Sustainable Agriculture: Volume 2: Functional Annotation for Crop Protection, 101-148.
Chen, Z., Wang, Q., Ma, J. et al. (2020). Impact of controlled-release urea on rice yield, nitrogen use efficiency and soil fertility in a single rice cropping system. Sci Rep, 10, 10432. https://doi.org/10.1038/s41598-020-67110-6.
Chong, I. Q., Azman, E. A., Ng, J. F., Ismail, R., Awang, A., Hasbullah, N. A., Murdad, R., Ahmed, O. H., Musah, A. A., Alam, M. A., Besar, N. A., Tajidin, N. E., and Jalloh, M. B. (Year). "Improving Selected Chemical Properties of a Paddy Soil in Sabah Amended with Calcium Silicate: A Laboratory Incubation Study. Sustainability (Switzerland), 14(20), pp. 1–13. Available at: https://doi.org/10.3390/su142013214.
Church, J.A., Monselesan, D., Gregory, J., & Marzeion, B. (2013). Evaluating the ability of process-based models to project sea-level change. Environmental Research Letters, 8(1), 014051. https://doi.org/10.1088/1748-9326/8/1/014051.
Cohen, J. (1992). Statistical Power Analysis. Current Directions in Psychological Science, 1(3), 98-101. https://doi.org/10.1111/1467-8721.ep10768783.
Collaud Coen, M., Andrews, E., Bigi, A., Martucci, G., Romanens, G., Vogt, F. P. A., & Vuilleumier, L. (2020). Effects of the prewhitening method, the time granularity, and the time segmentation on the Mann–Kendall trend detection and the associated Sen's slope. Atmospheric Measurement Techniques, 13(12), 6945-6964. https://doi.org/10.5194/amt-13-6945-2020.
Colley, R. (1985). Constraints Imposed by Acid Sulfate Soils on the Gambia's Bridge-barrage Scheme (No. 5). Great Lakes and Marine Waters Center, University of Michigan.
Conijn, J. G., Bindraban, P. S., Schröder, J. J., & Jongschaap, R. E. E. (2018). Can our global food system meet food demand within planetary boundaries? Agriculture, Ecosystems & Environment, 251, 244-256.
Cook, K. H., & Vizy, E. K. (2006). Coupled Model Simulations of the West African Monsoon System: Twentieth- and Twenty-First-Century Simulations. Journal of Climate, 19(15), 3681–3703. https://doi.org/10.1175/JCLI3814.1.
Corbeels, M., Berre, D., Rusinamhodzi, L., Lopez-Ridaura, S. (2018). Can we use crop modelling to identify climate change adaptation options? Agricultural and Forest Meteorology. https://doi.org/10.1016/j.agrformet.2018.02.026.
Corwin, D. L., & Scudiero, E. (2019). Review of soil salinity assessment for agriculture across multiple scales using proximal and remote sensors. In Advances in Agronomy (1st ed., Vol. 158). Elsevier Inc. https://doi.org/10.1016/bs.agron.2019.07.001.
Corwin, D. L., Rhoades, J. D., & Šimůnek, J. (2007). Leaching requirement for soil salinity control: Steady-state versus transient models. Agricultural Water Management, 90(3), 165-180.
Coser, T. R., de Figueiredo, C. C., Jovanovic, B., Moreira, T. N., Leite, G. G., Cabral Filho, S. L. S., Marchão, R. L. (2018). Short-term buildup of carbon from a

low-productivity pastureland to an agrisilviculture system in the Brazilian savannah. Agricultural Systems. https://doi.org/10.1016/j.agsy.2018.01.030.
Daoud, J. I. (2017). Multicollinearity and Regression Analysis. Journal of Physics: Conference Series, 949, 012009. https://doi.org/10.1088/1742-6596/949/1/012009.
Dasgupta, S., Moqbul Hossain, M. D., Huq, M., & Wheeler, D. (2016). Facing the hungry tide: Climate change, livelihood threats, and household responses in coastal Bangladesh. Climate Change Economics, 7(03), 1650007.
Davis, C. S. (2002). Statistical methods for the analysis of repeated measurements. Springer, New.
Davydenko, A., & Charith, K. (2020). A Visual Framework for Longitudinal and Panel Studies (with Examples in R) xd Plot. July 9–10. https://doi.org/10.6084/m9.figshare.12749432.
Day, J. J., & Hodges, K. I. (2018). Growing Land-Sea Temperature Contrast and the Intensification of Arctic Cyclones. Geophysical Research Letters, 45(8), 3857–3865. https://doi.org/10.1029/2018GL077587.
Dehni, A and Lounis M (2012). Remote sensing techniques for salt-affected soil mapping application to the Oran Region of Algeria. *Procedia Engineering* (33) 188 – 198.
Delima, A. J. P., & Lumintac, M. T. Q. (2019). Application of time series analysis for Philippines' inflation prediction. Int. J. Recent Technol. Eng, 8(1), 1761-1765.
Dewitte, O., Jones, A., Elbelrhiti, H., Horion, S., & Montanarella, L. (2012). Satellite remote sensing for soil mapping in Africa: An overview. Progress in physical geography, 36(4), 514-538.
Dong-Jin Kang, Koichi Futakuchi, Somsot Dumnoenngam, Ishii Ryuichi & Ryuichi Ishii (2007) High-Yielding Performance of A New Rice Variety, Ir53650In Mildly Improved Acid Sulfate Soil Conditions, Plant Production Science, 10:1, 64-67. Available at: https://doi.org/10.1626/pps.10.64.
Douaoui, A. E. K., Nicolas, H., & Walter, C. (2006). Detecting salinity hazards within a semiarid context using combining soil and remote-sensing data. *Geoderma*, *134*(1-2), 217-230. https://doi.org/10.1016/j.geoderma.2005.10.009.
Duan, M., & Zhang, X. (2021). Using remote sensing to identify soil types based on multiscale image texture features. Computers and Electronics in Agriculture, 187, 106272. https://doi.org/10.1016/j.compag.2021.106272.
Dunsmore, J.R, Blair A. Rains, G.D.N. Lowe, D.J. Moffatt. I.P. Anderson and J.B. Williams (1976). The Agricultural Development of The Gambia: An Agricultural, Environmental and Socioeconomic Analysis. Land Resource Study 22, Land Resources Division, Ministry of Overseas Development. Surrey, England.
Ekercin, S., and Ormeci, C., (2008). Estimating Soil Salinity Using Satellite Remote Sensing Data and Real-Time Field Sampling. Environmental Engineering Science, (25) 7. https://doi.org/10.1089/ees.2007.0061.
Ellis, A. R., Burchett, Woodrow. W., Harrar, S. W., & Bathke, A. C. (2017). Nonparametric inference for multivariate data: The R package npmv. Journal of Statistical Software, 76(1). https://doi.org/10.18637/jss.v076.i04.
Engman, E. T. (Ed.). (1998). Remote Sensing for Agriculture, Ecosystems, and Hydrology. Chair/Editor. 22-24 September 1998. Barcelona, Spain. Sponsored by CNR-National Research Council of Italy, NASA-National Aeronautics and Space Administration (USA), EOS-The European Optical Society, The

Commission of the European Communities, Directorate General for Science, Research, and Development, SPIE-The International Society for Optical Engineering.
Ervine DA, et al. Vulnerability of two estuaries to flooding and salinity intrusion. Water Science and Tech: Water Supply. 2007:7:125-136.
Fahad, S., Adnan, M., & Noor, M. A. (2019). Major Constraints for Global Rice Production. January, 0–22. https://doi.org/10.1016/B978-0-12-814332-2.00001-0.
Fan, X., Pedroli, B., Liu, G., Liu, Q., Liu, H., & Shu, L. (2012). Soil salinity development in the Yellow River Delta in relation to groundwater dynamics. Land Degradation & Development, 23(2), 175-189.
Fan, X., Weng, Y., & Tao, J. (2016). Towards decadal soil salinity mapping using Landsat time series data. International Journal of Applied Earth Observation and Geoinformation, 52, 32-41. https://doi.org/10.1016/j.jag.2016.05.009.
FAO & ICBA. (2023). Thematic 1: Farmers' guidelines on soil and water management in salt-affected areas. Rome, FAO. https://doi.org/10.4060/cc4200en
FAO (2011). State of the World's Land and Water Resources for Food and Agriculture (SOLAW). Food and Agriculture Organization of the United Nations, Rome.
FAO. (1997). The National Agricultural Research System of the Gambia: Analysis and Strategy for the Long Term. Field Document of FAO/TCP project TCP/GAM/6611. FAO, Rome. 193 p.
FAO. (2020). Crop prospects and food situation-Quarterly global report No. 1, March 2020. Rome.
FAO/AQUASTAT (2010). FAO Aquastat on-line database. Food and Agricultural Organization, Rome, Italy, Available: http://faostat.fao.org. Accessed date: 14 July 2020.
FAOSTAT (2019). Food and Agriculture Data. [WWW Document]. URL. http://www.fao.org/faostat. Accessed date: 14 July 2020.
Feka NZ, Ajonina GN. (2011). Drivers causing a decline of mangrove in West-Central Africa: a review. Int J Biodiversity Sci Ecosystem Serv Manage. https://doi.org/10.1080/21513732.2011.634436.
Fellow, D., Africa, W., & Management, L. (2006). Meeting the challenges of global rice production. 1–9. https://doi.org/10.1007/s10333-005-0031-5.
Feng, G., Zhang, Z., Wan, C., Lu, P., & Bakour, A. (2017). Effects of saline water irrigation on soil salinity and Yield of summer maize (Zea mays L.) in a subsurface drainage system. Agricultural Water Management, pp. 193, 205–213. https://doi.org/10.1016/j.agwat.2017.07.026
Fernandez-Buces, N., Siebe, C., Cram, S., & Palacio, J. L. (2006). Mapping soil salinity using a combined spectral response index for bare soil and vegetation: A case study in the former lake Texcoco, Mexico. Journal of Arid Environments, 65(4), 644-667.
Findley, D. F., Donald E. K., and Wills, K.C (2014). Generalizations of the Box-Jenkins airline model Developing and Evaluating Instructional Sensitive Assessments in Science View project Time Series Modeling and Seasonal Adjustment View project generalizations of the Box-Jenkins airline model. https://www.researchgate.net/publication/241616195.
Fischer, E. M., Beyerle, U., & Knutti, R. (2013). Robust spatially aggregated projections of climate extremes. Nature Climate Change, 3(12), 1033-1038.
Fitton, N., Alexander, P., Arnell, N., Bajzelj, B., Calvin, K., Doelman, J., Gerber, J., Havlík, P., Hasegawa, T., Herrero, M., Krisztin, T., Meijl, H., Powell, T.,

Sands, R., Stehfest, E., West, P., & Smith, P. (2019). The vulnerabilities of agricultural land and food production to future water scarcity. Global Environmental Change, 58. https://doi.org/10.1016/j.gloenvcha.2019.101944.

Food and Agriculture Organization of the United Nations (FAO). (2015). Climate change and food security: Risks and responses (ISBN 978-92-5-108998-9). FAO.

Foulkes, M.J. and Carvalho P. (2012). Roots and Uptake of Water and Nutrients In Meyers, R.A. (eds) Encyclopedia of Sustainability Science and Technology. Springer, New York, NY. https://doi.org/10.1007/978-1-4419-0851-3_195.

Fraser, R. H., Olthof, I., Carrière, M., Deschamps, A., & Pouliot, D. (2011). Detecting long-term changes to vegetation in northern Canada using the Landsat satellite image archive. Environmental Research Letters, 6(4), 045502.

Friedrich, S. and Pauly, M. (2017a). MATS: Inference for potentially singular and heteroscedastic MANOVA. arXiv preprint arXiv:1704.03731.

Friedrich, S., Brunner, E., and Pauly, M. (2017b). Permuting longitudinal data despite the dependencies. Journal of Multivariate Analysis, 153:255–265.

Friedrich, S., Konietschke, F., and Pauly, M. (2017c). GFD: An R package for the analysis of general factorial designs. Journal of Statistical Software, Code Snippets, 79(1):1–18.

Gao, X, Alvo M, Chen J, Li G (2008). "Nonparametric Multiple Comparison Procedures for Unbalanced One-Way Factorial Designs." Journal of Statistical Planning and Inference, 138(8), 2574–2591.

GBOS (2017). The Gambia 2017 Statistical Abstract. Nationally representative – Subnationally representative. https://chat.openai.com/c/48bfb148-fede-4cbe-a427-25079da3db17.

Gebremeskel, G., Gebremicael, T. G., Ki, M., Meresa, E., Gebremedhin, T., & Girmay, A. (2018). Salinization in the irrigated agriculture of Northern Ethiopia : An integrated approach of quantitative and spatial analysis. 206(May), 147–157. https://doi.org/10.1016/j.agwat.2018.05.007.

Gebreyes, M., Zinyengere, N., Theodory, T. F., & Speranza, C. I. (2017). Introduction. Beyond Agricultural Impacts, 1–11. https://doi.org/10.1016/B978-0-12-812624-0.00001-6.

Gedefaw, M., Yan, D., Wang, H., Qin, T., & Wang, K. (2019). Analysis of the Recent Trends of Two Climate Parameters over Two Eco-Regions of Ethiopia. Water, 11(1), 161. https://doi.org/10.3390/w11010161.

Giannini, A., Y. Kushnir, and M. A. Cane. 2001. Seasonality in the impact of ENSO and the North Atlantic High on Caribbean rainfall. Physics and Chemistry of the Earth 26:143-147.

Gibba, P., & Jallow, M. B. P. (2020). The Gambia National Framework for Climate Services (NFCS-GAM).

González-Gómez, P. A., Rodríguez-Sánchez, M. R., Laporte-Azcué, M., Santana, D. (2021). Calculating molten-salt central-receiver lifetime under creep-fatigue damage. Solar Energy, 213, 180-197. https://doi.org/10.1016/j.solener.2020.11.033.

Gorji, T., Ayseggul, T., Sertel, E. (2015). Soil salinity prediction, monitoring, and mapping using modern technologies. http://creativecommons.org/license/by-nc-nd/4.0/.

GoTG (2003) First National Communication under the UNFCCC. Department of State for Fisheries, Natural Resources and the Environment., Banjul the Gambia., 94p.

GoTG (2012) The Gambia's Second National Communication under the United Nations Framework Convention on Climate Change. Ministry of Forestry and the Environment, Banjul, 113p.

GoTG (2016). Gambia Coastal Zone Management Project. National Climate Change Policy of The Gambia: Final Report, Final Draft Policy. Compiled by Penny Urquhart. January 2016. Contract No.: 1363. GCCA Support Project to The Gambia for Integrated Coastal Zone Management and the Mainstreaming of Climate Change.

Günal, E., Wang, X., Kılıc, O. M., Budak, M., Al Obaid, S., Ansari, M. J., & Brestic, M. (2021). The potential of Landsat 8 OLI for mapping and monitoring soil salinity in an arid region: A case study in Dushak, Turkmenistan. PLoS ONE, 16(11 November), 1–14. https://doi.org/10.1371/journal.pone.0259695.

Guo, H., Wang, R., Garfin, G. M., Zhang, A., Lin, D., Liang, Q., & Wang, J. (2020). Rice drought risk assessment under climate change: Based on physical vulnerability a quantitative assessment method. Science of The Total Environment, 141481. https://doi:10.1016/j.scitotenv.2020.141481.

Gupta, M., Srivastava, P. K., Islam, T., & Ishak, A. M. B. (2014). Evaluation of TRMM rainfall for soil moisture prediction in a subtropical climate. Environmental Earth Sciences, 71, 4421-4431. https://doi.org/10.1007/s12665-013-2837-6.

Hammam, A., & Mohamed, E. (2020). Mapping soil salinity in the East Nile Delta using several methodological approaches of salinity assessment. The Egyptian Journal of Remote Sensing and Space Science, 23(2), 125-131. https://doi.org/10.1016/j.ejrs.2018.11.002.

He, F., Mazumdar, S., Tang, G., Bhatia, T., Anderson, S. J., Dew, M. A., Krafty, R., Nimgaonkar, V., Deshpande, S., Hall, M., & Reynolds, C. F. (2017). Nonparametric MANOVA approaches for non-normal multivariate outcomes with missing values. Communications in Statistics - Theory and Methods, 46(14), 7188–7200. https://doi.org/10.1080/03610926.2016.1146767

He, J., & Wang, C. L. (2017). How global brands incorporating local cultural elements increase consumer purchase likelihood: An empirical study in China. International Marketing Review. https://doi.org/10.1108/IMR-07-2016-0167.

He, Y., Lin, K., & Chen, X. (2013). Effect of land use and climate change on runoff in the Dongjiang basin of south China. Mathematical Problems in Engineering, 2013. https://doi.org/10.1155/2013/471429.

Hirsch, R. M., Slack, J. R., & Smith, R. A. (1982). Techniques of trend analysis for monthly water quality data. Water resources research, 18(1), 107–121. https://doi.org/10.1029/WR018i001p00107.

Hoang, T.M.L., Tran, T.N., Nguyen, T.K.T., Williams, B., Wurm, P., Bellairs, S., & Mundree, S. (2016). Improvement of salinity stress tolerance in rice: Challenges and opportunities. Agronomy, 2016, 6, 54; https://doi.org/10.3390/agronomy6040054.

Hoerling, M., Eischeid, J., Perlwitz, J. (2010). Regional Precipitation Trends: Distinguishing Natural Variability from Anthropogenic Forcing. Journal Title, Volume(Issue), 2131–2145. DOI: https://doi.org/10.1175/2009JCLI3420.1.

Huang, L., Sun, F., Yuan, S., Peng, S., and Wang, F. (2018). Responses of candidate green super rice and super hybrid rice varieties to simplified and reduced input practice. Field Crops Research 218:78-87.

Hunt, L.A. & Boote, K.J. (1998). Data for model operation, calibration, and evaluation. In: Tsuji, G.Y., Hoogenboom, G., Thornton, P.K. (eds)

Understanding Options for Agricultural Production. Systems Approaches for Sustainable Agricultural Development, vol 7. Springer, Dordrecht. https://doi.org/10.1007/978-94-017-3624-4_2.

Ibrahim, A., & Saito, K. (2022). Assessing genetic and agronomic gains in rice yield in sub-Saharan Africa: A meta-analysis. Field Crops Research, 287, 108652.

Iizumi, T., Kotoku, M., Kim, W., West, P. C., Gerber, J. S., & Brown, M. E. (2018). Uncertainties of potentials and recent changes in global yields of major crops resulting from census- and satellite-based yield datasets at multiple resolutions. PLoS One, 13(9), e0203809.

IPCC (2007). Climate Change 2007: Impacts, Adaptation and Vulnerability: Contribution of Working Group II to the Fourth Assessment Report of the Intergovernmental Panel on Climate Change. Cambridge, United Nations.

IPCC (2013). Climate change: the physical science basis. In: Stocker, T.F., Qin, D., Plattner, G.-K., Tignor, M., Allen, S.K., Boschung, J., Nauels, A., Xia, Y., Bex, V., Midgley, P.M. (Eds.), Contribution of Working Group I to the Fifth Assessment Report of the Intergovernmental Panel on Climate Change. Cambridge University Press, Cambridge, United Kingdom and New York, NY, USA.

IPCC (2014). Climate change 2014: impacts, adaptation, and vulnerability. In: Field, C.B., Barros, V.R., Dokken, D.J., Mach, K.J., Mastrandrea, M.D., Bilir, T.E., Chatterjee, M., Ebi, K.L., Estrada, Y.O., Genova, R.C., Girma, B., Kissel, E.S., Levy, A.N., MacCracken, S., Mastrandrea, P.R., White, L.L. (Eds.), Contribution of Working Group II to the Fifth Assessment Report of the Intergovernmental Panel on Climate Change. Cambridge University Press, Cambridge, United Kingdom and New York, NY, USA, pp. 1–32.

IPCC, (2022). Climate Change 2022: Impacts, Adaptation and Vulnerability. Contribution of Working Group II to the Sixth Assessment Report of the Intergovernmental Panel on Climate Change [H.-O. Pörtner, D.C. Roberts, M. Tignor, E.S. Poloczanska, K. Mintenbeck, A. Alegría, M. Craig, S. Langsdorf, S. Löschke, V. Möller, A. Okem, B. Rama (eds.)]. Cambridge University Press. Cambridge University Press, Cambridge, UK and New York, NY, USA, 3056 pp., https://doi:10.1017/9781009325844.

IPCC. (2013). Climate Change 2013: The Physical Science Basis. Contribution of Working Group I to the Fifth Assessment Report of the Intergovernmental Panel on Climate Change [Stocker, T.F., D. Qin, G.-K. Plattner, M. Tignor, S.K. Allen, J. Boschung, A. Nauels, Y. Xia, V. Bex and P.M. Midgley (eds.)]. Cambridge University Press, Cambridge, United Kingdom and New York, NY, USA, 1535 pp.

IPCC. (2019). Technical Summary. In: IPCC Special Report on the Ocean and Cryosphere in a Changing Climate [Pörtner, H. O., D. C. Roberts, V. Masson-Delmotte, P. Zhai, M. Tignor, E. Poloczanska, K. Mintenbeck, A. Alegría, M. Nicolai, A. Okem, J. Petzold, B. Rama and N. M. Weyer (eds.)]. Cambridge University Press, Cambridge.

Ivushkin, K., Bartholomeus, H., Bregt, A. K., Pulatov, A., Kempen, B., & de Sousa, L. (2019). Global mapping of soil salinity change. Remote Sensing of Environment, 231(June), 111260. https://doi.org/10.1016/j.rse.2019.111260.

Jaiswal, R. K., Lohani, A. K., & Tiwari, H. L. (2015). Statistical Analysis for Change Detection and Trend Assessment in Climatological Parameters. Environmental Processes, 2(4), 729–749. https://doi.org/10.1007/s40710-015-0105-3.

Jamil, I., Jun, W., Mughal, B., Raza, M. H., Imran, M. A., & Waheed, A. (2021). Does adapting climate-smart agricultural practices increase farmers' resilience to climate change? Environmental Science and Pollution Research, 28, 27238-27249.

Jarju, P.O. (2009). National Report on Adaptation of Water Resources in the Gambia. 1–23.

Jarju, B. (2020). Third National Communication of the Gambia under the UNFCCC. July. Machiwal, D., & Jha, M. K. (2012). Hydrologic time series analysis: Theory and practice. In Hydrologic Time Series Analysis: Theory and Practice. https://doi.org/10.1007/978-94-007-1861-6..

Jenkins, D. M., Holmes, Z. F., Ishida, K., et al. (2018). Autocorrelation analysis of the infrared spectra of synthetic and biogenic carbonates along the calcite–dolomite join. Physics and Chemistry of Minerals, 45(6), 563-574. https://doi.org/10.1007/s00269-018-0942-5.

John, A., Horne, A., Nathan, R., Stewardson, M., Webb, J. A., Wang, J., & Poff, N. L. (2020). "Climate change and freshwater ecology: Hydrological and ecological methods of comparable complexity are needed to predict risk." WIREs Water, https://doi.org/10.1002/wcc.692.

Johnson, R. A. and Wichern, D. W. (2007). Applied multivariate statistical analysis. Prentice Hall.

Jones, J. W., Antle, J. M., Basso, B., Boote, K. J., Conant, R. T., Foster, I., … Wheeler, T. R. (2017). Brief history of agricultural systems modeling. Agricultural Systems, 155, 240–254. https://doi:10.1016/j.agsy.2016.05.014.

Jones, M. C., & Cheung, W. W. L. (2014). Multi-model ensemble projections of climate change effects on global marine biodiversity. ICES Journal of Marine Science, 72(3), 741–752. https://doi:10.1093/icesjms/fsu172.

Jørgensen, B. B., Findlay, A. J., & Pellerin, A. (2019). The biogeochemical sulfur cycle of marine sediments. Frontiers in Microbiology, 10(APR), 1–27. https://doi.org/10.3389/fmicb.2019.00849.

Juglea, S., Kerr, Y., Mialon, A., Wigneron, J.-P., Lopez-Baeza, E., Cano, A., Albitar, A., Millan-Scheiding, C., Carmen Antolin, M., and Delwart, S. (2010). Modeling soil moisture at SMOS scale using an SVAT model over the Valencia Anchor Station, Hydrol. Earth Syst. Sci., 14, 831–846. https://doi.org/10.5194/hess-14-831-2010, 2010.

Kadykalo, A. N., López-Rodriguez, M. D., Ainscough, J., Droste, N., Ryu, H., Ávila-Flores, G. & Harmáčková, Z. V. (2019). Disentangling 'ecosystem services' and 'nature's contributions to people.' Ecosystems and People, 15(1), 269-287.

Kamali, B., Abbaspour, K. C., Wehrli, B., & Yang, H. (2018). Drought vulnerability assessment of maize in Sub-Saharan Africa: Insights from physical and social perspectives. Global and Planetary Change. https://doi.org/10.1016/j.gloplacha.2018.01.011.

Kano, Y., Harada, A. (2000). Stepwise variable selection in factor analysis. *Psychometrika* **65**, 7–22. https://doi.org/10.1007/BF02294182.

Kasim, N., Tiyip, T., Abliz, A., Nurmemet, I., Sawut, R., & Maihemuti, B. (2018). Mapping and modeling soil salinity using WorldView-2 data and EM38-KM2 in an arid region of the Keriya River, China. Photogrammetric Engineering & Remote Sensing, 84(1), 43-52.

Kawasaki, J., & Herath, S. (2011). Impact assessment of climate change on rice production in Khon Kaen province, Thailand. Journal of ISSAAS, 17, 14-28.

Kendall, M. (1975). Rank correlation measures. Charles Griffin, London, 202, 15.

Kephe, P. N., Ayisi, K. K., & Petja, B. M. (2021). Challenges and opportunities in crop simulation modeling under seasonal and projected climate change scenarios for crop production in South Africa. Agric & Food Security, 10, 10. https://doi.org/10.1186/s40066-020-00283-5.

Khaledian, Y., Brevik, E. C., Pereira, P., Cerdà, A., Fattah, M. A., & Tazikeh, H. (2017). *Modeling soil cation exchange capacity in multiple countries. CATENA, 158, 194–200.* https://doi:10.1016/j.catena.2017.07.002.

Khan, N. M., Rastoskuev, V. V., Sato, Y., & Shiozawa, S. (2005). Assessment of hydrosaline land degradation by using a simple approach of remote sensing indicators. Agricultural Water Management, 77(1-3), 96-109. https://doi.org/10.1016/j.agwat.2004.09.038.

Kherad-Pajouh, S., & Renaud, O. (2015). A general permutation approach for analyzing repeated measures ANOVA and mixed-model designs. Statistical Papers, 56, 947–967. https://doi.org/10.1007/s00362-014-0617-3.

Kissell, D.E., and L. Sonon. (2008). Soil test handbook for Georgia. Univ. Georgia Coop. Ext. Special Bul. 62.

Klein, T., Holzkämper, A., Calanca, P., & Fuhrer, J. (2014). Adaptation options under climate change for multifunctional agriculture: a simulation study for western Switzerland. Regional Environmental Change, 14, 167–184. https://doi.org/10.1007/s10113-013-0489-7.

Konietschke, F., Bathke, A., Harrar, S., and Pauly, M. (2015). Parametric and nonparametric bootstrap methods for general MANOVA. Journal of Multivariate Analysis, 140:291–301.

Kramer, D. B., Stevens, K., Williams, N. E., Sistla, S. A., Roddy, A. B., & Urquhart, G. R. (2019). Coastal livelihood transitions under globalization with implications for trans-ecosystem interactions. PloS One, 12(10), e0186683.

Krishnan, R., Sabin, T. P., Vellore, R., Mujumdar, M., Sanjay, J., Goswami, B. N., ... & Terray, P. (2016). Deciphering the desiccation trend of the South Asian monsoon hydroclimate in a warming world. Climate Dynamics, 47, 1007-1027.

Kronzucker, H. J., Szczerba, M. W., Schulze, L. M., & Britto, D. T. (2008). Non-reciprocal interactions between K^+ and Na^+ ions in barley (Hordeum vulgare L.). Journal of Experimental Botany, 59(10), 2793–2801. https://doi:10.1093/jxb/ern139.

Kumar, P., & Sharma, P. K. (2020). Soil Salinity and Food Security in India. *Frontiers in Sustainable Food Systems*. Frontiers Media S.A. https://doi.org/10.3389/fsufs.2020.533781.

Kumar, P., Sarangi, A., Singh, D. K., & Parihar, S. S. (2014). Evaluation of AquaCrop model in predicting wheat yield and water productivity under irrigated saline regimes. Irrigation and Drainage, 63(4), 474-487.

Lacy, Scott M.; Cleveland, David; and Soleri, Daniela, "Farmer choice of sorghum varieties in southern Mali: Managing Unpredictable Growing Environments and Resources" (2006). Sociology & Anthropology Faculty Publications. 16. https://digitalcommons.fairfield.edu/sociologyandanthropology-facultypubs/16.

Lal B, Gautam P, Panda BB, Raja R, Singh T, Tripathi R, et al. (2017) Crop and varietal diversification of rainfed rice-based cropping systems for higher productivity and profitability in Eastern India. PLoS ONE 12(4): e0175709. https://doi.org/10.1371/journal.pone.0175709.

Lambin, E. ., Rounsevell, M. D. ., & Geist, H. . (2000). Are agricultural land-use models able to predict changes in land-use intensity? Agriculture, Ecosystems & Environment, 82(1-3), 321–331. https://doi:10.1016/s0167-8809(00)00235-8.

Lamichhane, J. R., Debaeke, P., Steinberg, C., Pei, M.Y., Barbetti, M. J., Aubertot, J. N. (2018). Abiotic and biotic factors affecting crop seed germination and seedling emergence: a conceptual framework. Plant Soil 432, 1–28. https://doi.org/10.1007/s11104-018-3780-9.

Lamond, R., Whitney, D.A. (1992). Management of saline and sodic soils. Kansas State University, Department of Agronomy MF-1022. Making the case for reusing saline water and restoring salt-affected agricultural lands. wle.cgiar.org/news/makingcase-reusing-saline-water-and-restoring-salt-affected-agricultural-lands.

Li, Chaozhi. (2023). Predictors selection strategy based on stepwise random forests and logistic regression model. 46. https://doi.org/10.1117/12.2656859.

Li, H. Y., Shi, Z., Webster, R., & Triantafilis, J. (2013). Mapping the three-dimensional variation of soil salinity in a rice-paddy soil. Geoderma, 195, 31-41.

Li, X. and Kang, Y. (2020). 'Agricultural utilization and vegetation establishment on saline-sodic soils using a water–salt regulation method for scheduled drip irrigation,' Agricultural Water Management, 231(September 2019), p. 105995. Available at: https://doi.org/10.1016/j.agwat.2019.105995.

Li, X., & Kang, Y. (2019). Agricultural utilization and vegetation establishment on saline-sodic soils using a water–salt regulation method for scheduled drip irrigation. Agricultural Water Management, 226, 105995. https://doi.org/10.1016/j.agwat.2019.105995.

Liliane, T. N., & Charles, M. S. (2020). Factors affecting the yield of crops. Agronomy-climate change & food security, 9.

Liu, C., Bathke, A. C., & Harrar, S. W. (2011). A nonparametric version of Wilks' lambda—Asymptotic results and small sample approximations. Statistics & Probability Letters, 81(10), 1502–1506. https://doi:10.1016/j.spl.2011.04.012.

Liu, X., Liang, X., Li, X., Xu, X., Ou, J., Chen, Y. & Pei, F. (2017). A future land use simulation model (FLUS) for simulating multiple land use scenarios by coupling human and natural effects. Landscape and Urban Planning, 168, 94-116.

Lobell, D. B., & Field, C. B. (2007). Global scale climate–crop yield relationships and the impacts of recent warming. Environmental research letters, 2(1), 014002.

Lomborg, B. (2020). Welfare in the 21st century: Increasing development, reducing inequality, the impact of climate change, and the cost of climate policies. Technological Forecasting and Social Change, 156, 119981.

Lotze-Campen, H., Müller, C., Bondeau, A., Rost, S., Popp, A., & Lucht, W. (2008). Global food demand, productivity growth, and the scarcity of land and water resources: a spatially explicit mathematical programming approach. Potsdam Institute for Climate Impact Research (PIK), PO Box 60 12 03.

M'koumfida, B., Yaffa S, & Bah A. (2018). The Impacts of Saline-Water Intrusion on the Lives and Livelihoods of Gambian Rice-Growing Farmers. Res. Rev. J Ecol. Environ. Sci.|, 6(1), 1–7. http://www.rroij.com/open-access/the-impacts-of-salinewater-intrusion-on-the-lives-and-livelihoods-of-gambian-ricegrowingfarmers.pdf.

Mahajan, G. R., Manjunath, B. L., Latare, A. M., D'souza, R., Vishwakarma, S., & Singh, N. P. (2015). Fertility Status of the Unique Coastal Acid Saline Soils of Goa. Journal of the Indian Society of Soil Science, 63(2), 232-237. https://doi.org/10.5958/0974-0228.2015.00031.6.

Mahajan, G.R. et al. (2015). 'Fertility status of the unique coastal acid saline soils of Goa,' Journal of the Indian Society of Soil Science, 63(2), pp. 232–237. Available at: https://doi.org/10.5958/0974-0228.2015.00031.6.

Manandhar, R., Odeh, I. O. A., & Pontius, R. G. (2010). Analysis of twenty years of categorical land transitions in the Lower Hunter of New South Wales, Australia. Agriculture, Ecosystems & Environment, 135(4), 336-346. https://doi.org/10.1016/j.agee.2009.10.016.

Mandal, S., Vema, V. K., Kurian, C., Sudheer, K. P. (2020). Improving the crop productivity in rainfed areas with water harvesting structures and deficit irrigation strategies. Journal of Hydrology, 586, 124818. ISSN 0022-1694. https://doi.org/10.1016/j.jhydrol.2020.124818.

Mann, H. B. (1945). Nonparametric tests against trend. Econometrica: Journal of the Econometric Society, 245–259. https://doi.org/10.2307/1907187.

Manneh, B. (2004). Genetic, Physiological and Modelling Approaches Towards Tolerance to Salinity and Low Nitrogen Supply in Rice (Oryza Sativa L.). Wageningen University and Research. ProQuest Dissertations Publishing. 28239122.

Mariama, J. (2019). Genetic studies of salinity tolerance of mangrove rice varieties in Sierra Leone This thesis is submitted to the University of Ghana, Legon, in partial fulfillment of the requirements for the award of the degree of Doctor of Philosophy in West Africa center.

Marius, C. (1982). Acid sulfate soils of the mangrove area of Senegal and Gambia. Office de la Recherche Scientifique et Technique Outre-Mer, Paris, France.

Markhi, A., Laftouhi, N., Grusson, Y., & Soulaimani, A. (2019). Assessment of potential soil erosion and sediment yield in the semi-arid N′ fis basin (High Atlas, Morocco) using the SWAT model. Acta Geophysica, 67, 263-272.

Masoud, A. A., Koike, K., Atwia, M. G., El-Horiny, M. M., & Gemail, K. S. (2019). Mapping soil salinity using spectral mixture analysis of Landsat 8 OLI images to identify factors influencing salinization in an arid region. International Journal of Applied Earth Observation and Geoinformation, 83, 101944. https://doi.org/10.1016/j.jag.2019.101944.

Masoud, A.A., (2014). Predicting salt abundance in slightly saline soils from Landsat ETM+imagery using Spectral Mixture Analysis and soil spectrometry. Geoderma 217-218, 45–56. https://doi.org/10.1016/j.geoderma.2013.10.027.

Mbaye, M. L., Sy, K., Faty, B., & Sall, S. M. M. (2020). Impact of 1.5 and 2.0 °C global warming on the hydrology of the Faleme river basin. Journal of Hydrology: Regional Studies, 31, 100719. https://doi.org/10.1016/j.ejrh.2020.100719.

McConnell, B.B., & Jallow, S.O. (2022). Climate Change Adaptation in The Gambia: The Role of Kanyeleng Communication and Performance. Published online by Cambridge University Press: 02 August 2022. https://doi.org/10.1017/asr.2022.67.

McFarquhar, M., McKie, S., Emsley, R., Suckling, J., Elliott, R., & Williams, S. (2016). Multivariate and repeated measures (mrm): A new toolbox for dependent and multimodal group-level neuroimaging data. NeuroImage, 132:373–389.

McInnes, K. L., Macadam, I., Hubbert, G., & O'Grady, J. (2011). An assessment of current and future vulnerability to coastal inundation due to sea-level extremes in Victoria, southeast Australia. Journal of Climatology, https://doi.org/10.1002/joc.3405.

Mengel, M., Levermann, A., Frieler, K., and Marzeion, B., Winkelmann, R. (2016). Future sea level rise constrained by observations and long-term commitment. Proceedings of the National Academy of Sciences, 113(10), 2597-2602. https://doi.org/10.1073/pnas.1500515113.

Merabtene, T., Siddique, M., & Shanableh, A. (2016). Assessment of Seasonal and Annual Rainfall Trends and Variability in Sharjah City, UAE. Advances in Meteorology, 2016, Article ID 6206238. https://doi.org/10.1155/2016/6206238.

Metternicht, G. I., & Zinck, J. A. (2003). Remote sensing of soil salinity: Potentials and constraints. Remote Sensing of Environment, 85(1), 1–20. https://doi.org/10.1016/S0034-4257(02)00188-8.

Mishra, R. K. (2023). Fresh Water Availability and Its Global Challenge. Journal of Marine Science and Research, 2(1), 01–03. https://doi.org/10.58489/2836-5933/004.

Mohd-Aizat, A., Mohamad-Roslan, M.K., Wan Nor Azmin Sulaiman, Daljit Singh Karam (2014). The relationship between soil pH and selected soil properties in 48 years logged-over forest. International Journal of Environmental Sciences. 4-6. https://doi.org/10.6088/ijes.2014040600004.

Mondal, M. F., Asaduzzaman, M., & Asao, T. (2015). Adverse effects of allelopathy from legume crops and its possible avoidance. American Journal of Plant Sciences, 6(06), 804.

Mondal, R., & Bhat, A. (2021). Investigating the trophic ecology of freshwater fish communities from central and eastern Indian streams using stable isotope analysis. Community Ecology, 22, 203-215.

Montesinos López, O.A., Montesinos López, A., Crossa, J. (2022). Overfitting, Model Tuning, and Evaluation of Prediction Performance. In: Multivariate Statistical Machine Learning Methods for Genomic Prediction. Springer, Cham. https://doi.org/10.1007/978-3-030-89010-0_4.

Morgan, M.G., Mellon, C. (2011). Certainty, uncertainty, and climate change. Climatic Change 108, 707. https://doi.org/10.1007/s10584-011-0184-8.

Morton, J. F. (2007). The impact of climate change on smallholder and subsistence agriculture. Proceedings of the national academy of sciences, 104(50), 19680-19685. https://doi.org/10.1073/pnas.070185510.

Mukhopadhyay, R., Sarkar, B., Jat, H. S., Sharma, P. C., & Bolan, N. S. (2020). Soil salinity under climate change: Challenges for sustainable agriculture and food security. Journal of Environmental Management, 111736. https://doi.org/10.1016/j.jenvman.2020.111736.

Mungai, Rose; Amouzou Agbe, Guy Morel Kossivi. 2019. The Gambia: A Look at Agriculture. © World Bank, Washington, DC. http://hdl.handle.net/10986/34341 License: CC BY 3.0 IGO.

Munns, R., & Gilliham, M. (2015). Salinity tolerance of crops - what is the cost? New Phytologist, 208(3), 668–673. https://doi.org/10.1111/nph.13519.

Munns, R., Day, D. A., Fricke, W., Watt, M., Arsova, B., Barkla, B. J., Tyerman, S. D. (2019). Energy costs of salt tolerance in crop plants. New Phytologist. https://doi:10.1111/nph.15864.

Munns, R., James, R. A., Sirault, X. R. R., Furbank, R. T., & Jones, H. G. (2010). New phenotyping methods for screening wheat and barley for beneficial responses to water deficit. Journal of Experimental Botany, 61(12), 3499-3507. https://doi.org/10.1093/jxb/erq199.

Nanni, M., and Dematte, J. (2006). Spectral Reflectance Methodology in Comparison to Traditional Soil Analysis: Soil Sci. Soc. Am. J. 70:393–407. https://doi.org/10.2136/sssaj2003.0285.

Nawar, S., Buddenbaum, H., Hill, J., and Kozak, J. (2014). Modeling and Mapping Soil Salinity with Reflectance Spectroscopy and Landsat Data Using Two Quantitative Methods (PLSR and MARS). Remote Sens. 6, 10813-10834; https://doi.org/10.3390/rs61110813.

Negi, H. S., Singh, S. K., Kulkarni, A. V., & Semwal, B. S. (2010). Field-based spectral reflectance measurements of seasonal snow cover in the Indian Himalayas. International Journal of Remote Sensing, 31(9), 2393-2417.

Niang, A., Becker, M., Ewert, F., Dieng, I., Gaiser, T., Tanaka, A., Saito, K. (2017). Variability and determinants of yields in rice production systems of West Africa. Field Crops Research, 207, 1–12. https://doi:10.1016/j.fcr.2017.02.014.

Nielsen, J. Ø., & Reenberg, A. (2010). Cultural barriers to climate change adaptation: A case study from Northern Burkina Faso. Global Environmental Change, 20(1), 142–152. https://doi.org/10.1016/j.gloenvcha.2009.10.002.

Njie, M. & Corr, G. (2006). Water Resources Status and Management Framework in The Gambia. 1-23.

Nkurunziza, L., Watson, C. A., Öborn, I., Smith, H. G., Bergkvist, G., & Bengtsson, J. (2020). Socio-ecological factors determine crop performance in agricultural systems. Scientific Reports, 10(1). https://doi.org/10.1038/s41598-020-60927-1.

NRDS (2014). (Volume 5, Issue 2). Supported by the IFAD-Sponsored National Agricultural Land and Water Management Development Project (Nema) of the Ministry of Agriculture (MOA).

OECD/FAO (2019), OECD-FAO Agricultural Outlook 2019-2028, OECD Publishing, Paris/Food and Agriculture Organization of the United Nations, Rome. https://doi.org/10.1787/agr_outlook-2019-en.

Olesen, J. E., & Bindi, M. (2002). Consequences of climate change for European agricultural productivity, land use, and policy. European Journal of Agronomy, 16(4), 239–262. https://doi.oeg/10.1016/s1161-0301(02)00004-7.

Omuto CT, Vargas RR, El Mobarak AM, Mohamed N, Viatkin K, Yigini Y. 2020. Mapping of salt-affected soils: Technical manual. Rome, FAO. https://doi.org/10.4060/ca9215en.

Oyerinde, G. T., Hountondji, F. C. C., Lawin, A. E., Odofin, A. J., Afouda, A., & Diekkrüger, B. (2017). Improving Hydro-Climatic Projections with Bias-Correction in Sahelian Niger Basin, West Africa. Climate, 5(1), 8. https://doi.org/10.3390/cli5010008.

Panagea, I. S., Daliakopoulos, I. N., Tsanis, I. K., & Schwilch, G. (2016). Evaluation of promising technologies for soil salinity amelioration in Timpaki (Crete): a participatory approach. Solid Earth, 7, 177–191. https://doi.org/10.5194/se-7-177-2016.

Patel, D.P., Patel, M.M. and Patel, D.R. (2014) 'Implementation of ARIMA model to predict rain attenuation for KU-band 12 Ghz frequency', IOSR Journal of

Electronics and Communication Engineering (IOSR-JECE), Vol. 9, No. 1, pp.83–87, ISSN: 2278-8735.

Paul, D., & Lade, H. (2014). Plant-growth-promoting rhizobacteria to improve crop growth in saline soils: A review. *Agronomy for Sustainable Development*, 34(4), 737–752. https://doi.org/10.1007/s13593-014-0233-6.

Peat, Marwick, & Mitchell (1979). The Gambia estuary barrage study, stage II. Gambia River Basin Development Organization.

Peng, B., Guan, K., Tang, J., Ainsworth, E. A, Asseng, S., Bernacchi, C. J., Cooper, M., Delucia, E. H., Elliott, J. W., Ewert, F., Grant, R. F., Gustafson, D. I., Hammer, G. L., Jin, Z., Jones, J. W., Kimm, H., Lawrence, D. M., Li, Y., Lombardozzi, D. L. Marshall-Colon, A. Messina, C. D., Ort, D. R., Schnable, J. C., Vallejos, C. E., Wu, A., Yin, X., Zhou W. (2020). Towards a multiscale crop modeling framework for climate change adaptation assessment. Nature Plants 6, 338–348. https://doi.org/10.1038/s41477-020-0625-3.

Pesarin, F., & Salmaso, L. (2012). A review and some new results on permutation testing for multivariate problems. Statistical Computing, 22(4), 639–646. https://doi.org/10.1007/s11222-011-9261-0.

Petz, K. (2014). Mapping and modeling the effects of land use and land management change on ecosystem services from local ecosystems and landscapes to global biomes. Wageningen University and Research.

Pohlert T (2020) Non-Parametric Trend Tests and Change-Point Detection. https://creativecommons.org/licenses/by-nd/4.0/.

Pontius, R. G., & Petrova, S. H. (2010). Assessing a predictive model of land change using uncertain data. Environmental Modelling & Software, 25(3), 299-309. https://doi.org/10.1016/j.envsoft.2009.09.005.

Promchote, P., Wang, S.-Y. S., Yoon, J.-H., Johnson, P. G., Creech, E., Shen, Y., & Yao, M.-H. (2022). On the Changing Cool Season Affecting Rice Growth and Yield in Taiwan. Agronomy, 12(11), 2625. https://doi.org/10.3390/agronomy12112625.

Qureshi, A. S., Mohammed, M., Daba, A. W., Hailu, B., Belay, G., Tesfaye, A., & Ertebo, T. M. (2019). Improving agricultural productivity on salt-affected soils in Ethiopia: Farmers' perceptions and proposals. African Journal of Agricultural Research, 14(21), 897-906. https://doi.org/10.5897/AJAR2019.14077.

R Core Team (2016). R: A Language and Environment for Statistical Computing.RFounda-tion for Statistical Computing, Vienna, Austria. URL https://www.R-project.org/.

Radanielson, A. M., Gaydon, D. S., Li, T., Angeles, O., & Roth, C. H. (2018). Modeling salinity effect on rice growth and grain yield with ORYZA v3 and APSIM-Oryza. European Journal of Agronomy, 100(March), 44–55. https://doi.org/10.1016/j.eja.2018.01.015.

Ragatoa, D. S., Ogunjobi, K. O., Okhimamhe, A. A., Francis, S. D., & Adet, L. (2021). A Trend Analysis of Temperature in Selected Stations in Nigeria Using Three Different Approaches. Open Access Library Journal, 8(04), 1–20. https://doi.org/10.4236/oalib.1104371.

Rahman, A., Kang, S. Nagabhatla, N., Robert, M. (2017). Impact of temperature and rainfall variation on rice productivity in major ecosystems of Bangladesh. https://doi.org/10.1186/s40066-017-0089-5.

Rahman, M., Thomson, M. J., De Ocumpo, M., Edgar, J. A., Salam, M. A., Shah-E-Alam, M., and Ismail, A. (2019). Assessing trait contribution and mapping

novel QTL for salinity tolerance using the Bangladeshi rice landrace capsule. Rice 12:63 Open Access Journal.
Ramírez Villegas, J., & Thornton, P. K. (2015). Climate change impacts on African crop production. CCAFS Working Paper.
Rangesamy P., Marchuk A. 2011. Cation ratio of soil structural stability (CROSS). Soil Research, 49: 280-285.
Ravi, R. K., Valli, P. P. S., & Muthukumar, T. (2020). Physiological characterization of root endophytic Fusarium haematococcum for hydrolytic enzyme production, nutrient solubilization, and salinity tolerance. Biocatalysis and Agricultural Biotechnology, 43, 102392.
Ray, R. L., Ampim, P. A., & Gao, M. (2020). Crop protection under drought stress. Crop protection under changing climate, 145-170.
Richards, L., Ed. (1954). Diagnosis and improvement of saline and alkali soils. Agriculture Handbook 60. U.S. Department of Agriculture, Washington, DC.
Rippke, U., Ramirez-Villegas, J., Jarvis, A. (2016). Timescales of transformational climate change adaptation in sub-Saharan African agriculture. Nature Climate Change, 6, 605–609. DOI: https://doi.org/10.1038/nclimate2947.
Rodríguez, J. P., Beard, T. D. Jr., Bennett, E. M., Cumming, G. S., Cork, S. J., Agard, J., Dobson, A. P., & Peterson, G. D. (2006). Trade-offs across Space, Time, and Ecosystem Services. Ecology and Society, 11(1), [28]. https://www.jstor.org/stable/26267786.
Rondhi, M., Pratiwi, P.A., Handini, V.T., Sunartomo, A.F., Budiman, S.A. (2019). Agricultural Land Conversion and Food Policy in Indonesia: Historical Linkages, Current Challenges, and Future Directions. In: Mueller, L., Eulenstein, F. (eds) Current Trends in Landscape Research. Innovations in Landscape Research. Springer, Cham. https://doi.org/10.1007/978-3-030-30069-2_29.
Rosenstock, T. S., Nowak, A., & Girvetz, E. (Eds.). (2019). The Climate-Smart Agriculture Papers. https://doi:10.1007/978-3-319-92798-5.
Roudier, P., Ducharne, A., & Feyen, L. (2014). Climate change impacts on runoff in West Africa: a review. Hydrology and Earth System Sciences, 18(7), 2789-2801. https://doi.org/10.5194/hess-18-2789-2014.
Roudier, P., Sultan, B., Quirion, P., & Berg, A. (2011). The impact of future climate change on West African crop yields: What does the recent literature say? Global Environmental Change, 21(3), 1073–1083. https://doi.org/10.1016/j.gloenvcha.2011.04.007.
Sadeghi, F., Rezeizad, A. and Rahimi, M. (2021). 'Effect of Zinc and Magnesium Fertilizers on the Yield and Some Characteristics of Wheat (Triticum aestivum L.) Seeds in Two Years,' International Journal of Agronomy, 2021. Available at: https://doi.org/10.1155/2021/8857222.
Saleh, K., Wigneron, J. P., de Rosnay, P., Calvet, J. C., & Kerr, Y. (2006). Semi-empirical regressions at L-band applied to surface soil moisture retrievals over grass. Remote Sensing of Environment, 101(3), 415-426.
Sánchez, B., Rasmussen, A., & Porter, J. R. (2013). Temperatures and the growth and development of maize and rice: a review. Global Change Biology, 20(2), 408–417. https://doi:10.1111/gcb.12389.
Sanogo, S., Fink, A. H., Omotosho, J. A., Ba, A., Redl, R., & Ermert, V. (2015). Spatio-temporal characteristics of the recent rainfall recovery in West Africa. International Journal of Climatology, 35(15), 4589–4605. https://doi.org/10.1002/joc.4309.

Sarak, K. K. (2010). Global Warming Induced Sea Level Rise on Soil, Land and Crop Production Loss in Bangladesh. August, 77–80. Sari, N. N., Saputra.

Sari, N. N., Saputra, R. A., & Noor, M. (2023). Seventy Years of Rice Crop Cultivation in Tidal Swampland: Potential, Constraints, and Limitations (Vol. 1). Atlantis Press International BV. https://doi.org/10.2991/978-94-6463-128-9_23.

Schlenker, W., & Lobell, D. B. (2010). Robust negative impacts of climate change on African agriculture. Environmental Research Letters, 5(1), 014010. https://doi.org/10.1088/1748-9326/5/1/014010.

Schmugge, T. J., Kustas, W. P., Ritchie, J. C., Jackson, T. J., & Rango, A. (2002). Remote sensing in hydrology. Advances in Water Resources, 25(8-12), 1367–1385. https://doi.org/10.1016/s0309-1708(02)00065-9.

Scudiero, E., Skaggs, T. H., & Corwin, D. L. (2017). Simplifying field-scale assessment of spatiotemporal changes of soil salinity. Science of the Total Environment, 587–588, 273–281. https://doi.org/10.1016/j.scitotenv.2017.02.136

Segnon AC, Zougmoré RB, Green R, Ali Z, Carr TW, Houessionon P, M'boob S and Scheelbeek PFD (2022). Climate change adaptation options to inform the planning of agriculture and food systems in The Gambia: A systematic approach for stocktaking. Front. Sustain. Food Syst. 6:834867. https://doi.org/10.3389/fsufs.2022.834867.

Segnon, A. C., Zougmoré, R. B., Green, R., Ali, Z., Carr, T. W., Houessionon, P., M'boob, S., & Scheelbeek, P. F. D. (2022). Climate change adaptation options to inform the planning of agriculture and food systems in The Gambia: A systematic approach for stocktaking. Frontiers in Sustainable Food Systems, 6, 834867. https://doi.org/10.3389/fsufs.2022.834867.

Seneviratne, S.I., X. Zhang, M. Adnan, W. Badi, C. Dereczynski, A. Di Luca, S. Ghosh, I. Iskandar, J. Kossin, S. Lewis, F. Otto, I. Pinto, M. Satoh, S.M. Vicente-Serrano, M. Wehner, and B. Zhou, 2021: Weather and Climate Extreme Events in a Changing Climate. In Climate Change 2021: The Physical Science Basis. Contribution of Working Group I to the Sixth Assessment Report of the Intergovernmental Panel on Climate Change [Masson-Delmotte, V., P. Zhai, A. Pirani, S.L. Connors, C. Péan, S. Berger, N. Caud, Y. Chen, L. Goldfarb, M.I. Gomis, M. Huang, K. Leitzell, E. Lonnoy, J.B.R. Matthews, T.K. Maycock, T. Waterfield, O. Yelekçi, R. Yu, and B. Zhou (eds.)]. Cambridge University Press, Cambridge, United Kingdom and New York, NY, USA, pp. 1513–1766, https://doi:10.1017/9781009157896.013.

Senthilnathan, S. (2019, July 9). Usefulness of Correlation Analysis. Retrieved from SSRN: https://ssrn.com/abstract=3416918, or http://dx.doi.org/10.2139/ssrn.3416918.

Shackleton, S., Ziervogel, G., Sallu, S., Gill, T., & Tschakert, P. (2015). Why is socially just climate change adaptation in sub-Saharan Africa so challenging? A review of barriers identified from empirical cases. First published: 04 February 2015. https://doi.org/10.1002/wcc.335.

Shahbaz, M., & Ashraf, M. (2013). Improving salinity tolerance in cereals. Critical reviews in plant sciences, 32(4), 237-249.

Shepherd, M. A., Mackay, A. D., Monaghan, R., Vibart, R., Devantier, B., Wakelin, S. J., ... & Harrison, D. R. (2016). An Assessment of Climate Mitigation Co-

benefits Arising from the Freshwater Reforms: Appendices. Ministry for Primary Industries, Manatū Ahu Matua.

Shiferaw, B., Prasanna, B. M., Hellin, J., & Bänziger, M. (2011). Crops that feed the world 6. Past successes and future challenges to the role played by maize in global food security. Food Security, 3(3), 307-327. https://doi.org/10.1007/s12571-011-0140-5.

Shiferaw, B., Tesfaye, K., Kassie, M., Abate, T., Prasanna, B. M., & Menkir, A. (2014). Managing vulnerability to drought and enhancing livelihood resilience in sub-Saharan Africa: Technological, institutional and policy options. Weather and Climate Extremes, 3, 67-79. https://doi: 10.1016/j.wace.2014.04.004.

Shrivastava, P., & Kumar, R. (2015). Soil salinity: A serious environmental issue and plant growth promoting bacteria as one of the tools for its alleviation. Saudi Journal of Biological Sciences, 22(2), 123–131. http://dx.doi.org/10.1016/j.sjbs.2014.12.001.

Sienta, H., Hurley, J., Martin, L., Mcgrenra, D. (2019). Country Strategic Opportunities Programme 2019-2024, Republic of The Gambia.

Silliman & James R. (1980). University of Arizona. Arid Lands Information Center. U.S. Man and the Biosphere Secretariat, Department of State (Washington, D.C.) October. http://hdl.handle.net/10150/228159.

Sillmann, J., Kharin, V. V., Zhang, X., Zwiers, F. W., & Bronaugh, D. (2013). Climate extremes indices in the CMIP5 multimodel ensemble: Part 1. Model evaluation in the present climate. Journal of Geophysical Research: Atmospheres, 118(4), 1716–1733. https://doi.org/10.1002/jgrd.50203.

Singh, R. P., Oza, S. R., Chaudhari, K. N., & Dadhwal, V. K. (2005). Spatial and temporal patterns of surface soil moisture over India estimated using the surface wetness index from the SSM/I microwave radiometer. International Journal of Remote Sensing, 26(6), 1269-1276.

Sivakumar, M. V. K. (2017). Climate Extremes and Impacts on Agriculture. 621–647. https://doi.org/10.2134/agronmonogr60.2016.0003.

Sivakumar, M. V., Collins, C., Jay, A., & Hansen, J. (2014). Regional priorities for strengthening climate services for farmers in Africa and South Asia. CCAFS Working Paper.

Solomon, S., Qin, D., Manning, M., Chen, Z., Marquis, M., Averyt, K. B., Tignor, M., Miller, H. L. (Eds.). (2007). Climate Change 2007: The Physical Science Basis. Contribution of Working Group I to the Fourth Assessment Report of the Intergovernmental Panel on Climate Change. Cambridge University Press, Cambridge, United Kingdom and New York, NY, USA, 996 pp.

Sonko, E., Agodzo, S. K., & Antwi-Agyei, P. (2019). Evaluating the Yield Response of Maize (Zea mays L.) and Rice (Oryza sativa L.) to Future Climate Variability in The Gambia. Journal of Agricultural Studies, 7(2), 11. https://doi.org/10.5296/jas.v7i2.14664.

Sreelatha, A.K., Nisha, P., Kaledhonkar, M.J. (2022). Temporal Verifications in Soil Nutrient Dynamics of Rice_Prawn Integration in Acid Saline Pokkali Soils of Kerala, India. Journal of Soil Salinity and Water Quality 14(2), 259-265.

Srivastava, A. K., Pandey, M., Ghate, T., Kumar, V., Upadhyay, M. K., Majumdar, A., Suprasanna, P. (2021). Chemical intervention for enhancing growth and reducing grain arsenic accumulation in rice. Environmental Pollution, 276, 116719. https://doi/10.1016/j.envpol.2021.116719.

Srivastava, P., Wu, Q., & Giri, B. (2019). Chapter 1 Salinity : An Overview. July. https://doi.org/10.1007/978-3-030-18975-4

Stanzel, P., Kling, H., & Bauer, H. (2018). Climate change impacts West African rivers under an ensemble of CORDEX climate projections. Climate Services, 11, 36-48. https://doi.org/10.1016/j.cliser.2018.05.003.

Sullivan, G. M., & Feinn, R. (2012). Using Effect Size—or Why the P Value Is Not Enough. Journal of Graduate Medical Education, 4(3), 279–282. https://doi.org/10.4300/JGME-D-12-00156.1.

Sultan, B., & Gaetani, M. (2016). Agriculture in West Africa in the Twenty-First Century: Climate Change and Impacts Scenarios, and Potential for Adaptation. Frontiers in Plant Science, 7, 1262. https://doi.org/10.3389/fpls.2016.01262.

Sultan, B., Defrance, D., & Iizumi, T. (2019). Evidence of crop production losses in West Africa due to historical global warming in two crop models. Scientific reports, 9(1), 12834.

Sylla, M.B (1994). Soil Salinity and Acidity : Spatial Variability and Effects on Rice Production in West Africa. ISRA-Djibelor, BP 34, Ziguinchor, Senegal. DLO-The Winand Staring Centre for Integrated Land, Soil and Water Research, P.O. Box 125, 6700 AC Wageningen, The Netherlands. Mahajan, G. R.

Sylla, M.B., Nikiema, P.M., Gibba, P., Kebe, I., Klutse, N.A.B. (2016). Climate Change over West Africa: Recent Trends and Future Projections. In: Yaro, J., Hesselberg, J. (eds) Adaptation to Climate Change and Variability in Rural West Africa. Springer, Cham. https://doi.org/10.1007/978-3-319-31499-0_3.

Tabari, H., & Hosseinzadeh Talaee, P. (2011). Analysis of trends in temperature data in arid and semi-arid regions of Iran. Global and Planetary Change, 79(1-2), 1–10. https://doi:10.1016/j.gloplacha.2011.07.008.

Tahir, M., Ahmad, I., Shahid, M., Shah, G. M., Farooq, A. B. U., Akram, M., & Zakir, A. (2019). Regulation of antioxidant production, ion uptake, and productivity in potato (Solanum tuberosum L.) plant inoculated with growth-promoting salt tolerant Bacillus strains. Ecotoxicology and environmental safety, 178, 33-42.

Talat, N. (2020). Alleviation of soil salinization and the management of saline soils, climate change, and soil interactions. Climate Change and Soil Interactions, pp. 305–329. https://doi.org/10.1016/B978-0-12-818032-7.00011-4.

Tan, J., Ding, J., Han, L., Ge, X., Wang, X., Wang, J., Wang, R., Qin, S., Zhang, Z., & Li, Y. (2023). Exploring PlanetScope Satellite Capabilities for Soil Salinity Estimation and Mapping in Arid Regions Oases. Remote Sensing, 15(4). https://doi.org/10.3390/rs15041066.

Tanaka, A., Saito, K., Azoma, K., & Kobayashi, K. (2013). Factors affecting variation in farm yields of irrigated lowland rice in southern-central Benin. European Journal of Agronomy, 44, 46–53.

Thomson, J., & Rogers, W. E. (2014). Swell and sea in the emerging Arctic Ocean. Geophysical Research Letters, https://doi.org/10.1002/2014GL059983.

Thornton, I., & Giglioli, M. E. C. (1965). The Mangrove Swamps of Keneba, Lower Gambia River Basin. II. Sulfur and pH in the Profiles of Swamp Soils. Journal of Applied Ecology, 2(2), 257-269. URL: http://www.jstor.org/stable/2401478.

Thornton, P. K. (2010). Livestock production: recent trends, future prospects. Philosophical Transactions of the Royal Society B: Biological Sciences, 365(1554), 2853-2867. https://doi.org/10.1098/rstb.2010.0134.

Tian, F., Hou, M., Qiu, Y., Zhang, T., & Yuan, Y. (2020). Geoderma Salinity stress affects transpiration and plant growth under different salinity soil levels based on the thermal infrared remote (TIR) technique. Geoderma, 357(September 2019), 113961. https://doi.org/10.1016/j.geoderma.2019.113961.

Torres, M. A., West, A. J., Clark, K. E., Paris, G., Bouchez, J., Ponton, C., ... & Adkins, J. F. (2016). The acid and alkalinity budgets of weathering in the Andes–Amazon system: Insights into the erosional control of global biogeochemical cycles. Earth and Planetary Science Letters, 450, 381-391.

Tougui, I., Jilbab, A., & Mhamdi, J. E. (2021). Impact of the Choice of Cross-Validation Techniques on the Results of Machine Learning-Based Diagnostic Applications. *Healthcare Informatics Research, 27*(3), 189-199. https://doi.org/10.4258/hir.2021.27.3.189.

Trærup, S. L. M. (2010). Ensuring Sustainable Development within a Changing Climate. University of Copenhagen.

Tully, K. L., Weissman, D., Wyner, W. J., Miller, J., & Jordan, T. (2019). Soils in transition: saltwater intrusion alters soil chemistry in agricultural fields. Biogeochemistry, 142(3), 339–356. https://doi.org/10.1007/s10533-019-00538-9.

United States Department of Agriculture (USDA), Soil Quality Indicator: Soil Electrical Conductivity; Natural Resources Conservation Services: United States, 2011.

Van Nguyen, N., & Ferrero, A. (2006). Meeting the challenges of global rice production. Paddy and Water Environment, 4(1), 1–9. https://doi:10.1007/s10333-005-0031-5.

Van Nguyen, N., Ferrero, A. (2006).Meeting the challenges of global rice production. Paddy Water Environ 4, 1–9. https://doi.org/10.1007/s10333-005-0031-5.

Van Vuuren, D. P., Edmonds, J., Kainuma, M., Riahi, K., Thomson, A., Hibbard, K., Rose, S. K. (2011). The representative concentration pathways: an overview. Climatic Change, 109, 5-31. https://doi: 10.1007/s10584-011-0148-z.

Verbruggen, H., Kuik, O. (1991). Indicators of sustainable development: an overview. In: Kuik, O., Verbruggen, H. (eds) In Search of Indicators of Sustainable Development. Environment & Management, vol 1. Springer, Dordrecht. https://doi.org/10.1007/978-94-011-3246-6_1.

Verkerk M.P. & van Rens C.P.M., (2005), Saline intrusion in Gambia River after dam construction, Research Report, University of Twente, The Netherlands

Vigerstol, K. L., & Aukema, J. E. (2011). A comparison of tools for modeling freshwater ecosystem services. Journal of Environmental Management, 92(10), 2403-2409. https://doi.org/10.1016/j.jenvman.2011.06.040.

Virtasalo, J. J., Österholm, P., & Asmala, E. (2023). Estuarine flocculation dynamics of organic carbon and metals from boreal acid sulfate soils. 2883–2901.

Vogel, E., Donat, M. G., Alexander, L. V., Meinshausen, M., Ray, D. K., Karoly, D., ... & Frieler, K. (2019). The effects of climate extremes on global agricultural yields. Environmental Research Letters, 14(5), 054010.

Wang, F., Shi, Z., Biswas, A., Yang, S., & Ding, J. (2020). Multi-algorithm comparison for predicting soil salinity. *Geoderma, 365, 114211*. https://doi:10.1016/j.geoderma.2020.114211.

Wang, J., Peng, J., Li, H., Yin, C., Liu, W., Wang, T., & Zhang, H. (2021). Soil salinity mapping using machine learning algorithms with the sentinel-2 MSI in arid areas in China. Remote Sensing, 13(2), 1–14. https://doi.org/10.3390/rs13020305.

Wang, N., Xue, J., Peng, J., Biswas, A., He, Y., & Shi, Z. (2020). Integrating Remote Sensing and Landscape Characteristics to Estimate Soil Salinity Using Machine Learning Methods: A Case Study from Southern Xinjiang, China. *Remote Sensing, 12(24), 4118.* https://doi:10.3390/rs12244118.

Wang, Y., Deng, C., Liu, Y., Niu, Z., & Li, Y. (2018). Identifying change in spatial soil salinity accumulation in an inland river watershed, China. Science of The Total Environment, 621, 177-185. https://doi.org/10.1016/j.scitotenv.2017.11.222.

Wang, Z., Hassan, M. U., Nadeem, F., Wu, L., Zhang, F., & Li, X. (2020). Magnesium Fertilization Improves Crop Yield in Most Production Systems: A Meta-Analysis. Frontiers in Plant Science, 10(January), 1–10. https://doi.org/10.3389/fpls.2019.01727.

Warne, R. T. (2014). A Primer on Multivariate Analysis of Variance (MANOVA) for Behavioral Scientists. Practical Assessment, Research & Evaluation, 19(17), ISSN 1531-7714.

Webb, J. L. A. (1992). Ecological and economic change along the middle reaches of the Gambia River, 1945-1985. African Affairs, 91(365), 543–565. https://doi.org/10.1093/oxfordjournals.afraf.a098561.

Webber, H. A., Madramootoo, C. A., Bourgault, M., Horst, M. G., Stulina, G., & Smith, D. L. (2010). Adapting the CROPGRO model for saline soils: the case for a common bean crop. Irrigation Science, 28, 317-329.

Webber, H., Hoffmann, M., Rezaei, E.E. (2018). Crop Models as Tools for Agroclimatology. Agronomy Monographs. https://doi.org/10.2134/agronmonogr60.2016.0025.

Wei, Y., Shi, Z., Biswas, A., Yang, S., Ding, J., & Wang, F. (2020). Updated information on soil salinity in a typical oasis agroecosystem and desert-oasis ecotone: Case study conducted along the Tarim River, China. Science of the Total Environment, 716, 135387.

Welch, J. R., Vincent, J. R., Auffhammer, M., & Dawe, D. (2010). Rice yields in tropical/subtropical Asia exhibit large but opposing sensitivities to minimum and maximum temperatures. Proceedings of the National Academy of Sciences, 107(33), 14562-14567. https://doi.org/10.1073/pnas.1001222107.

Werner AD, et al. Impact of sea-level rise on seawater intrusion in coastal aquifers. Ground Water. 2009;47:197-204

Wheeler B (2016). lmPerm: Permutation Tests for Linear Models. R package version 2.1.0.URL https://CRAN.R-project.org/package=lmPerm.

Wicke B, Smeets E, Dornburg V, Vashev B, Gaiser T, Turkenburg W and Faaij A (2011). The global technical and economic potential of bioenergy from salt-affected soils. *Energy Environ. Sci.* (4): 2669-2681.

Wilhelmi, O. V., & Wilhite, D. A. (2002). Assessing Vulnerability to Agricultural Drought: A Nebraska Case Study. Natural Hazards, 25, 37–58. https://doi.org/10.1023/A:1013388814894.

Woodrow W. Burchett, Amanda R. Ellis, Solomon W. Harrar, Arne C. Bathke (2017). "Nonparametric Inference for Multivariate Data: The R Package npmv.," Journal of Statistical Software,76(4), 1-18.

World Meteorological Organization (WMO), "A Decade of Extremes: The Global Climate 2001-2010," Meteoworld, July 2013. Available at: https://public-old.wmo.int/en/meteoworld/decade-extremes. Accessed on 11/25/2022.

Xiao, S. & Zhang, J.-T. (2016). Modified Tests for Heteroscedastic Two-Way MANOVA. Journal of Advanced Statistics, 1(1):1.

Xu, X., Huang, G., Sun, C., Pereira, L. S., Ramos, T. B., Huang, Q., & Hao, Y. (2013). Assessing the effects of water table depth on water use, soil salinity, and wheat yield: Searching for a target depth for irrigated areas in the upper Yellow River basin. Agricultural Water Management, 125, 46–60. https://doi.org/10.1016/j.agwat.2013.04.004.

Yadav, S., Sandhu, N., Singh, V. K., Catolos, M., & Kumar, A. (2019). Genotyping-by-sequencing based QTL mapping for rice grain yield under reproductive stage drought stress tolerance. Scientific reports, 9(1), 14326.

Yang, Y., Liu, L., Singh, R. P., Meng, C., Ma, S., Jing, C., Li, Y., & Zhang, C. (2020). Nodule and root zone microbiota of salt-tolerant wild soybean in coastal sand and saline-alkali soil. Frontiers in Microbiology, 11, 2178. https://doi.org/10.3389/fmicb.2020.523142.

Yensen, N.P., (2008). Halophyte uses in the twenty-first century. In: Khan, M.A., Weber, D.J. (Eds.), Ecophysiology of High Salinity Tolerant Plants. Springer, Dordrecht, pp. 367-396.

Yira, Y., Diekkrüger, B., Steup, G., & Bossa, A. Y. (2017). Impact of climate change on hydrological conditions in a tropical West African catchment using an ensemble of climate simulations. Hydrology and Earth System Sciences, 21(4), 2143–2161. https://doi.org/10.5194/hess-21-2143-2017.

Yoshida, Takuma. (2023). Asymptotic theory for extreme value generalized additive models. https://doi.org/10.48550/arXiv.2303.02402.

Yue, S., Pilon, P., Phinney, B., & Cavadias, G. (2002). The influence of autocorrelation on the ability to detect trends in hydrological series. Hydrological Processes, 16(9), 1807–1829. https://doi.org/10.1002/hyp.1095.

Zabel F, Putzenlechner B, Mauser W (2014) Global Agricultural Land Resources – A High-Resolution Suitability Evaluation and Its Perspectives until 2100 under Climate Change Conditions. PLoS ONE 9(9): e107522. https://doi.org/10.1371/journal.pone.0107522.

Zaman, M., Shahid, S. A., & Heng, L. (2018). Guideline for Salinity Assessment, Mitigation and Adaptation Using Nuclear and Related Techniques. In Guideline for Salinity Assessment, Mitigation and Adaptation Using Nuclear and Related Techniques. https://doi.org/10.1007/978-3-319-96190-3.

Zeng, C., Zhu, A., Liu, F., Yang, L., Rossiter, D. G., Liu, J., & Wang, D. (2017). The impact of rainfall magnitude on the performance of digital soil mapping over low-relief areas using a land surface dynamic feedback method. Ecological Indicators, 72, 297-309. https://doi.org/10.1016/j.ecolind.2016.08.023.

Zhang, X., Huang, B., & Liu, F. (2020). Information extraction and dynamic evaluation of soil salinization with a remote sensing method in a typical county on the Huang-Huai-Hai Plain of China. Pedosphere, 30(4), 496–507. https://doi.org/10.1016/S1002-0160(17)60478–8.

Zhang, X., K. D. Harvey, W. D. Hogg, and T. R. Yuzyk (2001), Trends in Canadian streamflow, Water Resour. Res., 37(4), 987 – 998

Zhang, Xike, Gui Zhang, Luo Qiu, Bo Zhang, Yurong Sun, Zifan Gui, and Qiuwen Zhang. (2019). "A Modified Multifractal Detrended Fluctuation Analysis (MFDFA) Approach for Multifractal Analysis of Precipitation in Dongting Lake Basin, China" Water 11, no. 5: 891. https://doi.org/10.3390/w11050891.

Zhao, H. et al. (2020). 'Relationships between grain yield and agronomic traits of rice in southern China,' Chilean Journal of Agricultural Research, 80(1), pp. 72–79. Available at: https://doi.org/10.4067/s0718-58392020000100072.

Zheng Z, Zhang F, Ma F, Chai X, Zhu Z, Shi J, Zhang S. (2009). Spatiotemporal changes in soil salinity in a drip-irrigated field. Geoderma, 149: 243–248.

Zientek, L. R., & Thompson, B. (2009). Matrix Summaries Improve Research Reports: Secondary Analyses Using Published Literature. Educational Researcher, 38(5). https://doi.org/10.3102/0013189X09339056.

Zientek, L. R., & Thompson, B. (2009). Matrix summaries improve research reports: Secondary analyses using published literature. Educational Researcher. Retrieved from journals.sagepub.com.

Zinyengere, N., Crespo, O., Hachigonta, S., & Tadross, M. (2014). Local impacts of climate change and agronomic practices on dry land crops in Southern Africa. Agriculture, Ecosystems & Environment, 197, 1–10. https://doi.org/10.1016/j.agee.2014.07.002.

APPENDIX

Appendix 4.1. ANOVA-Type Statistic for Subset Algorithm Based on Factor Level: Site

Buiba	Kudang				rejected
Kudang	Mandina				rejected
Kudang	Pakaliba				rejected
Kudang	Tonitaba				rejected
Buiba	Kudang	Mandina			rejected
Buiba	Kudang	Pakaliba			rejected
Buiba	Kudang	Tonitaba			rejected
Kudang	Mandina	Pakaliba			rejected
Kudang	Mandina	Tonitaba			rejected
Kudang	Pakaliba	Tonitaba			rejected
Buiba	Kudang	Mandina	Pakaliba		rejected
Buiba	Kudang	Mandina	Tonitaba		rejected
Buiba	Kudang	Pakaliba	Tonitaba		rejected
Kudang	Mandina	Pakaliba	Tonitaba		rejected
Buiba	Kudang	Mandina	Pakaliba	Tonitaba	rejected

Appendix 4.2 Table 4. 11 ANOVA-type statistic for the subset algorithm based on variable level: Soil variables

ESP			rejected
Na^{+2}			rejected
EC_e (dS/m)			rejected
pH			rejected
Na^{+2}	ESP		rejected
EC_e (dS/m)	ESP		rejected
EC_e (dS/m)	Na^{+2}		rejected
pH	ESP		rejected
pH	Na^{+2}		rejected
pH(H_2O)	EC_e (dS/m)		rejected
EC_e (dS/m)	Na^{+2}	ESP	rejected
pH	Na^{+2}	ESP	rejected
pH	EC_e (dS/m)	ESP	rejected
pH	EC_e (dS/m)	Na^{+2})	rejected
EC_e (dS/m)	Na^{+2}	ESP	rejected

Appendix 5.1: SMK and Seasonal trend with and without serial correlation of annual climate variables in CRRS and LRR

Annual	**Standard Mann-Kendall Test (M.K.)**			**Prewhitening MK (**Yue Pilon**)**		
CRRS	Z	S.S.	P-value	AR(1)	SS	p-value
Tmax ^{0}C	-0.03	-4.0	0.97	0.61	0.00	0.80
Tmin ^{0}C	0.26	2.3	0.79	0.73	0.39	0.56
RF (mm)	2.59	224	**0.009**	0.15	3.57	**0.015**
LRR						
Tmax ^{0}C	0.38	3.40	0.70	0.64	0.66	0.94
Tmin ^{0}C	-0.36	-32.0	0.72	0.7	-0.66	0.41
RF (mm)	2.57	222	**0.01**	1.12	5.73	**0.011**
Seasonal	**Seasonal Mann-Kendall Test (Hirsch-Slack test)**			**Prewhitening MK** (Yue Pilon)		
CRRS	Z	S.S.	p-value	AR(1)	SS	p-value
Tmax ^{0}C	3.44	986	**<0.001**	0.68	0.53	0.63
Tmin^{0}C	-11.07	-318	**<2.2e**	0.75	-2.6	**0.009**
RF (mm)	0.04	2.0	0.97	0.58	0.00	0.88
LRR						
Tmax ^{0}C	1.79	70.1	0.07	0.64	-0.21	0.96
Tmin ^{0}C	-4.3	-1241	**<0.001**	0.77	-0.53	0.52
RF (mm)	1.65	341	0.09	0.64	0.00	0.41

Appendix 5.2 AIC values of tentative models for selecting a better model to predict climate variables and rice production in CRRS and LRR

ARIMA Model		Tmax RMSE	Tmin	RMSE	Rainfall
0,0,0	42.99	1.80	42.99	1.76	110.24
1,1,0	41.70	1.66	41.70	1.51	101.69
0,1,1	41.19	2.09	41.19	1.91	**100.88**
0,1,0	**37.69**	**1.65**	**37.69**	1.64	101.16
1,1,1	47.55	2.09	47.55	1.91	104.52

ARIMA Model		Tmax RMSE	Tmin	RMSE	Rainfall
0,0,0	39.68	1.61	47.59	1.98	111.62
1,1,0	37.60	**1.35**	38.36	**1.42**	103.81
0,1,1	37.45	1.81	37.82	1.98	102.08
0,1,0	**33.46**	1.55	**36.11**	1.66	**99.79**
1,1,1	44.28	1.81	44.75	1.98	108.70

Appendix 5.3 ACF and PACF for annual climate parameters

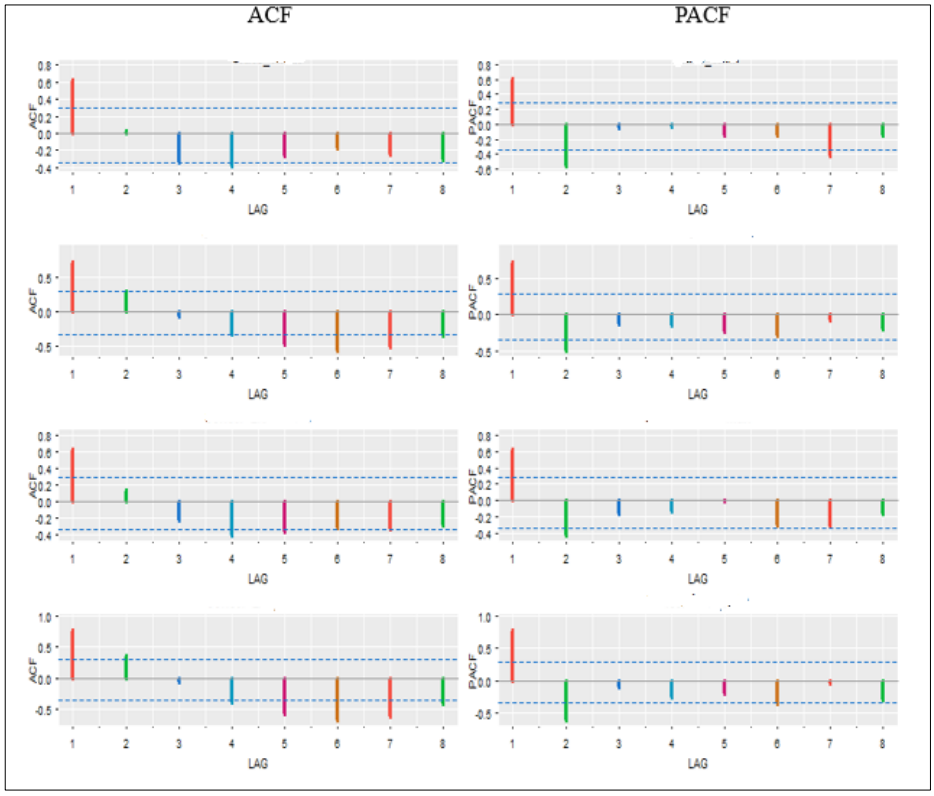

Appendix 5.4: Diagnostic checking of the models using Jlung-Box chi-square statistics and autocorrelation of residuals

(a) Maximum temperature (Tmax)

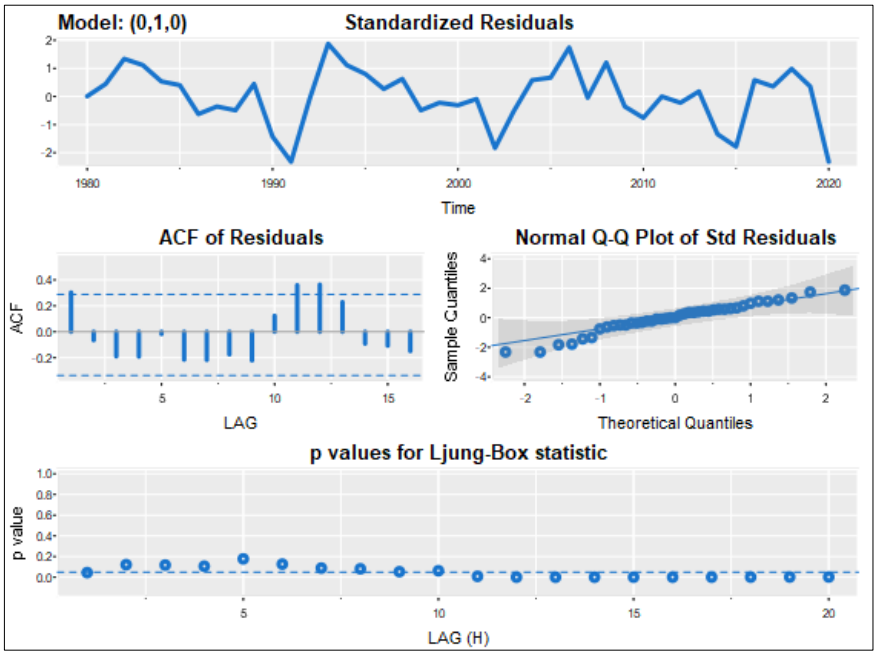

(b) Minimum temperature (Tmin)

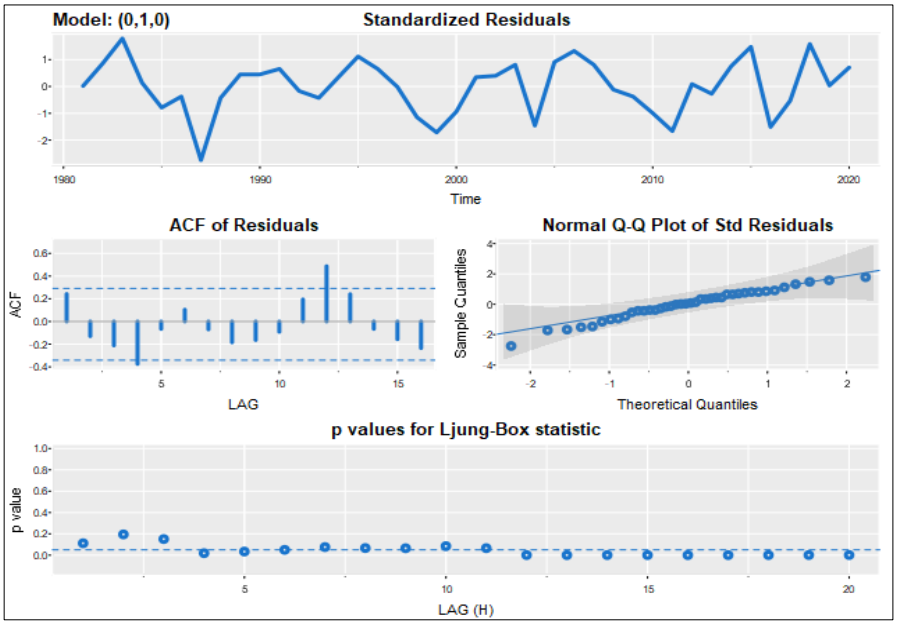

(c) Rainfall (RF)